Multivalent binding, cell rolling, and micropatterning for enhanced detection of circulating tumor cells

BY

JA HYE MYUNG
B.S., Chungam National University, 2004
M.S., Chungnam National University, 2006

Submitted as partial fulfillment of the requirements
for the degree of Doctor of Philosophy in Biopharmaceutical Sciences
in the Graduate College of the University of Illinois at Chicago, 2012

Chicago, Illinois

Doctoral Committee:

Seungpyo Hong, Chair and Advisor
David T. Eddington, Bioengineering
Michael Cho, Bioengineering
Robert E. Molokie
Richard A. Gemeinhart

ACKNOWLEDGEMENTS

It would not have been possible for me to finish this doctoral thesis without the help and support of many people around me. I would like to mention some of them here.

Above all, I would like to deeply thank Prof. Seungpyo Hong. This dissertation would not have been possible without his help, support, and patience. Throughout my whole Ph.D. study, he encouraged, mentored, and academically enlightened me. I also greatly appreciate Prof. David T. Eddington for his great scientific advice and generous support for my thesis project, especially through the monthly meetings. I thank Prof. Richard A. Gemeinhart and his group members for optical/fluorescence microscopy measurements. All blood-based experiments in this dissertation would not have been possible without the support of Prof. Robert E. Molokie and his team in the sickle cell center in UIC hospital. I also appreciate Prof. Michael Cho and his lab members for helpful discussion throughout the work and upright fluorescence microscopy measurements for my collaboration project. They have guided me throughout this journey with great scientific insights and helpful comments. I really appreciate them for their support and encouragement.

It was a great pleasure to have an opportunity to work with my wonderful colleagues in Dr. Hong's lab. I would like to give special thanks to Khyati A. Gajjar and Jelena Saric who assisted most of the experiments and proof-read my drafts, and Dr. Jin Woo Bae who performed NMR analysis and gave me great advices. I am very grateful to other group members, Suhair Sunoqrot, Yang Yang, Ryan M. Pearson, Hao-jui Hsu,

Sayam Uddin, Ye Eon Han, Eri Iwasaki, Jason Bugno, and other previous lab members for their generous contribution and help in my research.

Knowledge I have gained from such an interdisciplinary group in the department of Biopharmaceutical Sciences is invaluable. I sincerely thank all faculties in BPS for their guidance with great scientific insights and helpful comments. I appreciate Ernest Gemeinhart, Dr. Tsui-Ting Ho, Dr. Amrita Benerjee, and Dr. Sungpil Cho for their support and encouragement. I also thank to my collaborators, Dr. Cari A. Launiere and Dr. Shawn Oppegard in Dr. David T. Eddington's lab for PDMS gasket development and helpful discussion throughout the work.

Finally, I would like to thank my parents, Dr. Byung-Soo Myung and Mrs. Hee-Soo Cho, for their unequivocal support throughout my Ph.D. course, as always has been in my life. I would like to thank my siblings, Ji Hae and Ji Hwan, who have always supported me. I would like to express my deepest gratitude to my family for their understanding, unconditional support and encouragement during my whole life. I also greatly acknowledge my friends, Danbi, Tsui-Ting, Jian-You, and Minjee for their support, encouragement, and friendship. Without this wonderful team of support I could not have done what I have done.

This research has been financially supported by National Science Foundation, This investigation was conducted in a facility constructed with support from the National Institutes of Health, USA. I got supports, Dean's fellowship, Chancellor's supplementary fellowship, and W.E. van Doren Scholar Award from the University of Illinois at

Chicago. I also received a Global Alumni Scholarship from Alumni of Chungnam National University, Daejeon, Korea (ROK).

TABLE OF CONTENTS

LIST OF TABLES

LIST OF FIGURES

LIST OF ABBREVIATIONS

APC	Allophycocyanin
BSA	Bovine serum albumin
CEA	Carcinoembryonic antigen
CTC	Circulating tumor cell
CytoD	Cytochalasin D
DMEM	Dulbecco's modified eagle's medium
DsRED-MCF-7	*Discosoma sp.* Red fluorescent protein (DsRED)-transfected MCF-7
DTC	Disseminated tumor cell
EDC	1-ethyl-3-(3-dimethylaminopropyl) carbodiimide
EMT	Epithelial-to-mesenchymal transition
EpCAM	Epithelial cell adhesion molecule
E-selectin	Recombinant human E-selectin/Fc chimera
ESL-1	E-selectin ligand-1
FACS	Fluorescence activated cell sorter
FBS	Fetal bovine serum
FITC	Fluorescein isothiocyanate
G	Generation
HCELL	Hematopoietic cell E- and L-selectin ligand
HER-2	Human epidermal growth factor receptor-2
HUVEC	Human umbilical endothelial cells
IMDM	Isocove's Modified Dulbecco's Medium

k_a	Association rate constant
K_A	Association constant
k_d	Dissociation rate constant
K_D	Dissociation constant
MACS	Magnetic active cell sorting
NHS	N-hydroxylsuccinimide
NMR	Nuclear magnetic resonance
PAMAM	Poly(amidoamine)
PBS	Phosphate buffered saline
PDMS	Polydimethylsiloxane
PE	Phycoerythrin
PEG	Polyethylene glycol
PSA	Prostate specific antigen
P-selectin	Recombinant human P-selectin/Fc chimera
PSGL-1	P-selectin glycoprotein-1
RU	Resonance units
sLe^a	Sialyl Lewis^a
sLe^X	Sialyl Lewis^X
SEM	Standard error of the mean
SPR	Surface plasmon resonance
XPS	X-ray photoelectron scattering

CHAPTER 1

INTRODUCTION

1.1. Circulating Tumor Cells (CTCs) and Metastasis

1.1.1. Cancer Metastasis

Cancer metastasis is a pathological process by which cancer cells spread from the primary tumor site to other distant sites in body. Metastasis-related signaling in the primary cancer cells is triggered by various stimuli such as the tumor overgrowth beyond a millimeter or two and chemo/ratio-therapies [1]. Mostly, the adhesive mechanisms that normally keep cells tethered to the extracellular matrix are disrupted and the cancer cells become invasive and spread aggressively by the metastasis-enhancing signaling [2]. For instance, the gene expression of E-cadherin, a transmembrane protein for cell-cell adhesion, is down-regulated, which facilitates local invasiveness of cancer cells during cancer development [3]. The loss of cell adhesiveness is similar to a character transition of epithelial cells during epithelial-to-mesenchymal transition (EMT), which occurs in some epithelial tissues during normal development [4]. The cancer cells in primary site are also secreting angiogenic signals in response to hypoxia to form new blood vessels (angiogenesis) [5]. The formation of the new leaky vessels near tumors is not helpful only to supply the tumor with nutrients and oxygen, but also to provide an escape route for the metastatic cancer cells [6]. The escaping phenomenon of cancer cells from primary site to lymphatic or blood vessels is known as intravasation.

Although invasive cancer cells are escaping from the original site, they should pass other multistage process to form the metastases in remote sites. The escaped cancer cells must survive in the circulating system (lymph nodes or blood vessel), and the survival process is as inefficient

as only few cells reach to the target organ [7, 8]. After interacting with the endothelium, surrounding in lymph or blood vessels, the invasive cancer cells penetrate the lymph or blood vessels by crossing the basal lamina and the endothelium of the vessel [9]. The initial seeding cancer cells continue to survive and proliferate in foreign site (colonization). The cancer types or origins determine the sites of cancer metastasis such as lungs, bones, and liver, and cancer metastases can occur at multiple locations in body simultaneously [10].

1.1.2. Diagnosis of Cancer Metastasis

Although recent advances in diagnostic and therapeutic methods to treat primary tumors hold promise to decrease mortality of cancer, metastasis of cancer still poses a great challenge as patients often relapse [11-14]. Thus, research efforts on diagnosis and prognosis of metastatic cancer have been concentrated. Two pathways of the intravasated cancer cell circulation are involved to induce secondary tumor formation at distant sites from primary tumors, cancer metastasis; disseminated tumor cells (DTCs) through lymph node and circulating tumor cells (CTCs) through blood circulation [8].

The average number of DTCs in bone marrow is around 10-20 cells among millions of bone marrow cells, and the DTCs are currently enriched by a density gradient centrifugation method or a positive immunomagnetic enrichment method, followed by detection and characterization of DTCs [15]. Detection of DTCs for prognosis studies along with therapeutic treatments requires repeated samplings of bone marrow that is invasive, time-consuming, and often painful for the patients [16, 17].

Consequently, effective detection of CTCs in peripheral blood of cancer patients holds a promise as an alternative due to its minimally invasive and easy sampling procedures (i.e. blood drawing). The presence of CTCs in the peripheral blood is highly related to the metastasis of

major carcinomas, especially breast, prostate, and colorectal cancers [18-22]. The number of CTCs can be used as a biomarker to diagnose metastatic cancer in early stage and to monitor the disease progress upon anti-cancer therapies [23, 24]. CTC detection from blood, often as referred to "liquid biopsy", has thus attracted a great deal of scientific and clinical interests, particularly because this method can potentially replace the currently available tissue biopsy that is painful and difficult to collect [25]. To achieve sensitive CTC detection, a number of detection methods have been investigated, such as nucleic acid-based detection, size/density-based detection, and antibody-based detection against tumor cell surface markers. The commonly used surface markers include epithelial cell adhesion molecule (EpCAM) [18, 26], carcinoembryonic antigen (CEA) [27], and human epidermal growth factor receptor-2 (HER-2) [28, 29]. However, the clinical usage of CTCs has not yet been implemented for routine clinical practice because CTCs are extremely rare and estimated to be in the range of one tumor cell in the background of 10^6-10^9 normal blood cells [30, 31].

1.1.3. Cell Rolling: the Binding between CTCs and Endothelium

The process of CTC-mediated metastasis is not fully understood but one of the most plausible mechanisms involves a similar process of leukocyte homing, i.e. a naturally occurring cell rolling process [9]. The formation of transient ligand-receptor interactions occurs commonly between cells flowing in the blood and the vascular endothelium; this physiological process is known as cell rolling [32]. Rolling cells then firmly attach to the endothelial layers, followed by transmigration through the endothelium (diapedesis) to form secondary tumors [33]. Cell rolling plays a key role in biologically important processes such as recruitment of leukocytes to sites of inflammation, homing of hematopoietic progenitor cells, and CTC-induced metastasis. This behavior is typically mediated by dynamic interactions between selectins (E- and P-selectins) on

the vascular endothelial cell surface and transmembrane ligands on the carcinoma cell surface. Endothelial (E)-selectin (CD62E) is particularly noteworthy in disease by virtue of its expression on activated endothelium and on bone-skin microvascular linings, and many studies point to the key role played by E-selectin in being involved in the adhesion and homing of various types of cancer cells such as prostate [34], breast [35, 36], and colon carcinoma cells [37].

Thus, tumor cell separation based on the selectin-mediated (particularly, E-selectin) cell rolling behavior is being pursued as it mimics a physiological process, and eliminates labeling and label removal steps that are necessary for other immune-labeling detection methods [38]. However, given that a large class of cells, including leukocytes, platelets, neutrophils, mesenchymal and hematopoietic stem cells, and metastatic cancer cells all exhibit rolling on E-selectins, detection that is solely based on cell rolling has limitations for achieving sufficient specificity, which has hindered translation of the technology to a clinically significant device. If the cell recruitments from circulating blood of E-selectin are combined with the target tumor cell selectivity mediated by anti-EpCAM, this biomimetic surfaces will provide the enhanced capture efficiency and selectivity of CTCs.

1.2. Polymeric Materials for CTC Detection

As mentioned above, a number of detection methods have been investigated for sensitive detection of CTCs, and polymers have played a central role in detection mechanisms, including physical property-based separation using polymeric structures [39], targeted detection in solution (i.e., blood) using polymer-coated inorganic nanoparticles [26, 27], and surface capturing using polymer-immobilized surfaces [41], as summarized in **Fig. 1.1** and **Table 1.1**. This section will introduce the polymeric materials that have been used for CTC detection, followed by

comprehensive discussion of representative examples. Chemical structures of the commonly used polymers are illustrated in **Fig. 1.2**.

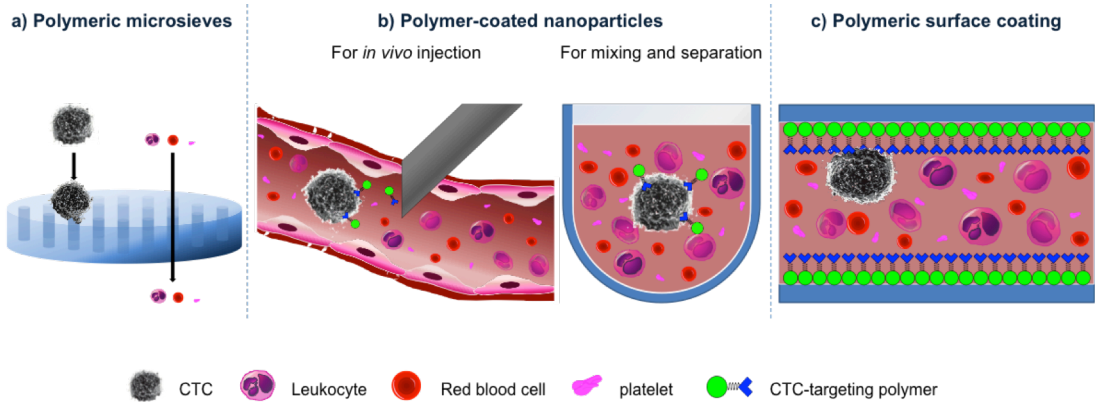

Figure 1.1. Illustrations of polymer-based CTC detection. The polymers play a crucial role in CTC detection via a) physical property-based CTC separation using polymeric microsieves, b) targeting using polymer-coated inorganic nanoparticles, and c) capturing using polymer-coated surfaces.

1.2.1. Polymeric structures for CTC detection: size and deformability-based separation

Characteristics of CTCs that are different from normal hematologic cells include their larger size and a low level of deformability [27, 42, 43, 44]. To separate CTCs based on such distinguishable physical properties, UV- or temperature-curable polymers such as parylene [39, 45, 46], polyurethane-methacrylate (PUMA) [42], and polydimethylsiloxane (PDMS) [47], have been fabricated as microscale sieves. As the separation mechanism is simply filtration-based, the polymeric microsieves can achieve high throughput CTC separation. The simple, cost-effective, and rapid processing of the polymers also makes the microsieve fabrication easy and fast. In addition, this method does not require immune-affinity or immunostaining, allowing isolation of immunologically intact CTCs, which is beneficial for the downstream analysis of the captured cells. However, the captured cells on the polymeric filtering systems are typically exposed to mechanical stress, which often induces cell damage, lysis, and cell cycle arrest [53]. The size

Table 1.1. Summary of recent investigations in CTC detection using polymers

Types		Mechanism	Description	Materials Used
Polymeric microsieves		Physical property differences between CTCs and leukocytes	Micro-sized filter systems fabricated using polymeric structure	parylene [39, 45, 46], PUMA [42], or PDMS [47]
Polymer-coated inorganic nanoparticles	***In vivo* injection**	Direct binding and detection of CTCs in blood stream	Polymeric coating or linkers combined with inorganic nanoparticles and CTC targeting ligands	PEG [40, 48, 49], or polymeric linkers [50]
	Mixing and separation	Isolation of CTCs from the drawn blood specimens		Amphiphilic triblock polymers consisting of PBA, PEA, and PMA [28], or SAM of MUA and MCH [27]
Polymer-immobilized surfaces		Binding and isolation of CTCs using polymer-engineered surfaces	CTC-capturing ligand-conjugated polymer coating on surfaces	Biopolymers such as alginate [51], SAM of MPTMS [52], or dendrimers [41]

variation of cancer cells can also derive the potential false negative or positive results [54]. To address the mechanical trauma to captured cells, Zheng *et al*. has recently devised a three-dimensional parylene-based filter system by combining the conventional two-dimensional filter systems with an additional bottom membrane to prevent the captured cells from exposure to the continuous mechanical forces [39]. They reported the overall tension applied to the trapped cells in the 3D microfilters was reduced by ~50%, compared to other 2D microfilters, resulting in a significant decrease in the cell lysis and cell membrane distortion of the filtrated cells. Another approach is the use of non-elastomeric polymers (e.g., PUMA) that provides a structurally robust CTC separation system [42]. Size-controlled pores on the PUMA wall that is lined in a

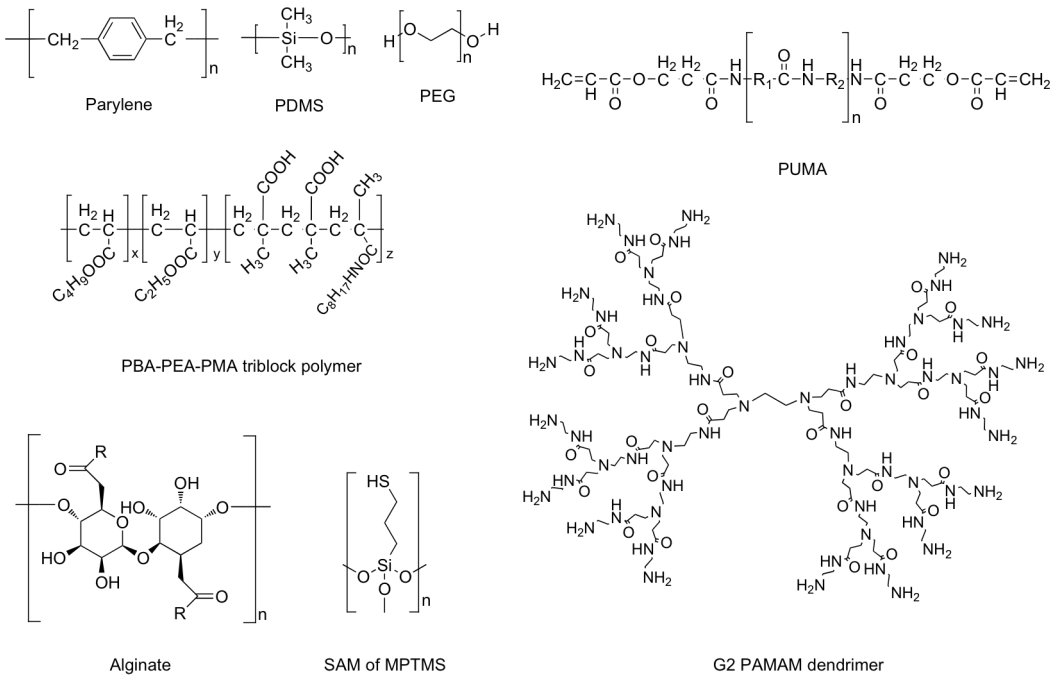

Figure 1.2. Chemical structures of polymers commonly used for CTC detection. Note that the chemical structure of G2 PAMAM dendrimer is given instead of G7 for structural simplicity.

serpentine-shaped channel separated CTCs from leukocytes and other hematologic cells, allowing for selective collection of CTCs at the outlet of the device. The polymer deposition of elastomeric polymers such as PDMS can be also employed to make a shear-modulated microfilter for CTC detection [47]. Using PDMS that allows precise filter fabrication via soft lithography, Tan *et al*. demonstrated that the rounded bases of the crescent-shaped isolation wells minimized the external trauma, and the multiple arrays of the isolation wells with 5 μm pores effectively isolated CTCs from the whole blood.

1.2.2. Polymer-coated inorganic nanoparticles for CTC targeting and capturing

1.2.2.1. Injectable System

To simultaneously detect and kill CTCs in the bloodstream, linear polymers conjugated with CTC targeting ligands have been employed to coat the surfaces of inorganic nanoparticles, making them an injectable form. A recent advance in this *in vivo* CTC detection approach has been achieved in a xenograft mouse model using PEGylated inorganic nanoparticles, consisting of inorganic core (golden carbon nanotube or cylindrical neodymium-iron-boron magnetic nanoparticles), poly(ethylene glycol) (PEG) outer layer, and targeting agents (folate or anti-CD44) [40, 48]. The PEG outer layers allowed the surface conjugation of targeting ligands and enhance water-phase stability of the inorganic nanomaterials. The inorganic nanoparticle cores enabled imaging of the whole blood circulation using photoacoustic/photothermal flow cytometry [40, 48]. By taking advantage of the multifunctionality of the nanoparticles, folate receptor-overexpressing CTCs in the bloodstream were detected by targeting, magnetic enrichment, signal amplification, and multicolour recognition in a sequential manner.

The advantages of this type of approaches include the real-time CTC monitoring capability *in vivo*, which eliminates the necessity of blood sampling or sample preparation steps. Furthermore, the injectable nanoparticles typically induce the phagocytic clearance of CTCs upon binding, such that the isolation steps of CTCs from blood cells are not necessary. However, for the CTC-targeted, injectable nanoparticles to be effective, rapid clearance by reticuloendothelial system, high shear stress of the blood circulation, immune responses, and undesired accumulation in organs need to be overcome [50, 55]. This method can also result in potential false positive signals due to expression of the target antigens/markers on normal cells, non-specific binding of the nanoparticles (specificity), and background noise (the signal-to-background ratio). As noted above, PEGylation of the inorganic nanoparticles has been frequently used to address some of the issues by enhancing their circulation time while reducing their non-specific binding [56-58].

1.2.2.1. Mixing and separation from drawn blood specimens

Another approach using polymer-coated inorganic nanoparticles containing CTC-targeting molecules includes CTC detection upon mixing with blood specimens that are drawn from patients. The magnetic properties of inorganic nanoparticles or the fluorescence from surface-coated fluorophores enable to employ magnetic active cell sorting (MACS) [23] or a fluorescence-activated cell sorter (FACS) [55], respectively. For example, CellSearch^{TM}, the only FDA-approved CTC detection system for breast, prostate, and colorectal metastatic cancers, is based on iron oxide (Fe_3O_4) nanoparticles. The iron oxide nanoparticles are coated with antibodies (anti-EpCAM) against CTC surface markers (EpCAM) through polymeric linkers [23, 59]. Upon binding to CTCs in 7.5 mL of whole blood specimens, the magnetic nanoparticles bound to CTCs can be isolated by applying an external magnetic field [23]. The captured EpCAM-positive CTCs are confirmed by following post-analysis of cytokeratin-positive and CD45-negative properties of CTCs. Although reliable and stable, the CellSearch™ system has limitations such as complicated sample processing with additional steps needed for plasma removal and magnetic antibody labeling and limited sensitivity with a median 1.2 cells/mL detected from patients with metastatic cancer. Moreover, the CTC detection sensitivity of this assay is highly dependent on the binding capacity of the magnetic particles and sensitivity/selectivity of anti-EpCAM. In particular, the size of the currently used iron oxide (Fe_3O_4) nanoparticles is approximately 200 nm in diameter, which has a relatively low surface-to-volume ratio causing lower binding capacity and less stability in whole blood (aggregation or precipitation) [28]. In order to enhance the detection properties of the inorganic particles, Xu *et al.* reported that magnetic nanoparticles with smaller diameter (30 nm) enhanced their diffusivity in viscous samples and binding affinity [28]. The iron oxide nanoparticles were coated with an amphiphilic triblock polymer consisting of polybutylacrylate (PBA, hydrophobic), polyethylacrylate (PEA, hydrophobic), and polymethacrylic acid (PMA, hydrophilic), along with a hydrophobic hydrocarbon side chain, which enhanced physical stability and allowed further surface functionalization of the nanoparticle surfaces.

1.2.3. Polymer-coated surfaces for CTC capture

1.2.3.1. Biopolymers, hybrids, and silane chemistries

Instead of mixing with the withdrawn blood specimens, the CTC-targeting nanoparticles have been immobilized on a surface to induce the CTC adhesion onto the surface via immune-affinity. As opposed to using the expensive analytical tools such as MACS or FACS, the surface detection only requires typical glass slide-sized surfaces to isolate the intact CTCs with minimal damages, allowing for downstream molecular analysis of the cells. Direct capture of CTCs from whole blood specimens on the surface avoids potential false negative outputs resulted from the loss of CTCs during multiple sample preparation steps in the cases of MACS or FACS analysis [60, 61].

Various types of biopolymers and hybrids have been used to modify the nanoscale topography of the surface to increase surface-to-volume ratios and surface roughness, and to facilitate immobilization of CTC-targeting ligands. The surfaces of PDMS microfluidic devices have been modified with polymeric materials [51]. For example, biopolymers, such as alginate hydrogel [51] and self-assembled DNA nanostructures [62], have been incorporated onto the surface to increase CTC capture efficiency by altering the surface topography. Furthermore, other functions such as efficient release of the isolated CTCs from the surface upon simple stimulation (e.g. alginate lyase for alginate hydrogel) have been also engineered using the degradability of the biopolymers [51]. Additionally, hybrids such as a combination of β-cyclodextrin and carbon nanotubes [63] have also been used as surface coating agents to improve CTC detection of the surfaces.

The silane chemistry for surface functionalization of PDMS-based microfluidic devices has been widely used because it allows facile, precise, and reproducible surface functionalization. Although a PDMS-microfluidic device called CTC-chip does not primarily rely on polymers, we

cover this technology because of its functionalization via the silane chemistry that is similar to inorganic polymer chemistry and its advanced development stage in the CTC detection area. The first generation of CTC-chip, an immune-affinity ligand-coated microfluidic device with 78,000 microposts developed by a team led by Haber and Toner [60], showed a great potential for simple and cost-effective CTC detection. They used the surfaces that are modified via a series of SAM of 3-mercaptopropyo trimethoxysilane (MPTMS), N-y-maleimidobutyryloxy succinimide ester (GMBS), and NeutrAvidin, allowing for immobilization of biotinylated aEpCAM that captures CTCs. The microposts incorporated into the fluidic channels enhanced the hydrodynamic efficiency of the flow, resulting in sensitive detection of CTCs under flow. The CTC-chip does not require multiple processing steps in sample preparation and has shown enhanced sensitivity as compared to the CellSearch™ with a median of 67 cells/mL detected from whole blood samples of patients under comparable conditions [64]. The combined effect of anti-EpCAM-based specificity and the micropost-enhanced hydrodynamic efficiency enabled a capturing of over 60%. Although promising and advanced, the CTC-chip technology still needs to overcome several hindrances to achieve its clinical translation. The micropost-based system exhibited high capture yield at low flow rate (1-2 mL per hour) [65], but the capture yield substantially decreased with an increase in flow rate (higher than 2.5 mL/hr) due to the insufficient time for CTCs to bind to the surface [65]. In addition, these new approaches of topographical modifications have some limitation, such as their sophisticated fabrication, the utility of corrosive materials, and non-specific binding on the surface patterns. It has been also reported that the first generation of CTC chip showed poor mixing efficiency of viscous flow (low diffusivity) [52]. In an effort of addressing these issues, subsequent studies have incorporated herringbone patterns on the ceiling of the microfluidic device, increasing the mixing efficiency [52]. Mittal *et al.* have also reported that the insertion of a fluid-permeable polycarbonate layer inside the channel increased the pulling-down force to tow the cells to the surface, resulting in enhanced CTC detection [65].

1.2.3.2. PAMAM Dendrimers

Compared to other surface chemistry for CTC detection, the surface modification using three-dimensional, spherical poly(amidoamine) (PAMAM) dendrimers offers a unique opportunity to take advantage of naturally occurring strong multivalent binding effect [41]. The multivalent binding effect and its mediator, dendrimers, will be discussed further in next section.

1.3. Multivalency in Nanoengineered Surface Detection

1.3.1. Multivalent Binding Effect

Multivalent binding is the simultaneous binding of multiple ligands to multiple receptors in biological systems, which is central to a number of pathological processes, including the attachment of viral, parasitic, mycoplasmal, and bacterial pathogens [66-68]. These biological activities have been extensively investigated to promote targeting of specific cell types [69-73], and biological multivalent inhibitors have yielded quantitative measurements of binding avidities, with increases by 1-9 orders of magnitude [74-76].

1.3.2. PAMAM Dendrimers

To induce the multivalent binding effect efficiently, the selection of scaffolds and linkers is crucial for a multivalent conjugate with cell/tissue-specific ligands [77]. In particular, poly(amidoamine) (PAMAM) dendrimers have been reported to be an excellent mediator for multivalent effect because pre-organization/orientation of ligand, polymer backbone topology, and easy deformability all contribute for strong multivalent binding to cell surfaces [69]. Three-

dimensional structure of the dendrimer organizes the ligands into a small region of space, as compared to what is obtained if the ligands are conjugated to a similar molecular weight linear polymer [69, 78]. This geometric advantage may reduce the energy of deformation (entropy) of ligands on dendrimer surface to bind with their receptors and eventually enhance the binding avidity, resulting in significantly enhanced detection/capture efficiency. Further, it has been known that the carboxylated dendrimer has good accessibility of target cells to the immobilized targeting ligands [71], and reduced denaturation of the ligand during immobilization [79]. The advantages of enhanced binding avidity through dendrimer-mediated multivalent effect could significantly improve detection of human disease-related rare cells (<0.1% subpopulation) such as circulating tumor cells (CTCs) in peripheral blood.

1.4. Outline of Dissertation Organization

Two different biomimetic approaches such as cell rolling and multivalent binding are hired to enhance the detection sensitivity and specificity of rare CTCs in blood specimens in this dissertation, as depicted in **Fig. 1.3**. Chapter 2 focused to evaluate the effect of the first biomimetic approach, E-selectin-mediated cell rolling, for cell recruitment from flow. Although PAMAM dendrimer is known to mediate the multivalent binding (the second biomimetic approach we hired), the multivalent binding effect after dendrimer immobilization on the surface needs to be confirmed. To prove the multivalent binding effect on the dendrimer-immobilized surface for tumor cell detection, chapter 4 compared the binding strength of the dendrimer-anti-EpCAM-immobilized surface with cancer cells with that of the PEG (a linear polymer)-anti-EpCAM-immobilized surface. Along with the biomimetic approaches for CTC detection, CD24, a transmembrane protein on MCF-7 cells, was investigated as a ligand against E-selectin as described in chapter 3. The combination of two different biomimetic approaches was used to

develop the multifunctional surfaces with three different types of antibodies in chapter 5. The chapter 5 also includes quantitative analyses (capture efficiency measurement) on the multifunctional surfaces using *in vitro* cancer cells in blood samples withdrawn from healthy donors, providing a guideline for future diagnostic device design.

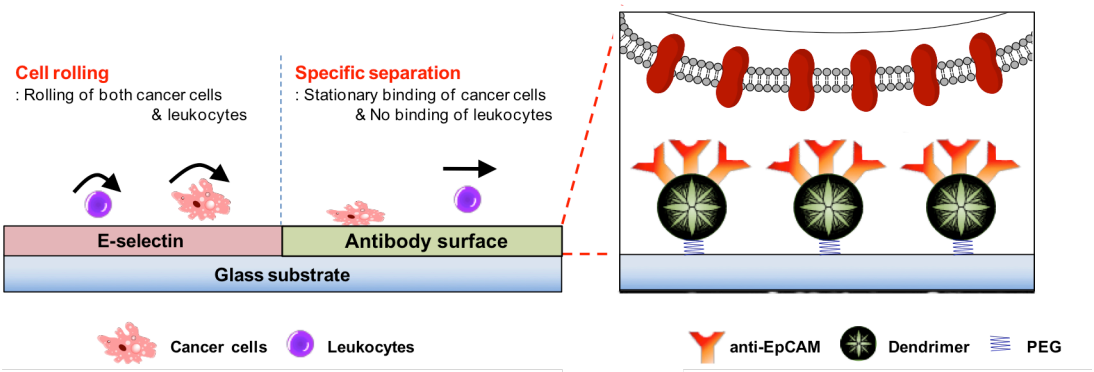

Figure 1.3. A schematic diagram of CTC capturing on biomimetic surface. The inset diagram represents the biomimetic surfaces that have the immobilized dendrimer with anti-EpCAM, resulting in the combination effect of cell rolling and multivalent binding for cancer cell capturing.

1.5. REFERENCES

1. Muraoka, R.S., et al., *Blockade of TGF-beta inhibits mammary tumor cell viability, migration, and metastases.* J Clin Invest, 2002. **109**(12): p. 1551-1559.

2. Cheng, G.Z., et al., *Twist transcriptionally up-regulates AKT2 in breast cancer cells leading to increased migration, invasion, and resistance to paclitaxel.* Cancer Res, 2007. **67**(5): p. 1979-1987.

3. Lu, Z.M., et al., *Downregulation of caveolin-1 function by EGF leads to the loss of E-cadherin, increased transcriptional activity of beta-catenin, and enhanced tumor cell invasion.* Cancer Cell, 2003. **4**(6): p. 499-515.

4. Mani, S.A., et al., *The epithelial-mesenchymal transition generates cells with properties of stem cells.* Cell, 2008. **133**(4): p. 704-715.

5. Shweiki, D., et al., *Vascular endothelial growth-factor induced by hypoxia may mediate hypoxia-initiated angiogenesis.* Nature, 1992. **359**(6398): p. 843-845.

6. Zhong, H., et al., *Overexpression of hypoxia-inducible factor 1 alpha in common human cancers and their metastases.* Cancer Res, 1999. **59**(22): p. 5830-5835.

7. Ashworth, T.R., *A case of cancer in which cells similar to those in the tumors were seen in the blood after death.* Aus Med J, 1869. **15**: p. 146-149.

8. Slade, M.J., et al., *Comparison of bone marrow, disseminated tumour cells and blood-circulating tumour cells in breast cancer patients after primary treatment.* Brit J Cancer, 2009. **100**(1): p. 160-166.

9. Mantovani, A., et al., *Cancer-related inflammation.* Nature, 2008. **454**(7203): p. 436-44.

10. Disibio, G. and S.W. French, *Metastatic patterns of cancers - Results from a large autopsy study.* Arch Pathol Lab Med, 2008. **132**(6): p. 931-939.

11. Karnon, J., et al., *Health care costs for the treatment of breast cancer recurrent events: estimates from a UK-based patient-level analysis.* Br J Cancer, 2007. **97**(4): p. 479-485.

12. Dong, F., A.S. Budhu, and X.W. Wang, *Translating the metastasis paradigm from scientific theory to clinical oncology.* Clin Cancer Res, 2009. **15**(8): p. 2588-93.

13. Pepper, M.S., *Lymphangiogenesis and tumor metastasis: myth or reality?* Clin Cancer Res, 2001. **7**(3): p. 462-8.

14. Hüsemann, Y., et al., *Systemic Spread Is an Early Step in Breast Cancer.* Cancer Cell, 2008. **13**(1): p. 58-68.

15. Riethdorf, S. and K. Pantel, *Disseminated tumor cells in bone marrow and circulating tumor cells in blood of breast cancer patients: current state of detection and characterization.* Pathobiology, 2008. **75**(2): p. 140-8.

16. Alix-Panabieres, C., V. Muller, and K. Pantel, *Current status in human breast cancer micrometastasis.* Curr Opin Oncol, 2007. **19**(6): p. 558-63.

17. Lacroix, M., *Significance, detection and markers of disseminated breast cancer cells.* Endocr Relat Cancer, 2006. **13**(4): p. 1033-67.

18. Allard, W.J., et al., *Tumor cells circulate in the peripheral blood of all major carcinomas but not in healthy subjects or patients with nonmalignant diseases.* Clin Cancer Res, 2004. **10**(20): p. 6897-904.

19. Chiang, A.C. and J. Massague, *Molecular basis of metastasis.* N Engl J Med, 2008. **359**(26): p. 2814-23.

20. Cristofanilli, M., et al., *Circulating tumor cells, disease progression, and survival in metastatic breast cancer.* N Engl J Med, 2004. **351**(8): p. 781-91.

21. Paget, S., *The distribution of secondary growths in cancer of the breast. 1889.* Cancer Metastasis Rev, 1989. **8**(2): p. 98-101.

22. Danila, D.C., et al., *Circulating tumors cells as biomarkers: progress toward biomarker qualification.* Cancer J, 2011. **17**(6): p. 438-50.

23. Riethdorf, S., et al., *Detection of circulating tumor cells in peripheral blood of patients with metastatic breast cancer: a validation study of the CellSearch system.* Clin Cancer Res, 2007. **13**(3): p. 920-8.

24. Riethdorf, S., et al., *Detection and HER2 expression of circulating tumor cells: prospective monitoring in breast cancer patients treated in the neoadjuvant GeparQuattro trial.* Clin Cancer Res, 2010. **16**(9): p. 2634-45.

25. van de Stolpe, A., et al., *Circulating tumor cell isolation and diagnostics: toward routine clinical use.* Cancer Res, 2011. **71**(18): p. 5955-60.

26. Momburg, F., et al., *Immunohistochemical study of the expression of a Mr 34,000 human epithelium-specific surface glycoprotein in normal and malignant tissues.* Cancer Res, 1987. **47**(11): p. 2883-91.

27. Balasubramanian, S., et al., *Micromachine-enabled capture and isolation of cancer cells in complex media.* Angew Chem Int Ed Engl, 2011. **50**(18): p. 4161-4.

28. Xu, H., et al., *Antibody conjugated magnetic iron oxide nanoparticles for cancer cell separation in fresh whole blood.* Biomaterials, 2011. **32**(36): p. 9758-65.

29. Mi, Y., et al., *Herceptin functionalized polyhedral oligomeric silsesquioxane - conjugated oligomers - silica/iron oxide nanoparticles for tumor cell sorting and detection.* Biomaterials, 2011. **32**(32): p. 8226-33.

30. Pantel, K. and M. Otte, *Occult micrometastasis: enrichment, identification and characterization of single disseminated tumour cells.* Semin Cancer Biol, 2001. **11**(5): p. 327-37.

31. Zieglschmid, V., C. Hollmann, and O. Bocher, *Detection of disseminated tumor cells in peripheral blood.* Crit Rev Clin Lab Sci, 2005. **42**(2): p. 155-96.

32. Tedder, T.F., et al., *The selectins: vascular adhesion molecules.* Faseb J, 1995. **9**(10): p. 866-73.

33. Mackay, C.R., *Moving targets: cell migration inhibitors as new anti-inflammatory therapies.* Nat Immunol, 2008. **9**(9): p. 988-98.

34. Dimitroff, C.J., et al., *Rolling of human bone-metastatic prostate tumor cells on human bone marrow endothelium under shear flow is mediated by E-selectin.* Cancer Res, 2004. **64**(15): p. 5261-9.

35. Giavazzi, R., et al., *Rolling and adhesion of human tumor cells on vascular endothelium under physiological flow conditions.* J Clin Invest, 1993. **92**(6): p. 3038-44.

36. Yuan, K., et al., *Alterations in human breast cancer adhesion-motility in response to changes in cell surface glycoproteins displaying alpha-L-fucose moieties.* Int J Oncol, 2008. **32**(4): p. 797-807.

37. Tremblay, P.L., J. Huot, and F.A. Auger, *Mechanisms by which E-selectin regulates diapedesis of colon cancer cells under flow conditions.* Cancer Res, 2008. **68**(13): p. 5167-76.

38. Greenberg, A.W. and D.A. Hammer, *Cell separation mediated by differential rolling adhesion.* Biotechnol Bioeng, 2001. **73**(2): p. 111-24.

39. Zheng, S., et al., *3D microfilter device for viable circulating tumor cell (CTC) enrichment from blood.* Biomed Microdevices, 2011. **13**(1): p. 203-13.

40. Galanzha, E.I., et al., *In vivo magnetic enrichment and multiplex photoacoustic detection of circulating tumour cells.* Nat Nanotechnol, 2009. **4**(12): p. 855-60.

41. Myung, J.H., et al., *Dendrimer-mediated multivalent binding for the enhanced capture of tumor cells.* Angew Chem Int Ed Engl, 2011. **50**(49): p. 11769-72.

42. Kuo, J.S., et al., *Deformability considerations in filtration of biological cells.* Lab Chip, 2010. **10**(7): p. 837-42.

43. Weiss, L. and D.S. Dimitrov, *A fluid mechanical analysis of the velocity, adhesion, and destruction of cancer cells in capillaries during metastasis.* Cell Biophys, 1984. **6**(1): p. 9-22.

44. Pinzani, P., et al., *Isolation by size of epithelial tumor cells in peripheral blood of patients with breast cancer: correlation with real-time reverse transcriptase-polymerase chain reaction results and feasibility of molecular analysis by laser microdissection.* Hum Pathol, 2006. **37**(6): p. 711-8.

45. Lin, H.K., et al., *Portable filter-based microdevice for detection and characterization of circulating tumor cells.* Clin Cancer Res, 2010. **16**(20): p. 5011-8.

46. Zheng, S., et al., *Membrane microfilter device for selective capture, electrolysis and genomic analysis of human circulating tumor cells.* J Chromatogr A, 2007. **1162**(2): p. 154-61.

47. Tan, S.J., et al., *Microdevice for the isolation and enumeration of cancer cells from blood.* Biomed Microdevices, 2009. **11**(4): p. 883-92.

48. Galanzha, E.I., J.W. Kim, and V.P. Zharov, *Nanotechnology-based molecular photoacoustic and photothermal flow cytometry platform for in-vivo detection and killing of circulating cancer stem cells.* J Biophotonics, 2009. **2**(12): p. 725-35.

49. Thiery, J.P., *Epithelial-mesenchymal transitions in development and pathologies.* Curr Opin Cell Biol, 2003. **15**(6): p. 740-746.

50. He, W., et al., *In vivo quantitation of rare circulating tumor cells by multiphoton intravital flow cytometry.* Proc Natl Acad Sci U S A, 2007. **104**(28): p. 11760-5.

51. Shah, A.M., et al., *Biopolymer System for Cell Recovery from Microfluidic Cell Capture Devices.* Anal Chem, 2012.

52. Stott, S.L., et al., *Isolation of circulating tumor cells using a microvortex-generating herringbone-chip.* Proc Natl Acad Sci U S A, 2010. **107**(43): p. 18392-7.

53. Chang, S.F., et al., *Tumor cell cycle arrest induced by shear stress: Roles of integrins and Smad.* Proc Natl Acad Sci U S A, 2008. **105**(10): p. 3927-32.

54. Attard, G., et al., *Reporting the capture efficiency of a filter-based microdevice: a CTC is not a CTC unless it is CD45 negative--letter.* Clin Cancer Res, 2011. **17**(9): p. 3048-9; author reply 3050.

55. He, W., et al., *Quantitation of circulating tumor cells in blood samples from ovarian and prostate cancer patients using tumor-specific fluorescent ligands.* Int J Cancer, 2008. **123**(8): p. 1968-73.

56. Sun, C., R. Sze, and M. Zhang, *Folic acid-PEG conjugated superparamagnetic nanoparticles for targeted cellular uptake and detection by MRI.* J Biomed Mater Res A, 2006. **78**(3): p. 550-7.

57. Owens, D.E., 3rd and N.A. Peppas, *Opsonization, biodistribution, and pharmacokinetics of polymeric nanoparticles.* Int J Pharm, 2006. **307**(1): p. 93-102.

58. Zhang, Y., N. Kohler, and M. Zhang, *Surface modification of superparamagnetic magnetite nanoparticles and their intracellular uptake.* Biomaterials, 2002. **23**(7): p. 1553-61.

59. Danila, D.C., et al., *Circulating tumor cell number and prognosis in progressive castration-resistant prostate cancer.* Clin Cancer Res, 2007. **13**(23): p. 7053-8.

60. Nagrath, S., et al., *Isolation of rare circulating tumour cells in cancer patients by microchip technology.* Nature, 2007. **450**(7173): p. 1235-9.

61. Hoshino, K., et al., *Microchip-based immunomagnetic detection of circulating tumor cells.* Lab Chip, 2011. **11**(20): p. 3449-57.

62. Koyfman, A.Y., G.B. Braun, and N.O. Reich, *Cell-targeted self-assembled DNA nanostructures.* J Am Chem Soc, 2009. **131**(40): p. 14237-9.

63. Zhao, J., et al., *Highly sensitive identification of cancer cells by combining the new tetrathiafulvalene derivative with a beta-cyclodextrin/multi-walled carbon nanotubes modified GCE.* Analyst, 2010. **135**(11): p. 2965-9.

64. Maheswaran, S., et al., *Detection of mutations in EGFR in circulating lung-cancer cells.* N Engl J Med, 2008. **359**(4): p. 366-77.

65. Mittal, S., et al., *Antibody-functionalized fluid-permeable surfaces for rolling cell capture at high flow rates.* Biophys J, 2012. **102**(4): p. 721-30.

66. Mammen, M., S.K. Choi, and G.M. Whitesides, *Polyvalent interactions in biological systems: Implications for design and use of multivalent ligands and inhibitors.* Angew Chem Int Ed Engl, 1998. **37**(20): p. 2755-2794.

67. Lee, R.T. and Y.C. Lee, *Affinity enhancement by multivalent lectin-carbohydrate interaction.* Glycoconj J, 2000. **17**(7-9): p. 543-51.

68. Mourez, M., et al., *Designing a polyvalent inhibitor of anthrax toxin.* Nat Biotechnol, 2001. **19**(10): p. 958-61.

69. Hong, S., et al., *The binding avidity of a nanoparticle-based multivalent targeted drug delivery platform.* Chem Biol, 2007. **14**(1): p. 107-15.

70. Kiessling, L.L. and N.L. Pohl, *Strength in numbers: non-natural polyvalent carbohydrate derivatives.* Chem Biol, 1996. **3**(2): p. 71-7.

71. Quintana, A., et al., *Design and function of a dendrimer-based therapeutic nanodevice targeted to tumor cells through the folate receptor.* Pharm Res, 2002. **19**(9): p. 1310-6.

72. Peer, D., et al., *Nanocarriers as an emerging platform for cancer therapy.* Nat Nanotechnol, 2007. **2**(12): p. 751-60.

73. Weissleder, R., et al., *Cell-specific targeting of nanoparticles by multivalent attachment of small molecules.* Nat Biotechnol, 2005. **23**(11): p. 1418-23.

74. Christensen, T., et al., *Additivity and the physical basis of multivalency effects: a thermodynamic investigation of the calcium EDTA interaction.* J Am Chem Soc, 2003. **125**(24): p. 7357-66.

75. Gestwicki, J.E., et al., *Selective immobilization of multivalent ligands for surface plasmon resonance and fluorescence microscopy.* Anal Biochem, 2002. **305**(2): p. 149-55.

76. Kitov, P.I. and D.R. Bundle, *On the nature of the multivalency effect: a thermodynamic model.* J Am Chem Soc, 2003. **125**(52): p. 16271-84.

77. Lindhorst, T., *Artificial Multivalent Sugar Ligands to Understand and Manipulate Carbohydrate-Protein Interactions*, in *Host-Guest Chemistry*, S. Penadés, Editor 2002, Springer Berlin / Heidelberg. p. 201-235.

78. Reuter, J.D., et al., *Inhibition of viral adhesion and infection by sialic-acid-conjugated dendritic polymers.* Bioconjug Chem, 1999. **10**(2): p. 271-8.

79. Ajikumar, P.K., et al., *Carboxyl-terminated dendrimer-coated bioactive interface for protein microarray: high-sensitivity detection of antigen in complex biological samples.* Langmuir, 2007. **23**(10): p. 5670-7.

CHAPTER 2

ENHANCED TUMOR CELL ISOLATION BY A BIOMIMETIC COMBINATION OF TWO PROTEINS: IMPLICATION FOR EFFECTIVE SEPARATION OF CTCs

2.1. INTRODUCTION

Although recent advances in diagnostic and therapeutic methods to treat primary tumors hold promise to decrease mortality of cancer, metastasis of cancer still poses a great challenge as patients often relapse [1-4]. Disseminated and circulating tumor cells (DTCs and CTCs, respectively) are known to induce secondary tumor formation at distant sites from primary tumors, known as metastasis [5-7]. The process of metastasis is not fully understood but one of the most plausible mechanisms involves a similar process of leukocyte homing, i.e. a naturally occurring cell rolling process [8]. Rolling cells then firmly attach to the endothelial layers, followed by transmigration through the endothelium (diapedesis) to form secondary tumors [9]. Thus, research efforts on diagnosis and prognosis of metastatic cancer have been concentrated on detection of DTCs in bone marrow (BM) and CTCs in blood [10]. Detection of DTCs for prognosis studies along with therapeutic treatments requires repeated samplings of BM that is invasive, time-consuming, and often painful for the patients [11, 12]. Consequently, effective detection of CTCs in peripheral blood of cancer patients holds a promise as an alternative due to its minimally invasive and easy sampling procedures (i.e. blood drawing). However the clinical usage of CTCs has not yet been implemented for routine clinical practice because CTCs are extremely rare and estimated to be in the range of one tumor cell in the background of 10^6-10^9 normal blood cells [13, 14].

To date, most methods for CTC detection are based on immunofluorescence labeling using CTC markers such as epithelial-cell-adhesion-molecule (EpCAM) [10, 15]. Recent progress in this field includes the development of an automated enrichment and immunocytochemical detection system for CTCs (CellSearch™, Veridex, LLC) that has been approved by the Food and Drug Administration (FDA) for clinical use in metastatic breast cancer patients [16, 17]. Although reliable and stable, the CellSearch™ system has limitations such as complicated sample processing with additional steps needed for plasma removal and magnetic antibody labeling and limited sensitivity with a median 1.2 cells/mL detected from patients with metastatic cancer. Another promising technology for CTC detection and isolation has been recently published by Nagrath et al. using a microfluidic device containing 78,000 anti-EpCAM coated microposts which has increased its sensitivity and specificity for CTC capturing [18]. The CTC-chip does not require multiple processing steps in sample preparation and has shown enhanced sensitivity as compared to the CellSearch™ with a median of 67 cells/mL detected from whole blood samples of patients under comparable conditions [19]. The combined effect of anti-EpCAM-based specificity and the micropost-enhanced hydrodynamic efficiency enabled a capturing of over 60%. However, the enhanced hydrodynamic efficiency relying on the microposts limits the utility of the device at higher flow rates where a significant decrease in the capture efficiency has been observed.

The formation of transient ligand-receptor interactions occurs commonly between cells flowing in the blood and the vascular endothelium; this physiological process is known as cell rolling [20]. Cell rolling plays a key role in biologically important processes such as recruitment of leukocytes to sites of inflammation, homing of hematopoietic progenitor cells, and CTC-induced metastasis. This behavior is typically mediated by dynamic interactions between selectins (E- and P-selectins) on the vascular endothelial cell surface and membrane ligands on the carcinoma cell surface. Endothelial (E)-selectin (CD62E) is particularly noteworthy in

disease by virtue of its expression on activated endothelium and on bone-skin microvascular linings, and many studies point to the key role played by E-selectin in being involved in the adhesion and homing of various types of cancer cells such as prostate [21], breast [22, 23], and colon carcinoma cells [24]. Thus, tumor cell separation based on the selectin-mediated cell rolling behavior is being pursued as it mimics a physiological process, and eliminates labeling and label removal steps that are necessary for other immune-labeling detection methods [25]. Recently, a tube-type flow chamber that is co-immobilized with E-selectin and TRAIL achieved concurrent dual functions of inducing rolling and apoptosis of various cell lines [26]. However, given that a large class of cells, including leukocytes, platelets, neutrophils, mesenchymal and hematopoietic stem cells, and metastatic cancer cells all exhibit rolling on selectins, detection that is solely based on cell rolling has limitations for achieving sufficient specificity, which has hindered translation of the technology to a clinically significant device.

The specific capturing and potential enrichment of CTCs using anti-EpCAM and selectin, respectively, inspired a biofunctionalized surface that mimics biological complexity may detect and isolate target cells at a greater sensitivity and specificity. This concept is supported by the initial physiological interactions between CTCs and endothelium in the bloodstream, which include concurrent rolling and stationary binding steps. Towards this aim, we investigated the following: i) two proteins with distinct biofunctions (selectin to induce rolling and anti-EpCAM to statically capture target cells) can be co-immobilized; ii) a combined rolling and stationary binding can be induced by the mixture of the proteins; and iii) the biomimetic combination enhances overall capture efficiency of the surface. In this paper, these are tested using biofunctional surfaces with immobilized selectins and anti-EpCAM. The surfaces are characterized by X-ray photoelectron scattering (XPS) and fluorescence microscopy using fluorophore-conjugated antibodies. As a proof-of-concept study for the hypothesis of enhanced separation capacity and capture efficiency using protein mixtures, the surfaces are tested using *in*

vitro cell lines (MCF-7 cells as a CTC model and HL-60 cells as a leukocyte model) under flow conditions. The effects of the combination of rolling (E-selectin) and stationary binding (anti-EpCAM) on capture efficiency are compared to a surface functionalized solely with anti-EpCAM or selectins. Here we report, for the first time to our knowledge, that combination of dynamic rolling and stationary binding significantly enhances capture efficiency of target cells, which holds great promise to develop a simple, effective device for CTC detection.

2.2. MATERIALS AND METHODS

2.2.1. Materials

Recombinant human P-selectin/Fc chimera (P-selectin), E-selectin/Fc chimera (E-selectin), anti-human EpCAM/TROP1 antibody (anti-EpCAM), fluorescein-conjugated mouse monoclonal anti-human E-selectin (fluorescein-anti-E-selectin), and allophycocyanin (APC)-conjugated mouse monoclonal anti-human EpCAM/TROP1 (APC-anti-EpCAM) were all purchased from R&D systems (Minneapolis, MN). Unconjugated goat anti-Human IgG (H + L) was acquired from Pierce biotechnology, Inc (Rockford, IL). The epoxy-functionalized glass surfaces (SuperEpoxy2®) were purchased by TeleChem International, Inc (Sunnyvale, CA). All other chemicals were obtained from Sigma-Aldrich (St. Louis, MO) and used without further purification.

2.2.2. Surface functionalization by immobilization of adhesive proteins

All individual proteins and/or mixture of P-selectin, E-selectin, and anti-EpCAM were immobilized on epoxy functionalized glass surfaces. A general scheme of the surface functionalization via protein immobilization is outlined in **Fig. 2.1**. The coating areas were defined by a polydimethylsiloxane (PDMS) gasket to confine protein solutions in a desired area,

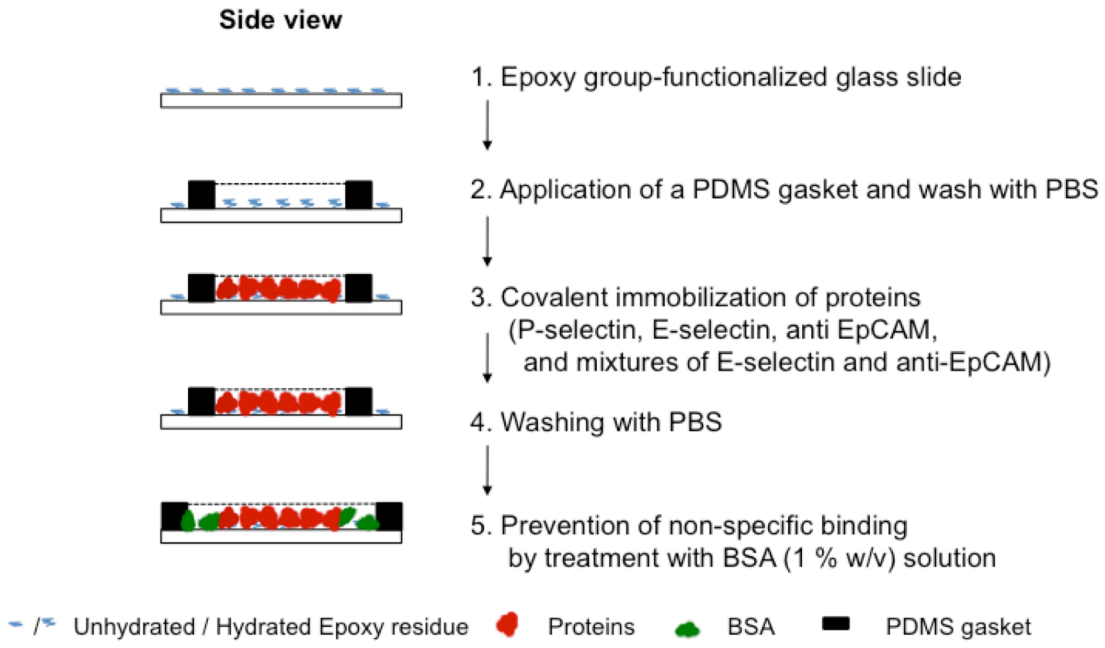

Figure 2.1. Surface functionalization by immobilization of proteins.

resulting in a clear interface between protein-coated and uncoated regions. For the surfaces functionalized with a single protein, 300 µL of each protein (P-selectin, E-selectin, or anti-EpCAM) at a concentration of 5 µg/mL in PBS buffer (Cellgro®, without Ca^{2+}, Mg^{2+}) was added on an approximately 2 cm^2 area of a slide defined by a PDMS gasket, followed by incubation at RT for 4 hrs with constant gentle shaking on a plate shaker. The PDMS gasket was then removed, and the whole slide surface was washed with PBS three times. Potential non-specific binding of both protein-coated and uncoated regions was blocked by the final incubation with 1% (w/v) bovine serum albumin (BSA) in PBS buffer (BSA solution). The subsequent experiments using the surfaces were immediately performed, or stored in PBS buffer at 4 °C. Additionally, mixtures of E-selectin and anti-EpCAM were immobilized at various ratios under the same condition described above. A fixed concentration of anti-EpCAM at 10 µg/mL was used with various amounts of E-selectin. The final total weights (in µg) of anti-EpCAM and E-selectin were 1.5:0, 1.5:0.3, 1.5:1.5, and 1.5:7.5.

2.2.3. Characterization of the functionalized surfaces by fluorescence microscopy

The co-immobilization process of anti-EpCAM and E-selectin was characterized using APC-anti-EpCAM and fluorescein-anti-E-selectin, respectively. The surfaces functionalized with P-selectin was explicitly characterized previously [27]. As neither fluorophore-tagged EpCAM nor fluorescent secondary antibody specific to anti-EpCAM is commercially available, APC-anti-EpCAM was co-immobilized with E-selectin, and red fluorescence was observed from the surface. For detection of E-selectin, anti-EpCAM/E-selectin-immobilized slides were incubated with fluorescein-conjugated anti-E-selectin (25 μg/mL) at 4 ºC for 1 hr, followed by a washing step (three times using PBS buffer). All slides were then mounted using Vectashield® mounting medium (Vector laboratories, Inc., Burlingame, CA), and air bubbles in the mounting medium were gently removed by applying pressure to the cover slides. The fluorescence images were taken using an Olympus IX70 inverted microscope equipped with a fluorescence illuminator (IX 70-S1F2, Olympus America, Inc., Center Valley, PA) using a 10× objective, a CCD camera (QImaging Retiga 1300B, Olympus America, Inc.) and filters for FITC (450 nm excitation and 535 nm emission) and APC (560 nm excitation and 645 nm emission). For each image (triplicate for each sample), 5 regions of equal size were randomly selected, and the total pixel intensity values within these regions were acquired using ImageJ (NIH). The slide treated with the BSA solution was used as background and its intensity value was subtracted from all sample slides. The intensities obtained from the protein mixture-immobilized slides were normalized based on those functionalized with a single protein (anti-EpCAM or E-selectin) to compare the relative amounts.

2.2.4. Characterization of the surfaces by X-ray photoelectron spectroscopy (XPS)

Protein-immobilized surfaces were characterized by XPS [27]. XPS measurements were performed using an Axis 165 X-ray photoelectron spectrometer (Kratos Analytical, Manchester, U.K.) equipped with a monochromatic AlKα source (hv = 1486.6 eV, 150W) and a hemispherical analyzer. The % mass concentrations were obtained from high-resolution spectra of the C 1s, O 1s, N 1s, and S 2p regions at an X-ray irradiating angle of 30° with pass energy of 80 eV and a step size of 0.5 eV, carried on 5 scans per each spectrum.

2.2.5. Cell lines

HL-60 and MCF-7 cells were purchased from ATCC (Manassas, VA). *Discosoma sp.* Red fluorescent protein (DsRED)-transfected MCF-7 (DsRED-MCF-7) cells that were transfected using an HIV-1-based lentiviral vector [28] were a generous gift of Prof. William Beck at UIC.

HL-60 cells were cultured in IMDM media supplemented with 20% (v/v) fetal bovine serum (FBS) and 1% (v/v) penicillin/streptomycin in a humidified incubator at 37 °C and 5% CO_2. MCF-7 cells and DsRED-MCF-7 cells were cultured in DMEM media that were supplemented with 10% (v/v) FBS and 1% (v/v) penicillin/streptomycin under the same condition of incubation for HL-60 cells. Prior to cell culture, to enrich the transfected (fluorescent) cell population, DsRED-MCF-7 cells were isolated from non-transfected MCF-7 cells via dilution of cell suspension (10^3 cells in 10 mL of media in a petri dish) and selection of the transfected MCF-7 cells using a fluorescence microscope (Olympus IX70). HL-60, MCF-7, and DsRED-MCF-7 cells were prepared by resuspension in their own supplemented media with anti-IgG and kept on ice during the subsequent cell rolling experiments [29].

2.2.6. Flow chamber experiments

A typical flow chamber experiment was performed as following. A glass slide functionalized by protein immobilization, a gasket (30 mm (L) × 10mm (W) × 0.25 mm (D), Glycotech, Gaithersburg, MD), and a rectangular parallel plate flow chamber (Glycotech) were assembled in line under vacuum. To observe cellular interactions with the biofunctionalized surfaces, individual cell lines (HL-60 or MCF-7) as well as mixtures of the two cell lines (HL-60 and DsRED-MCF-7) at a concentration between 10^5 and10^7 cells/mL were injected into the flow chamber at various flow rates (0.08-1.28 dyn/cm^2) using a syringe pump (New Era pump Systems Inc., Farmingdale, NY). Note that, in this flow chamber, 200 μL/min of flow rate is correspondent to 0.32 dyn/cm^2 of a wall shear stress, 32 s^{-1} of a wall shear rate, and 80 μm/sec of near-wall non-adherent cell velocity according to the Goldman equation [30].

2.2.7. Observation of cellular responses on various functional surfaces

Throughout this study, the cellular behaviors on the various surfaces in the flow chamber were all monitored using the Olympus IX70 microscope and images were recorded using a CCD camera. Rolling velocities of cells on the immobilized proteins were calculated based on the images taken every second for 1 min, using ImageJ. Cell rolling was defined when the rolling velocities were less than 50% of the free stream velocity (e.g. slower than 40 μm/sec at a flow rate of 200 μL/min). Rolling dynamic data was presented as mean ± standard error of the mean (SEM) values of repetitive observations. To confirm the statistical significance between data points, the rolling velocities of more than 40 cells per image were tracked in independent at least 5 replicates.

To evaluate separation of the two cell populations in the mixtures, fluorescent DsRED-MCF-7 cells were used as a CTC model so that they could be easily distinguished from the non-fluorescent leukocyte model (HL-60 cells) in a 50:50 mixture. The surface interactions of the cell mixture on each type of proteins, as well as the cell separation at the interface between E-selectin

(left) and anti-EpCAM (right)-coated regions were visualized using the fluorescent and bright fields for 1 min. The merged images of the fluorescent and bright fields were taken in the absence of the flow.

The DsRED-MCF-7 capture efficiency of the surfaces functionalized with E-selectin/anti-EpCAM combinations was measured as follows. The slides functionalized with the different ratios of E-selectin/anti-EpCAM combinations were prepared, and DsRED-MCF-7 cells (suspended in PBS at 2,500 cells/mL with anti-IgG) were injected into a flow chamber, followed by repetitive syringe pushing in and withdrawing at 100 μL/min (0.16 dyn/cm^2). The numbers of captured cells on a pre-defined area of protein-immobilized surface were counted using a microscope at each cycle. A cycle consisting of forward flow (pushing) for 2.5 min, and backward flow (withdrawing) for 2.5 min, and PBS washing for 1 min. As the known number of DsRED-MCF-7 cells was perfused into the flow chamber, the number of captured cells could be translated into the capture efficiency (%). The measured capture efficiencies of the protein mixture-immobilized slides were statistically analyzed by comparing to those of the anti-EpCAM-immobilized slides using one-factor ANOVA (SPSS software, Chicago, IL). In addition, as pair-wise comparisons among levels of weight for post-hoc analyses, Fisher's least significant difference (LSD) tests with 95% simultaneous confidence intervals were considered statistically significant (***** as shown in **Fig. 2.6**).

2.3. RESULTS

2.3.1. Confirmation of immobilization of E-selectin, anti-EpCAM, and combinations of the proteins on glass substrates

Surface functionalization by protein immobilization was confirmed by fluorescence microscopy and XPS, as summarized in **Fig. 2.2**, **Tables 2.1** and **2.2**, respectively. The

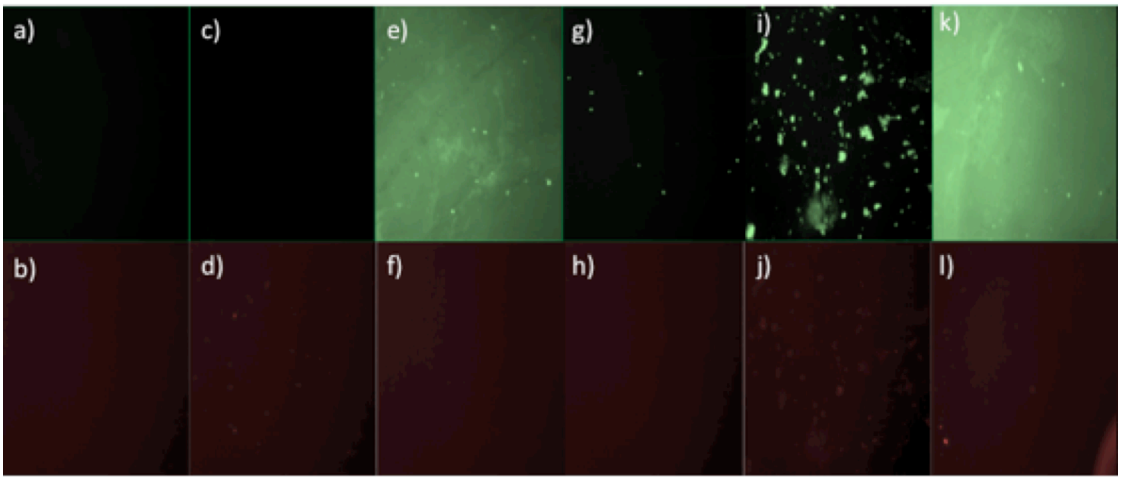

Figure 2.2. Immunostaining images of the surface of BSA (a) and b)), anti-EpCAM (c) and d)) or E-selectin (e) and f))-immobilized and the combinations (g) - l)) of anti-EpCAM and E-selectin -immobilized slides. The images of the upper low (a), c), e), g), i) and k))and those of the bottom low (b), d), f), h), j) and l))were representative to E-selectin and anti-EpCAM on the surfaces, respectively.

commercially available epoxy-terminated slides with highly reactive coupling efficiency (via amine/hydroxyl/thiol-based chemistries) and low fluorescence background allowed quantitative and reliable surface analyses using the two techniques. The presence of E-selectin on the surface was observed by immunostaining using fluorescein-anti-E-selectin (green fluorescence). APC-anti-EpCAM (red fluorescence) was used instead of non-fluorescent anti-EpCAM to image the surface immobilized anti-EpCAM by fluorescence microscopy. **Table 2.1** summarizes the measured fluorescence intensities of the various bioadhesive surfaces. For the surfaces functionalized with E-selectin/anti-EpCAM mixtures, the measured fluorescence intensities of each fluorophore well dictate the compositions of each protein. With an increase of the amount of E-selectin immobilized, the green fluorescence intensity was obviously increased, but minimal changes in the red fluorescence intensity were also observed.

The immobilization of anti-EpCAM and/or E-selectin was quantitatively confirmed by an increase in carbon and nitrogen compositions and decreased silicon detection in the underlying glass substrate, as measured by XPS analysis (**Table 2.2**). Furthermore, as the amount of

Table 2.1. Immunostaining results of surfaces immobilized with E-selectin, anti-EpCAM, and mixtures of the two proteins.

	Anti-EpCAM 1.5 μg	E-selectin 1.5 μg	Anti-EpCAM 1.5 μg: E-selectin **0.3** μg	Anti-EpCAM 1.5 μg: E-selectin **1.5** μg	Anti-EpCAM 1.5 μg: E-selectin **7.5** μg
FITC-anti-E-selectin (for E-selectin detection)	-	1	0.04 ± 0.01	0.66 ± 0.06	1.31 ± 0.02
APC-anti-EpCAM (for anti-EpCAM detection)	1	-	0.88 ± 0.31	0.96 ± 0.70	0.61 ± 0.31

Note that all the fluorescence intensities were normalized based on the intensities measured on the surfaces with individual proteins

Table 2. 2. Atomic compositions of functionalized slides with various proteins, as measured by XPS.

	Control (mass conc. %)	E-Selectin (mass conc. %)	Anti-EpCAM (mass conc. %)	Anti-EpCAM 1.5 μg: E-selectin **0.3** μg (mass conc. %)	Anti-EpCAM 1.5 μg: E-selectin **1.5** μg (mass conc. %)	Anti-EpCAM 1.5 μg: E-selectin **7.5** μg (mass conc. %)
C 1s	11.3	21.6	26.2	32.5	40.2	36.9
N 1s	0.0	5.4	2.6	3.5	4.6	6.5
O 1s	59.7	51.9	39.2	43.3	35.5	40.7
Si 2p	29.0	21.1	32.0	20.7	19.7	15.9
N/C ratio	0.0	0.3	0.1	0.1	0.1	0.2
C/O ratio	0.2	0.4	0.7	0.8	1.1	0.9

immobilized E-selectin in the mixture of anti-EpCAM and E-selectin was increased, the amounts of carbon and nitrogen on the surface were increased with a decreased silicon composition. All surfaces immobilized with proteins had a high degree of coverage, as evidenced by the lack of visible underlying silicon. The measured nitrogen content likely corresponds to the degree of

protein coverage on the glass surface, which is supported by the increased nitrogen composition when the total amount of proteins immobilized was increased.

2.3.2. Interactions of cells on the protein-immobilized surfaces

Cell interactions with the protein-immobilized surfaces under flow were assessed using a commercially available rectangular parallel-plate flow chamber. A breast cancer cell line, MCF-7 was employed as a CTC model. The rolling behavior of the MCF-7 cells was compared with that of HL-60 cells, a human myeloid leukocytic cell line, which expresses a high level of sialyl Lewis^x and exhibits rolling on selectins mediated primarily by P-selectin glycoprotein-1 (PSGL-1) [31, 32].

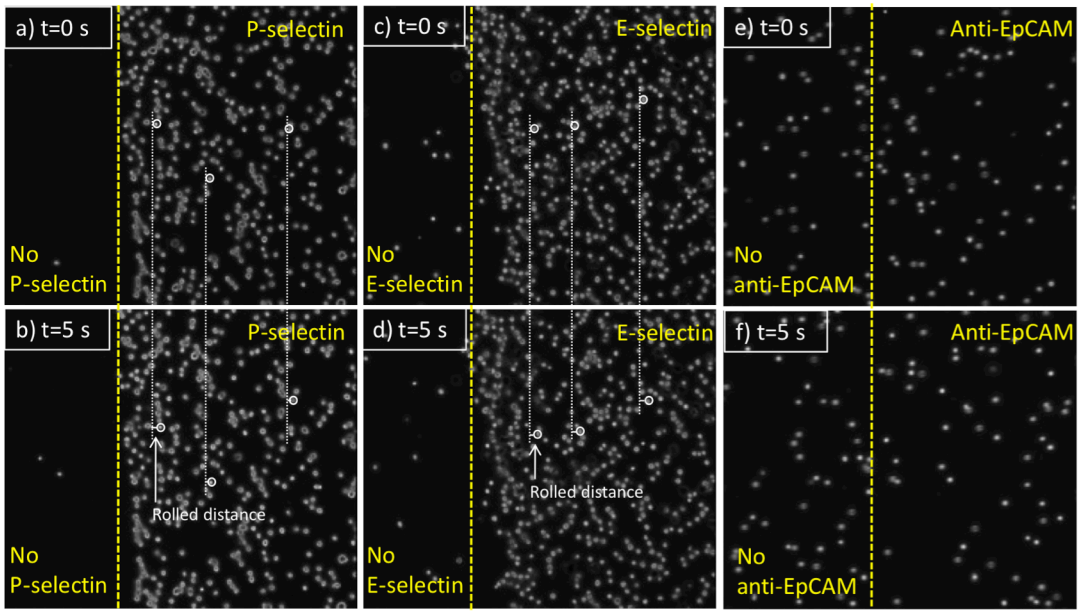

Figure 2.3. Time-course images of HL-60 cells under shear stress of 0.32 dyn/cm^2 on P-selectin (a) and b)), E-selectin (c) and d), and anti-EpCAM (e) and f))-immobilized surfaces. The rolling velocities (mean ± SEM, n=200) of the cells on P-selectin and E-selectin were 2.26 ± 0.28 and 2.12 ± 0.15 μm/sec, respectively, whereas there was no interaction observed between the cells and anti-EpCAM-coated surface. Flow directions of three sets were from left through right.

Each sets (a and b, c and d, and e and f) of **Fig. 2.3** show HL-60 cells on P-selectin, E-selectin, and anti-EpCAM coated surfaces at t = 0 s (a randomly-picked starting recording time during the flow experiment) and 5 s (5 sec after the starting time), respectively. Note that the HL-60 cells on anti-EpCAM-coated slide observed in the images at 0 s were non-adherent cells that were vertically close to the surface. As previously reported, HL-60 cells exhibited stable rolling on both P- and E- selectin-immobilized slides at velocities of 2.26 ± 0.28 and 2.12 ± 0.15 μm/sec, respectively, under 0.32 dyn/cm^2 of shear stress. HL-60 cells showed no interactions with the immobilized anti-EpCAM, traveling the flow path in the chamber at the speed of free stream velocity. In contrast, as shown in **Fig. 2.4**, MCF-7 cells did not interact with immobilized P-selectin, but exhibited the rolling response on the E-selectin coated surfaces. The rolling velocities of MCF-7 on E-selectin-immobilized slides (4.24 ± 0.31 μm/sec) were faster than

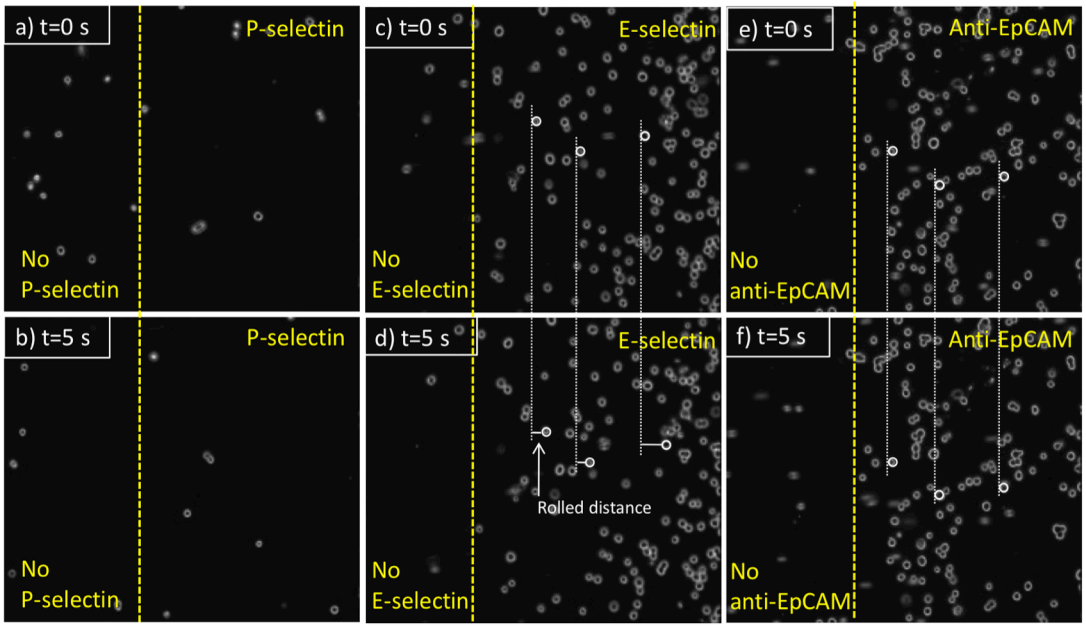

Figure 2.4. Time-course images of MCF-7 cells under shear stress of 0.32 dyn/cm^2 on P-selectin (a) and b)), E-selectin (c) and d)), and anti-EpCAM (c) and d))-immobilized surfaces. MCF-7 cells exhibited the rolling behavior on the E-selectin-coated surface (4.24 ± 0.31 μm/sec) or captured on the anti-EpCAM-coated surface. However, there was no interaction observed between the cells and the P-selectin-coated surface. Flow directions of three sets were from left through right. All of the rolling dynamic data is represented as mean ± SEM values (n=200).

those of HL-60 (2.12 ± 0.15 μm/sec). It should be noted that the rolling velocities of MCF-7 cells varied between experiments with relatively high standard errors, whereas the velocities of HL-60 cells on E-selectin-immobilized slides were relatively consistent between experiments. Unlike HL-60 cells, however, MCF-7 cells exhibited a strong interaction with immobilized anti-EpCAM slides, rolling very slowly (0.09 ± 0.03 μm/sec), so that they appeared to be stationary captured on the surface. Additionally, the rolling velocities of HL-60 and MCF-7 cells on E-selectin were measured at 4 different shear stresses (0.08-1.28 dyn/cm^2) as shown in **Fig. 2.5**. The rolling velocity of MCF-7 cells was significantly increased with an increase of the shear stress (~3.2-8.0 μm/sec) whereas the rolling response of HL-60 cells was less dependent upon the flow rate change (~1.5-2.3 μm/sec).

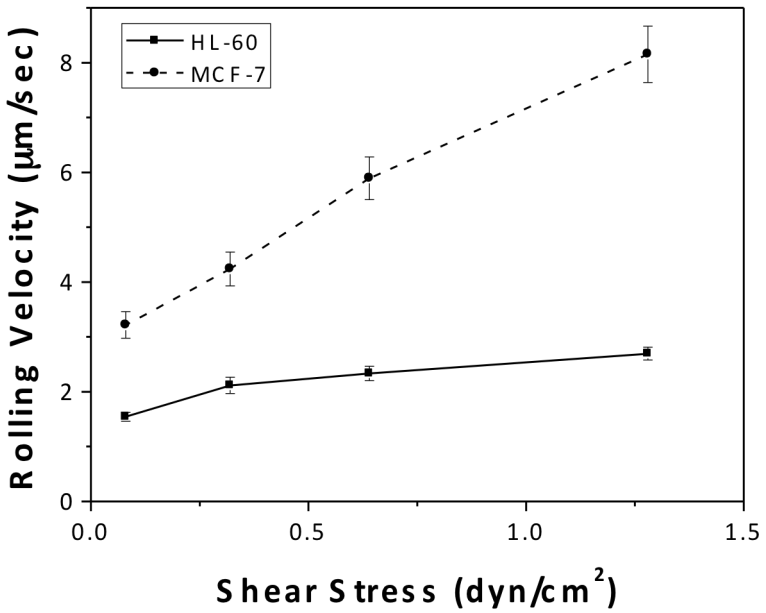

Figure 2.5. Cell rolling velocities of HL-60 and MCF-7 cells on E-selectin-immobilized slides at various shear stresses (0.08 dyn/cm^2, 0.32 dyn/cm^2, 0.64 dyn/cm^2, and 1.28 dyn/cm^2). Note that the rolling response of HL-60 cells is minimally affected by an increase in shear stress, whereas MCF-7 cells show rolling highly dependent upon shear stress. All of the rolling dynamic data is represented as mean ± SEM values.

2.3.3. Enhanced separation of tumor cells from two cell populations using combinations of anti-EpCAM and E-selectin

Interactions of mixtures of the two cell lines with various surfaces functionalized by P-selectin, E-selectin, anti-EpCAM, and combinations of E-selectin/anti-EpCAM were observed under flow conditions, as shown in **Fig. 2.6**. Note that DsRED-MCF-7 cells were used for easy recognition, as appeared to be red in the all images taken by a fluorescence microscope. As shown in **Fig. 2.6a**, P-selectin induced rolling of HL-60 but did not interact with DsRED-MCF-7 cells, which is consistent with the results using non-transfected MCF-7 cells as shown in **Fig. 2.4**. E-selectin, on the other hand, caused both cells to roll as presented in **Fig. 2.6b**. The surface with anti-EpCAM alone induced stationary adhesion of DsRED-MCF-7 cells exclusively. Although HL-60 cells had no interaction with anti-EpCAM, some of them were still located on the images

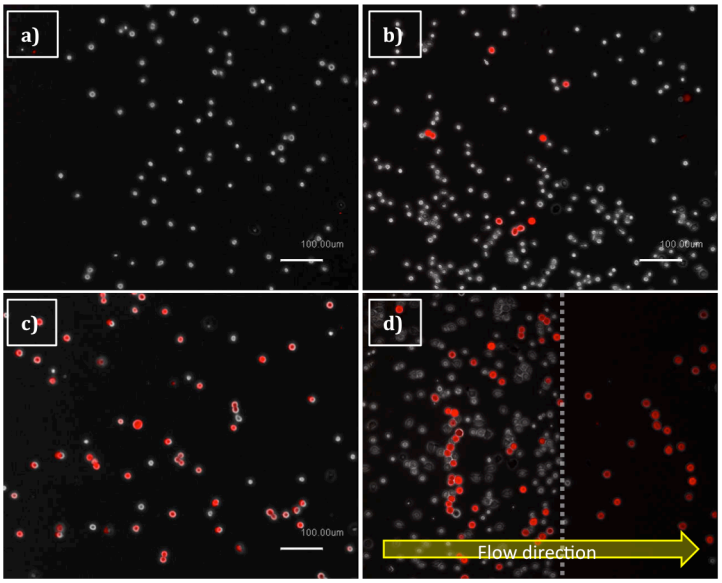

Figure 2.6. Images of HL-60 and DsRED-transfected MCF-7 cells (red cells) on a) P-selectin, b) E-selectin, c) anti-EpCAM, and d) patterned E-selectin/anti-EpCAM coated surfaces, under shear stress of 0.32 dyn/cm^2. The patterned surface with E-selectin and anti-EpCAM (shown in d) achieved efficient isolation of DsRED-transfected MCF-7 (a CTC model: red cells) cells from the mixture with HL-60 (a leukocyte model: white cells), on the anti-EpCAM coated region.

of the anti-EpCAM-immobilized surface (**Fig. 2.6c**), but these cells were in the bulk flow and not captured on the slide. As shown in **Fig. 2.6d**, the combined, but spatially separated E-selectin and anti-EpCAM in deed provided an enhanced separation of MCF-7 cells from the cell mixture, compared to the surface functionalized with E-selectin. Both cell types rolled on the E-selectin coated region (the left-hand side of the image), followed by clear separation of the pure MCF-7 cells in the adjacent anti-EpCAM coated region (the right-hand side).

2.3.4. Enhanced capturing of tumor cells using combinations of anti-EpCAM and E-selectin

The effect of E-selectin addition to the anti-EpCAM coated surface was further examined by a quantitative analysis of capture efficiency of DsRED-MCF-7 cells. **Fig. 2.7a and b** demonstrate a statistically significant enhancement in capture efficiency with the surface

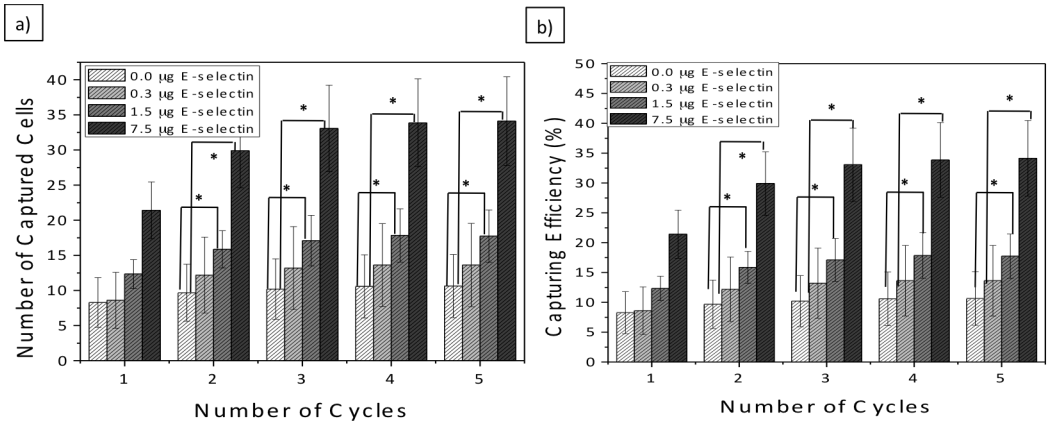

Figure 2.7. a) Number of captured cells and b) capture efficiencies of the surfaces immobilized with the mixtures of anti-EpCAM and E-selectin. The number of DsRED-MCF-7 cells on each surface was counted and the capture efficiency was calculated based on the total number of MCF-7 cells injected into the flow chamber. The flow experiments were performed at a shear stress of 0.16 dyn/cm^2. The average capture efficiencies of the surfaces with the mixture of E-selectin and anti-EpCAM were generally higher than those with anti-EpCAM alone. With an increase in E-selectin concentration, the capture efficiency of the surfaces was further enhanced as high as 3-fold. The measured capture efficiencies were compared by statistical analysis using one-factor ANOVA (SPSS software) and Fisher's least significant difference (LSD) tests with 95% simultaneous confidence intervals were marked *. Error bars: SEM. * $p < 0.05$.

immobilized with the mixtures (anti-EpCAM and E-selectin), as compared to the surface with anti-EpCAM only. As shown in **Fig. 2.7a and b**, the average number of captured cells by the surfaces with the two proteins was enhanced in an E-selectin concentration dependent manner. The enhancement of capture efficiency of the surface with E-selectin/anti-EpCAM compared to one with anti-EpCAM alone was observed to be as high as 3-fold.

To further evaluate cell capture under various conditions, a series of experiments in which DsRED-MCF-7 cells (2,500 cells/mL of PBS buffer) were spiked with HL-60 (2,500 cells/mL of PBS buffer) under the presence of anti-IgG was conducted. The rolling velocity of HL-60 cells

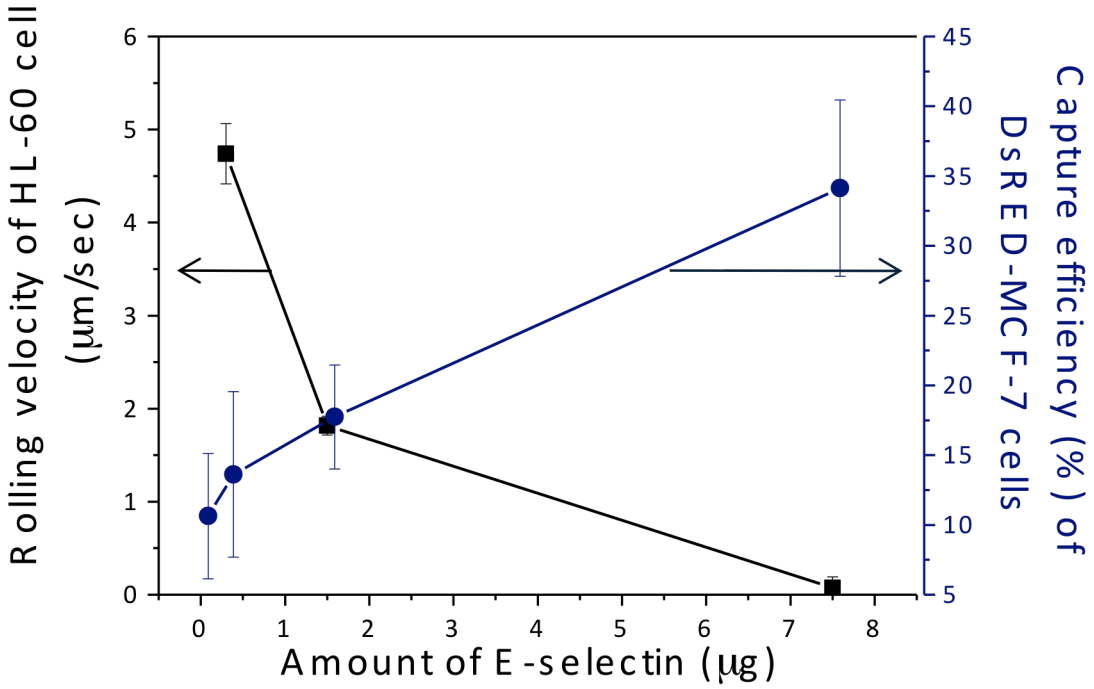

Figure 2.8. Effect of the amount of E-selectin added to E-selectin/anti-EpCAM mixture on rolling velocity of HL-60 cells and capture efficiency of DsRED-MCF-7 cells. Mixture of the two cell populations (1:1) were injected onto the surfaces co-immobilized with anti-EpCAM and E-selectin under the presence of anti-IgG at a shear stress of 0.16 dyn/cm^2. The amount of immobilized E-selectin was increased from 0, 0.3, and 1.5 to 7.5 μg, while the amount of immobilized anti-EpCAM was constant at 1.5 μg. The rolling velocities of HL-60 cells on each slides were 4.74 ± 0.32 (0.3 μg), 1.82 ± 0.10 (1.5 μg), and 0.07 ± 0.12 (7.5 μg of E-selectin) μm/sec. Error bar: SEM.

was measured at a flow rate of 200 μL/min (0.32 dyn/cm^2). **Fig. 2.8** quantitatively presents capture efficiency of DsRED-MCF-7 cells and rolling velocities of HL-60 on surfaces with co-immobilized E-selectin and anti-EpCAM at various ratios. As the amount of E-selectin in the total immobilized proteins was increased, the capture efficiency of DsRED-MCF-7 cells was increased, while the rolling velocity of HL-60 cells was decreased.

2.4. DISCUSSION

This study investigated three phenomena: i) two proteins with distinct biological functions can be co-immobilized; ii) rolling and stationary binding of tumor cells can be controlled by immobilized proteins; and iii) the protein combination enhances overall capture efficiency of tumor cells.

Tables 2.1 and 2.2 demonstrate co-immobilization of the two proteins. The red fluorescence from APC and the green fluorescence from fluorescein from the surfaces immobilized with either anti-EpCAM or E-selectin have little to no spectral overlap (**Fig. 2.2**). Furthermore, the even distribution of detected fluorescence (**Fig. 2.2**) indicates that uniform immobilization of both anti-EpCAM and E-selectin was achieved. The specific correlation between fluorescence and protein presentation on the slides was confirmed by two experiments. First, the control surfaces treated with BSA exhibited neither red nor green fluorescence, indicating that non-specific protein adsorption was minimal, which is consistent with a previous report [33]. Second, although E-selectin/APC-anti-EpCAM combinations showed a slightly decreased red fluorescence intensities (by ~30%) compared to the surfaces functionalized solely with anti-EpCAM at the same concentration, the decrease was marginal. By way of contrast, the green fluorescence intensities from fluorescein-anti-E-selectin substantially increased, in a non-linear fashion, with an increase of the immobilized amount of E-selectin in the protein mixtures.

Rolling and stationary binding were individually assessed to test the second phenomenon. As shown in **Fig. 2.3, 2.4, and 2.5**, we have found that the MCF-7 response on different surfaces can be controlled from no interaction (P-selectin) and the rolling response (E-selectin) to stationary binding (anti-EpCAM). The rolling velocities of the HL-60 cells that have a high level of PSGL-1 or sialyl Lewis X (sLe^x) expression were less shear stress-dependent than those of the MCF-7 cells (carcinoma cells) [34]. It is most likely caused by the regulation mechanisms by which leukocytic cells such as HL-60 maintain constant rolling velocities under varying flow conditions (**Fig. 2.5**) whereas carcinoma cells do not [35, 36]. Although the transient binding for rolling is a state between firm adhesion and the lack of the adhesion (i.e. no interaction), the rolling of leukocytic cells through selectins is highly stable due to a high density of selectin ligands presented on the leukocytic cells and their resistance against hydrodynamic force applied on the cells [37]. As a result, leukocytic cells are known to have a nearly constant rolling speed *in vivo* over a wide range of shear stresses [38]. It is also suspected that leukocytic cells maintain a constant rolling speed by shear dependent compensation mechanisms such as increasing the number of tethers and the number of selectin bonds so that they can be uniformly exposed to activating stimuli [35]. MCF-7 cells (Carcinoma cells), on the other hand, seem to lack these mechanisms, given that they are more susceptible to changes in shear stress (**Fig. 2.5**). Moreover, the formation of metastatic cancers often exhibits the organ selectivity because of the different interactions between the ligands of cancer cells and the organ-specific selectins of endothelial cells for the extravasation of CTCs, which does not require CTCs to adapt the controlling mechanism of the leukocytic cells [39].

MCF-7 cells exhibit the rolling behavior only on E-selectin, and as reported by Aigner et al. [34], MCF-7 cells do not interact with P-selectin. Although MCF-7 cells express CD24, a P-selectin ligand, a lack of decoration with sLe^x results in weak interactions that are not strong enough to stably support rolling on P-selectin [34]. E-selectin-mediated rolling of MCF-7 cells

under flow was reported by Toezeren et al [40]. Under the presence of laminar flow, they reported that the adhesion capacity and rolling behavior of MCF-7 cells on human umbilical endothelial cells (HUVECs) were blocked by treatment with antibody against E-selectin on the surface of HUVECs, without providing clear evidence. We have shown that clear interaction of MCF-7 cells with immobilized E-selectin in **Fig. 2.4**, and the behavior of MCF-7 cells was compared with HL-60. However, it is still unclear which interaction induces the observed rolling response. As a ligand of MCF-7 cells against E-selectin needs to be identified because MCF-7 cells lack most of the known ligands against E-selectin such as PSGL-1 [34], CD44 [41], and sLe^x [34]. There have been no definitive reports that clearly identify ligands of MCF-7 cells against E-selectin in the literature.

Adherent proteins that are involved in the metastasis process are randomly co-distributed on the endothelium [42]. Thus, our hypothesis was that cooperation of adherent proteins to trap tumor cells would be more efficient than the activity of one of them alone. The surfaces with the protein mixtures (anti-EpCAM and E-selectin) in deed more efficiently recognize DsRED-MCF-7 cells out of the cell mixture with HL-60 cells than the surfaces functionalized solely with anti-EpCAMs (**Fig. 2.6 and 2.7**). The protein combinations used in this study clearly demonstrate great potential to improve sensitivity and specificity of CTC separation and capturing from the whole blood. One can argue that an increase of E-selectin composition in the protein mixture may lead pre-occupation of the surface by abundant cells such as leukocytes (HL-60 in this study), resulting in binding interruption of CTCs (MCF-7 in our study). However, it would be not be the case because HL-60 cells exhibit the continuous dynamic rolling response whereas MCF-7 cells remain statically adhered on the surface. That is, a thorough washing step will remove all the rolling cells, leaving only captured cells behind on the surface. Further, it is shown that the enhanced capture efficiency by addition of E-selectin to anti-EpCAM is not interrupted by competitive binding of HL-60 cells. Instead, it is our expectation that E-selectin would be

effective in pulling CTCs (MCF-7 cells in this research) along with leukocytes out of the blood flow, inducing rolling, thereby reducing the velocities of the flowing cells, which would facilitate stationary binding of CTCs by adjacent anti-EpCAM on the surface. Furthermore, given that cells exhibit significantly different rolling velocities and different levels of interactions with various proteins, the surface responses of different types of cells are expected to be easily controlled by various combinations of proteins.

Taken together, it is obvious that the addition of E-selectin can induce the rolling of various cell types to be readily accessible by anti-EpCAM that recognizes/captures tumor cells, resulting in substantially enhanced capture efficiency of tumor cells by the surface – more than 3-fold enhancement as compared to the surface with anti-EpCAM alone. The E-selectin-induced tumor cell rolling most likely maximizes the chance of the tumor cells to interact with anti-EpCAM on the surface, resulting in effective stationary binding.

2.5. SUMMARY

We have achieved the evenly distributed, stable immobilization of proteins: P-selectin, E-selectin, anti-EpCAM, and mixtures of the proteins, using epoxy-functionalized glass slides. The immobilized proteins maintained their own biological adhesive functions that induce cell rolling and stationary binding in each specific protein-dependent manner. The patterning and combination of these immobilized proteins as a step towards mimicking physiological complexity can be used to design therapeutic or diagnostic devices for capturing specific cells using their enhanced separation capacity and capture efficiency. We are presently translating these results to a device to capture CTCs from the mixture of other cell lines and whole blood. In addition to the potential use of this device as a metastatic cancer treatment tool by filtering CTCs from the bloodstream, the advantages of this device include the ability to collect CTCs from whole blood under continuous flow without labeling or damaging the CTCs. Therefore, the collected CTCs

can be extracted and potentially be subject of further analysis such as genetic understanding and responses for currently available therapeutic drugs by culture expansion.

2.6. REFERENCES

1. Karnon, J., et al., *Health care costs for the treatment of breast cancer recurrent events: estimates from a UK-based patient-level analysis.* Br J Cancer, 2007. **97**(4): p. 479-485.
2. Dong, F., A.S. Budhu, and X.W. Wang, *Translating the metastasis paradigm from scientific theory to clinical oncology.* Clin Cancer Res, 2009. **15**(8): p. 2588-93.
3. Pepper, M.S., *Lymphangiogenesis and tumor metastasis: myth or reality?* Clin Cancer Res, 2001. **7**(3): p. 462-8.
4. Hüsemann, Y., et al., *Systemic Spread Is an Early Step in Breast Cancer.* Cancer Cell, 2008. **13**(1): p. 58-68.
5. Chiang, A.C. and J. Massague, *Molecular basis of metastasis.* N Engl J Med, 2008. **359**(26): p. 2814-23.
6. Cristofanilli, M., et al., *Circulating tumor cells, disease progression, and survival in metastatic breast cancer.* N Engl J Med, 2004. **351**(8): p. 781-91.
7. Paget, S., *The distribution of secondary growths in cancer of the breast. 1889.* Cancer Metastasis Rev, 1989. **8**(2): p. 98-101.
8. Mantovani, A., et al., *Cancer-related inflammation.* Nature, 2008. **454**(7203): p. 436-44.
9. Mackay, C.R., *Moving targets: cell migration inhibitors as new anti-inflammatory therapies.* Nat Immunol, 2008. **9**(9): p. 988-98.
10. Riethdorf, S. and K. Pantel, *Disseminated tumor cells in bone marrow and circulating tumor cells in blood of breast cancer patients: current state of detection and characterization.* Pathobiology, 2008. **75**(2): p. 140-8.
11. Alix-Panabieres, C., V. Muller, and K. Pantel, *Current status in human breast cancer micrometastasis.* Curr Opin Oncol, 2007. **19**(6): p. 558-63.
12. Lacroix, M., *Significance, detection and markers of disseminated breast cancer cells.* Endocr Relat Cancer, 2006. **13**(4): p. 1033-67.

13. Pantel, K. and M. Otte, *Occult micrometastasis: enrichment, identification and characterization of single disseminated tumour cells.* Semin Cancer Biol, 2001. **11**(5): p. 327-37.

14. Zieglschmid, V., C. Hollmann, and O. Bocher, *Detection of disseminated tumor cells in peripheral blood.* Crit Rev Clin Lab Sci, 2005. **42**(2): p. 155-96.

15. Krivacic, R.T., et al., *A rare-cell detector for cancer.* Proc Natl Acad Sci U S A, 2004. **101**(29): p. 10501-4.

16. Danila, D.C., et al., *Circulating tumor cell number and prognosis in progressive castration-resistant prostate cancer.* Clin Cancer Res, 2007. **13**(23): p. 7053-8.

17. Riethdorf, S., et al., *Detection of circulating tumor cells in peripheral blood of patients with metastatic breast cancer: a validation study of the CellSearch system.* Clin Cancer Res, 2007. **13**(3): p. 920-8.

18. Nagrath, S., et al., *Isolation of rare circulating tumour cells in cancer patients by microchip technology.* Nature, 2007. **450**(7173): p. 1235-9.

19. Maheswaran, S., et al., *Detection of mutations in EGFR in circulating lung-cancer cells.* N Engl J Med, 2008. **359**(4): p. 366-77.

20. Tedder, T.F., et al., *The selectins: vascular adhesion molecules.* Faseb J, 1995. **9**(10): p. 866-73.

21. Dimitroff, C.J., et al., *Rolling of human bone-metastatic prostate tumor cells on human bone marrow endothelium under shear flow is mediated by E-selectin.* Cancer Res, 2004. **64**(15): p. 5261-9.

22. Giavazzi, R., et al., *Rolling and adhesion of human tumor cells on vascular endothelium under physiological flow conditions.* J Clin Invest, 1993. **92**(6): p. 3038-44.

23. Yuan, K., et al., *Alterations in human breast cancer adhesion-motility in response to changes in cell surface glycoproteins displaying alpha-L-fucose moieties.* Int J Oncol, 2008. **32**(4): p. 797-807.

24. Tremblay, P.L., J. Huot, and F.A. Auger, *Mechanisms by which E-selectin regulates diapedesis of colon cancer cells under flow conditions.* Cancer Res, 2008. **68**(13): p. 5167-76.

25. Greenberg, A.W. and D.A. Hammer, *Cell separation mediated by differential rolling adhesion.* Biotechnol Bioeng, 2001. **73**(2): p. 111-24.

26. Rana, K., J.L. Liesveld, and M.R. King, *Delivery of apoptotic signal to rolling cancer cells: a novel biomimetic technique using immobilized TRAIL and E-selectin.* Biotechnol Bioeng, 2009. **102**(6): p. 1692-702.

27. Hong, S., et al., *Covalent immobilization of p-selectin enhances cell rolling.* Langmuir, 2007. **23**(24): p. 12261-8.

28. Ramezani, A. and R.G. Hawley, *Generation of HIV-1-based lentiviral vector particles.* Curr Protoc Mol Biol, 2002. **Chapter 16**: p. Unit 16 22.

29. Nilsson, R. and H.O. Sjogren, *Antigen-independent binding of rat immunoglobulins in a radioimmunoassay. Solutions to an unusual background problem.* J Immunol Methods, 1984. **66**(1): p. 17-25.

30. Goldman, A.J., R.G. Cox, and H. Brenner, *Slow viscous motion of a sphere parallel to a plane wall--II Couette flow.* Chemical Engineering Science, 1967. **22**(4): p. 653-660.

31. Kobzdej, M.M., et al., *Discordant expression of selectin ligands and sialyl Lewis x-related epitopes on murine myeloid cells.* Blood, 2002. **100**(13): p. 4485-94.

32. Zou, X., et al., *PSGL-1 derived from human neutrophils is a high-efficiency ligand for endothelium-expressed E-selectin under flow.* Am J Physiol Cell Physiol, 2005. **289**(2): p. C415-24.

33. Brorson, S.H., *Bovine serum albumin (BSA) as a reagent against non-specific immunogold labeling on LR-White and epoxy resin.* Micron, 1997. **28**(3): p. 189-95.

34. Aigner, S., et al., *CD24 mediates rolling of breast carcinoma cells on P-selectin.* Faseb J, 1998. **12**(12): p. 1241-51.

35. Chen, S. and T.A. Springer, *An automatic braking system that stabilizes leukocyte rolling by an increase in selectin bond number with shear.* J Cell Biol, 1999. **144**(1): p. 185-200.

36. Sachs, L., *Control of growth and normal differentiation in leukemic cells: regulation of the developmental program and restoration of the normal phenotype in myeloid leukemia.* J Cell Physiol Suppl, 1982. **1**: p. 151-64.

37. Lawrence, M.B. and T.A. Springer, *Leukocytes roll on a selectin at physiologic flow rates: distinction from and prerequisite for adhesion through integrins.* Cell, 1991. **65**(5): p. 859-73.

38. Atherton, A. and G.V. Born, *Relationship between the velocity of rolling granulocytes and that of the blood flow in venules.* J Physiol, 1973. **233**(1): p. 157-65.

39. Gout, S., P.L. Tremblay, and J. Huot, *Selectins and selectin ligands in extravasation of cancer cells and organ selectivity of metastasis.* Clin Exp Metastasis, 2008. **25**(4): p. 335-44.

40. Tozeren, A., et al., *E-selectin-mediated dynamic interactions of breast- and colon-cancer cells with endothelial-cell monolayers.* Int J Cancer, 1995. **60**(3): p. 426-31.

41. Zen, K., et al., *CD44v4 is a major E-selectin ligand that mediates breast cancer cell transendothelial migration.* PLoS ONE, 2008. **3**(3): p. e1826.

42. Ley, K., et al., *Getting to the site of inflammation: the leukocyte adhesion cascade updated.* Nat Rev Immunol, 2007. **7**(9): p. 678-689.

43. Ajikumar, P.K., et al., *Carboxyl-terminated dendrimer-coated bioactive interface for protein microarray: high-sensitivity detection of antigen in complex biological samples.* Langmuir, 2007. **23**(10): p. 5670-7.

CHAPTER 3

DIRECT MEASUREMENTS ON CD24-MEDIATED ROLLING OF HUMAN BREAST CANCER MCF-7 CELLS ON E-SELECTIN

3.1. INTRODUCTION

Adhesive interactions between tumor cells and the vascular endothelium are necessary to promote cancer metastasis induced by circulating tumor cells (CTCs) [1, 2]. The transient adhesion of cells to the endothelium in blood circulation, known as cell rolling, is the early event of the adhesive interactions that are mediated by adhesive proteins such as selectins on the endothelium and specific ligands on the cancer cell surface [3, 4]. To date, three types of selectins have been identified, E-selectin (CD62E), L-selectin (CD62L), and P-selectin (CD62P) [5]. Among them, E-selectin, an inducible endothelial cell-surface glycoprotein [6], has been suggested as one of the major receptors responsible for causing the metastasis of primary tumors such as breast [7], colon [3], and prostate cancers [8, 9]. E-selectin has been also shown to mediate the adhesion of leukocytes or carcinoma cells to cytokine-activated human endothelial cells [10, 11]. Information regarding the ligands for E-selectin on the cancer cells would thus be crucial to understand the mechanism of metastasis and to potentially find a way to prohibit the spreading of primary cancers in patients.

Earlier reports have shown high-affinity binding between E-selectin and its ligands such as E-selectin ligand-1 (ESL-1) [12], P-selectin glycoprotein ligand-1 (PSGL-1) [13, 14], and sialyl Lewis X (sLe^x) and related sulfated structures including sialyl Lewis^a (sLe^a) [15, 16]. In addition to these known ligands for E-selectin, it is reported that the following molecules also have binding affinity to E-selectin; CD43 [17], hematopoietic cell E- and L-selectin ligand (HCELL; a specialized glycoform of CD44) [10], β2 integrins [18], and CD44v4 [19]. In our previous report,

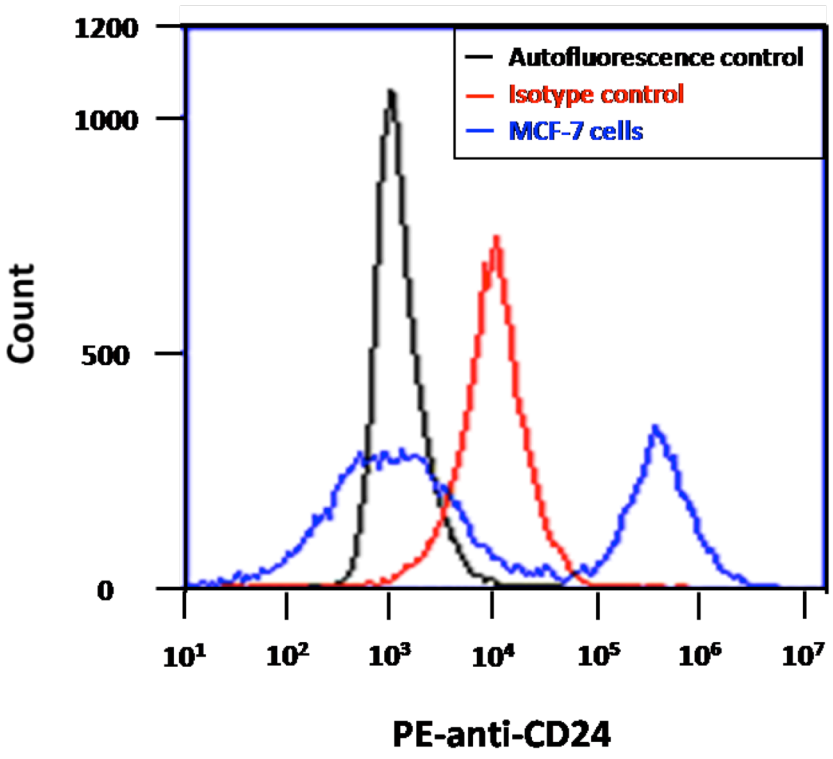

Figure 3.1. FACS histograms of PE fluorescence intensities from MCF-7 cells. The cells were treated with PE-conjugated anti-CD24 (blue), PE-conjugated anti-$IgG_{2a,k}$ for an isotype control [red], or were untreated (black). Based on the fluorescence intensity of each group, it was confirmed that MCF-7 cells have two subpopulations, CD24 negative and CD24 positive.

MCF-7 cells exhibited the rolling behavior only on E-selectin-immobilized surfaces under flow but no interactions with P-selectin [20]. However, to the best of our knowledge, a ligand against E-selectin present on MCF-7 cells has not been identified since MCF-7 cells lack all the known E-selectin ligands listed above [19, 21, 22].

CD24, which is highly expressed by MCF-7 cells, is a mucin-like glycosylphosphatidyl-inositol-linked cell surface protein consisting of 27 amino acids [23]. Expression of CD24 from MCF-7 cells was assessed using a fluorescence activated cell sorter (FACS) as shown in **Fig. 3.1**. This protein is also expressed by early stage B-cells and neutrophils, whereas it is not expressed by normal T-cells and monocytes [23]. Previous reports have also shown that it is highly expressed on several non-hematopoietic tumors such as breast carcinomas, epithelial ovarian

cancer, small and non-small cell lung carcinoma, prostate cancer, pancreatic cancer, and renal cell carcinoma [9, 24, 25]. A higher expression level of CD24 on cells in cancer patients has been correlated with a decreased survival rate, and thus CD24 has demonstrated potential to be used as a marker for more aggressive cancers [24, 26]. In cancer cell lines, the expression of CD24 molecules is known to enhance the metastatic properties of carcinoma cells, e.g. the adhesiveness [25, 26] and invasion *in vitro* [27] and *in vivo* [28, 29]. Moreover, expedited cell growth and metastatic properties of MCF-7 cells were inhibited by cross-linking of CD24 using anti-human CD24 rabbit polyclonal antibodies on the cell surface [30]. Based on the *in vitro* and *in vivo* connection between CD24 and the cancer cell properties as well as our previous observation of MCF-7 cell rolling, the possibility that CD24 may be a ligand for E-selectin has emerged.

In this chapter, we hypothesize that CD24 is a ligand for E-selectin, which mediates cell rolling. To test the hypothesis, the binding kinetics of CD24 with E-selectin were measured directly and quantitatively using surface plasmon resonance (SPR) provided by BIAcore® technology. We have also found that the rolling response of the CD24-positive MCF-7 cells was completely blocked by anti-CD24 pre-treatment to the cells. Additionally, we have tested the rolling velocities of MCF-7 cells treated with cytochalasin D (cytoD), an actin-disrupting agent, revealing that the cellular mechanics, such as actin-filament dynamics, play a role in the rolling mechanism mediated by CD24 and E-selectin. The involvement of the actin filament was further supported by the observed no rolling but stationary binding of CD24-coated microspheres on E-selectin. Our results presented here support our hypothesis that CD24 is a ligand for E-selectin and induces the rolling of the MCF-7 cells.

3.2. MATERIALS AND METHOD

3.2.1. Materials

Recombinant human E-selectin/Fc chimera (E-selectin) and anti-human epithelial-cell-adhesion-molecule (EpCAM)/TROP1 antibody (anti-EpCAM) were purchased from R&D systems (Minneapolis, MN). Recombinant human CD24 and sLe^x–PAA-Biotin were purchased from Santa Cruz Biotechnology, Inc (Santa Cruz, CA) and Glycotech (Gaithersburg, MD), respectively. Unconjugated goat anti-Human IgG (H + L) was acquired from Pierce Biotechnology, Inc (Rockford, IL). The epoxy-functionalized glass surfaces (SuperEpoxy2®) were purchased from TeleChem International, Inc (Sunnyvale, CA). PE mouse IgG2a (k isotype control), PE mouse anti-human CD24, and purified mouse anti-human CD24 were obtained from BD Pharmingen™ (BD biosciences, San Jose, CA). All other chemicals were obtained from Sigma-Aldrich (St. Louis, MO), unless otherwise specified, and used without further purification.

3.2.2. Flow Cytometry Measurements of CD24 expression

CD24 expression of MCF-7 cells was measured using a fluorescence activated cell sorter (FACS, Beckman Coulter EPICS Elite ESP, Miami, FL). Trypsinized MCF-7 cells (50 μL of 1×10^7 cells/mL solution in PBS with 1% FBS) were incubated with 10 μL of PE-conjugated anti-CD24 on ice for 15 min, centrifuged at 1800 rpm for 5 min, and resuspended in the FBS-containing PBS for the FACS measurements. The control groups include the untreated cells as a negative control, the cells treated with 10 μL of anti-$IgG_{2a,\,k}$, an isotype of anti-CD24, as an isotype control.

3.2.3. Surface plasmon resonance measurements

BIAcore® X instrument (GE Healthcare, Pittsburgh, PA) was used for quantitative and direct measurements of the binding kinetics of CD24 and sLe^x with E-selectin at 25 °C. The E-

selectin was immobilized on CM5 sensor chips (GE Healthcare) using the amine coupling kit (GE Healthcare) as described earlier (**Fig. 3.2**.) [31]. Briefly, 6 µL of E-selectin solution (1 mg/mL in PBS buffer) was diluted in 144 µL of sodium acetate buffer (immobilization buffer, 10 mM, pH 5.0). The protein solution (70 µL) was then injected into the channel 2 of a sensor chip CM5 that was pre-activated by 70 µL of a mixture of 1-ethyl-3-(3-dimethylaminopropyl) carbodiimide (EDC) and N-hydroxylsuccinimide (NHS). After protein immobilization, the remaining reactive ester residues were blocked by the injection of 70 µL ethanolamine (pH 8.5). The whole protein immobilization process was carried out at a flow rate of 5 µL/min using HBS-EP (GE Healthcare) as a running buffer.

CM5 sensor chips with an immobilized shift of more than 8,000 resonance units (RU, approximately 8 ng/mm^2 of surface presentation) were used for subsequent protein binding

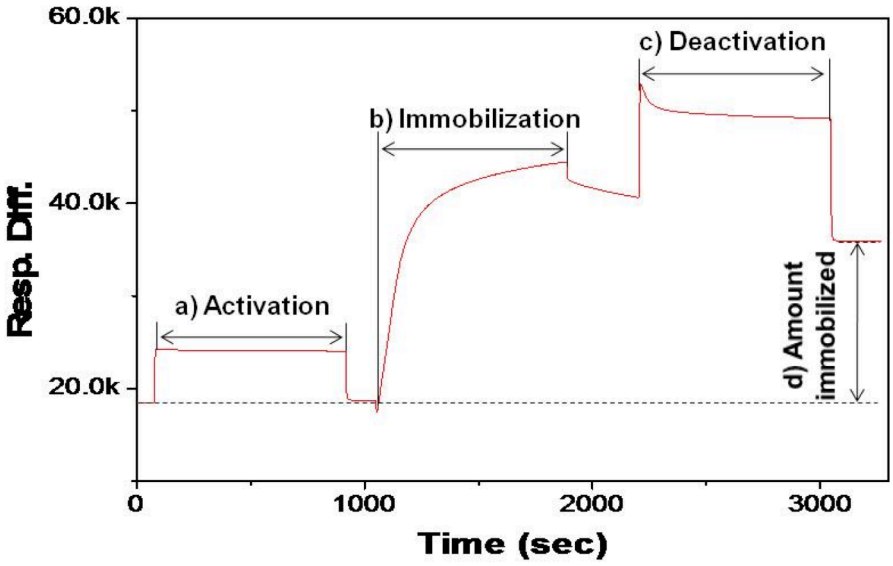

Figure 3.2. A SPR sensorgram of E-selectin immobilization on a CM5 sensor chip. The amount of the immobilized protein on the sensor chip was determined by the difference in resonance unit before and after immobilization of E-selectin (d). The sensor chips with the immobilized shift of more than 8,000 RU were used for subsequent binding analyses. The immobilization process was performed by three steps: (a) activation of the CM5 sensor chip using a mixture of EDC and NHS; (b) injection of E-selectin; and (c) termination of the remaining reactive ester residues on the sensor chip using ethanolamine.

analyses (**Fig. 3.2**). The protein-immobilized sensor chips were rinsed with PBS buffer (10 mM, running buffer) until a stable baseline (equilibrium) was obtained, prior to the injection of the analytes. To perform binding assays, 50 μL of CD24 or sLe^x in PBS buffer at a series of concentrations was injected into the two channels (channel 2 with E-selectin and channel 1 as reference) at a flow rate of 50 μL/min, which allowed the analytes to interact with the chip surface for 1 min, followed by flowing the running buffer for 5 min. After obtaining the binding curves, the sensor chip surface was regenerated using Glycin-HCl (10 mM, pH 2.5 or pH 3.0) buffer for further experiments. To confirm that the response is a result of the specific interactions, the responses (in RU) from the channel 2 were subtracted by those from the channel 1, represented as differences in responses. All sensorgrams were recorded from the start of the injection to the end of the dissociation phase, and were shifted to overlay at the same baseline resonance level. All binding kinetics parameters were obtained by fitting a 1:1 binding model provided by the BIAevaluation software and represented as the mean value ± standard deviation from three independent measurements.

3.2.4. Cell culture and treatments

MCF-7 cells purchased from ATCC (Manassas, VA) were grown in DMEM media supplemented with 10% (v/v) FBS and 1% (v/v) penicillin/streptomycin in a humidified incubator at 37 °C and 5% CO_2. Prior to all flow-chamber experiments, MCF-7 cells at a concentration of 2 × 10^5 cells/mL (5 mL) were pre-treated with 240 μg/mL of anti-IgG solution to prevent potential non-specific binding [32]. To block CD24 on the MCF-7 cell surface, 100 μL of anti-CD24 (0.5 mg/mL) was added into the cell suspension and incubated for 15 min. The final suspensions were kept on ice throughout the subsequent cell rolling experiments. To investigate the effect of actin-filament dynamics on the cell rolling behavior of MCF-7 cells, 5 mL of the cells at 2 × 10^5 cells/mL was treated with 40 μM of cytoD for 60 min and were resuspended in the supplemented DMEM media for the flow chamber experiments [33, 34].

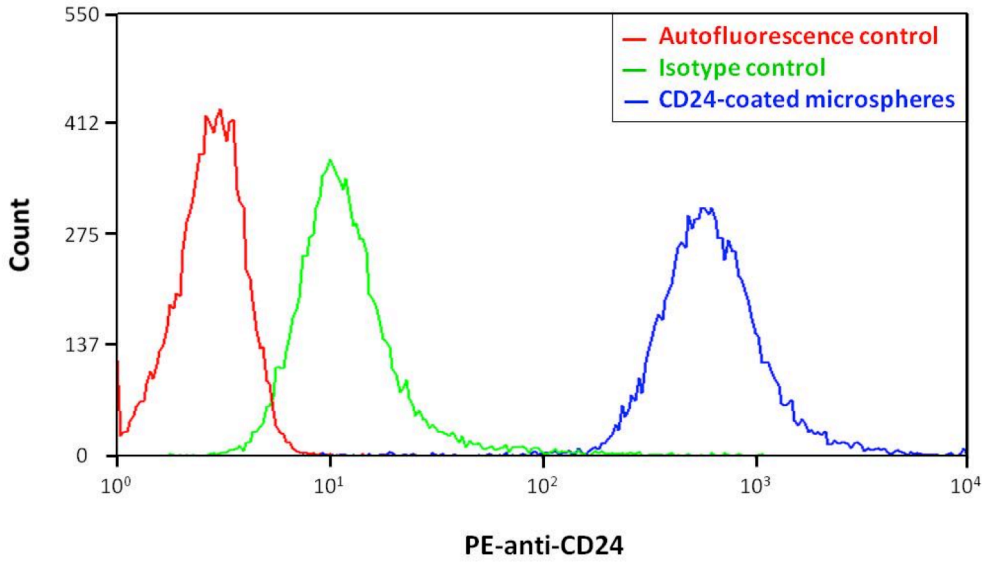

Figure 3.3. FACS histograms of PE fluorescence intensities from the various microspheres. The microspheres were treated with PE-conjugated anti-CD24 (blue), PE-conjugated anti-$IgG_{2a,\,k}$ for an isotype control (green), or were untreated [red]. The significantly increased fluorescence intensity from the CD24-coated microspheres confirms that CD24 coating was performed successfully.

3.2.5. Preparation of CD24- and sLe^x-coated microspheres

Recombinant human CD24 was used after dialysis (Slide-A-Lyzer® mini dialysis units with 10,000 MWCO, Thermo scientific, Rockford, IL) to remove impurities for high conjugation efficiency of the subsequent reaction with a biotin reagent. The purified, recombinant CD24 proteins were biotinylated using 10 mM EZ-Link® Sulfo-NHS-LC-Biotin (20-fold molar excess, Thermo scientific) for 2 hr on ice, and the biotinylated CD24 proteins were re-purified by dialysis using a Slide-A-Lyzer® mini dialysis unit. Streptavidin-coated microspheres (104.8 µL, 1×10^7 beads, 9.95 µm O.D., ProActive® microspheres, Bangs Laboratories, Inc, Fishers, IN) in 1% (w/v) bovine serum albumin (BSA) in PBS buffer (10 mM, Cellgro®, with 2 mM Ca^{2+}) (BSA solution) were washed three times using a centrifuge at 10,000 rpm for 2 min. The biotinylated CD24 (100 nM) was conjugated to the microspheres in BSA solution by the spontaneous interaction between

streptavidin and biotin after 1 hr of incubation at room temperature. The coating of CD24 molecules on microspheres was confirmed by flow cytometry (**Fig. 3.3**) using the same immunostaining condition for the confirmation of CD24 expression on MCF-7 cell using phycoerythrin (PE)-anti-CD24. In parallel, sLe^x-coated microspheres were also prepared using the biotinylated sLe^x (100 nM) as previously described [35]. The density of CD24 and sLe^x on microspheres might not be exactly identical, but presumably very similar due to the reasons such as the same streptavidin density on microspheres and the similar efficiencies of biotinylation of CD24 and sLe^x. For parallel flow chamber experiments, CD24 or sLe^x-coated microspheres were resuspended in 10 mL BSA solution (1×10^6 microspheres/mL). To investigate potential

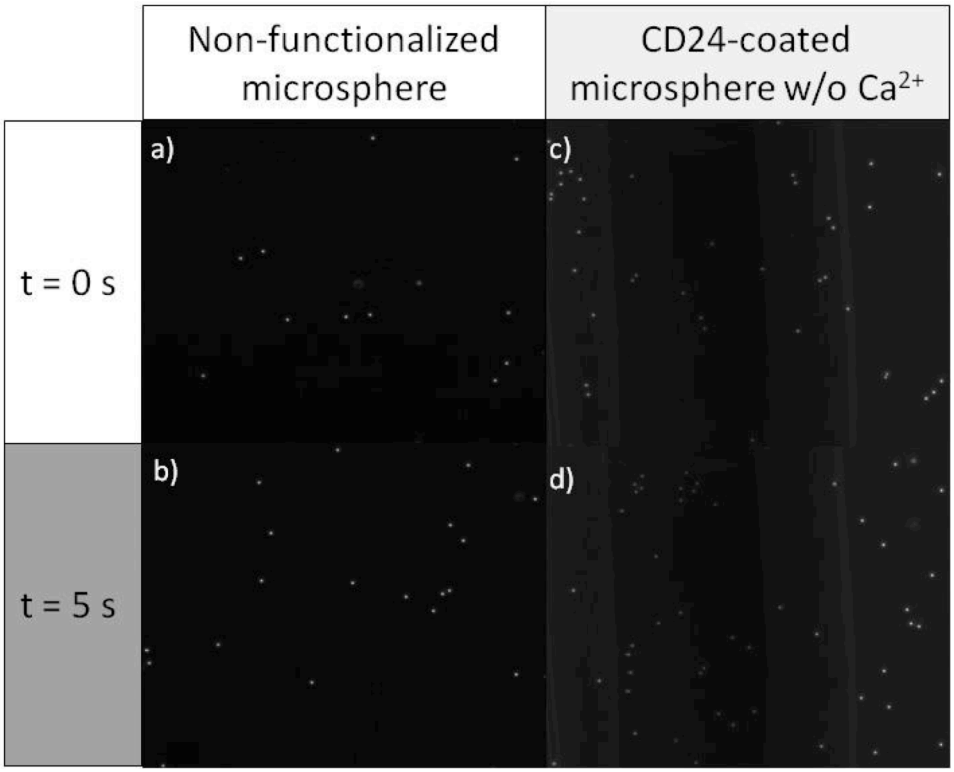

Figure 3.4. Time-course images of (a and b) nonfunctionalized microspheres and (c and d) CD24-coated microspheres without Ca^{2+} in buffer, both under shear stress of 0.08 dyn/cm^2 on E-selectin-immobilized surfaces. No interactions between the microspheres and the surfaces were observed in the either condition, indicating that non-specific interaction of the microspheres is minimal and the CD24/E-selectin interaction is Ca^{2+} dependent.

non-specific interactions of microspheres themselves with E-selectin, a flow-chamber experiment (described in detail below) was performed using non-functionalized microspheres, confirming that there is no non-specific binding (**Fig. 3.4**).

3.2.6. Surface functionalization by immobilization of adhesive proteins

A general scheme of the adhesive protein immobilization, along with the characterization of the surfaces, is described in our previous publication [20]. Briefly, 150 μL of each protein (E-selectin or anti-EpCAM) at a concentration of 5 μg/mL in PBS buffer was added on an approximately 1 cm^2 area of an epoxy functionalized glass slide defined by a polydimethylsiloxane (PDMS) gasket. After incubation at room temperature for 4 hr with constant gentle shaking, the PDMS gasket was removed, and the whole slide surface was washed with PBS three times. Potential non-specific binding of both protein-coated and uncoated regions was blocked by a final incubation with BSA solution. Experiments using the functionalized surfaces were performed immediately.

3.2.7. Flow chamber experiments

Flow chamber experiments were also performed according to our previous report [20]. The biofunctionalized glass slide, a gasket (30 mm (L) × 10mm (W) × 0.25 mm (D), Glycotech), and a rectangular parallel plate flow chamber (Glycotech) were assembled in line under vacuum. To observe cellular interactions, MCF-7 cell suspensions with or without anti-CD24 treatment as well as CD24- or sLe^x-coated microsphere suspensions were injected into the flow chamber at various flow rates (ranging from 50 to 200 μL/min) using a syringe pump (New Era pump Systems Inc., Farmingdale, NY). Note that, in this flow chamber, 50 μL/min of flow rate is correspondent to 0.08 dyn/cm^2 of a wall shear stress, 8 s^{-1} of a wall shear rate, and 20 μm/sec of near-wall non-adherent cell velocity according to the Goldman equation [36]. All cellular responses in the flow chamber were monitored using an Olympus IX70 inverted microscope (IX

70-S1F2, Olympus America, Inc., Center Valley, PA) and images were recorded using a 10× objective and a CCD camera (QImaging Retiga 1300B, Olympus America, Inc.). Rolling velocities of cells and the functionalized microspheres on the immobilized proteins were measured, based on the images taken every second for 1 min in repetitive observations using ImageJ (NIH). Cell rolling was defined when the rolling velocities were less than 50% of the free stream velocity (e.g. slower than 10 μm/sec at a flow rate of 50 μL/min). In addition to the flow-based experiments using the functionalized microspheres, the same number of CD24-coated microspheres (1×10^6 microspheres/mL in BSA solution) was incubated with each protein-immobilized surface for 1 min and the number of protein-immobilized microspheres per 1 mm^2 that remained on the surface was counted after flowing PBS buffer for 1 min.

3.3. RESULTS AND DISCUSSION

We have previously reported MCF-7 cell rolling on immobilized E-selectin [20]. However, as indicated, it was unclear which ligand was responsible for inducing the rolling behavior since the cells do not express any known ligands for E-selectin. The purpose of this study was therefore to identify the ligand of MCF-7 cells. Given that cells that maintain a high level of CD24 expression have enhanced invasive and adhesive properties which can potentially related to cancer metastasis [24, 28], we hypothesized that CD24 may mediate the rolling response of MCF-7 cells on E-selectin.

3.3.1. Flow Cytometry Measurements of CD24 expression

CD24 expression of MCF-7 cells was measured using a FACS. The FACS histograms of the PE fluorescence intensities are shown in **Fig. 3.1**. MCF-7 cells were divided into two groups based on CD24 expression; CD24-positive and CD24-negative subpopulations, which is

consistent with a previous report [37]. The CD24-positive subpopulation showed the strongest fluorescence intensity, indicating high expression of CD24. The fluorescence intensity of the $CD24^-$ subpopulation was similar to that of the non-treated cells. The anti-$IgG_{2a,k}$-treated MCF-7 cells exhibited a lower intensity than $CD24^+$ group but higher than the untreated cells.

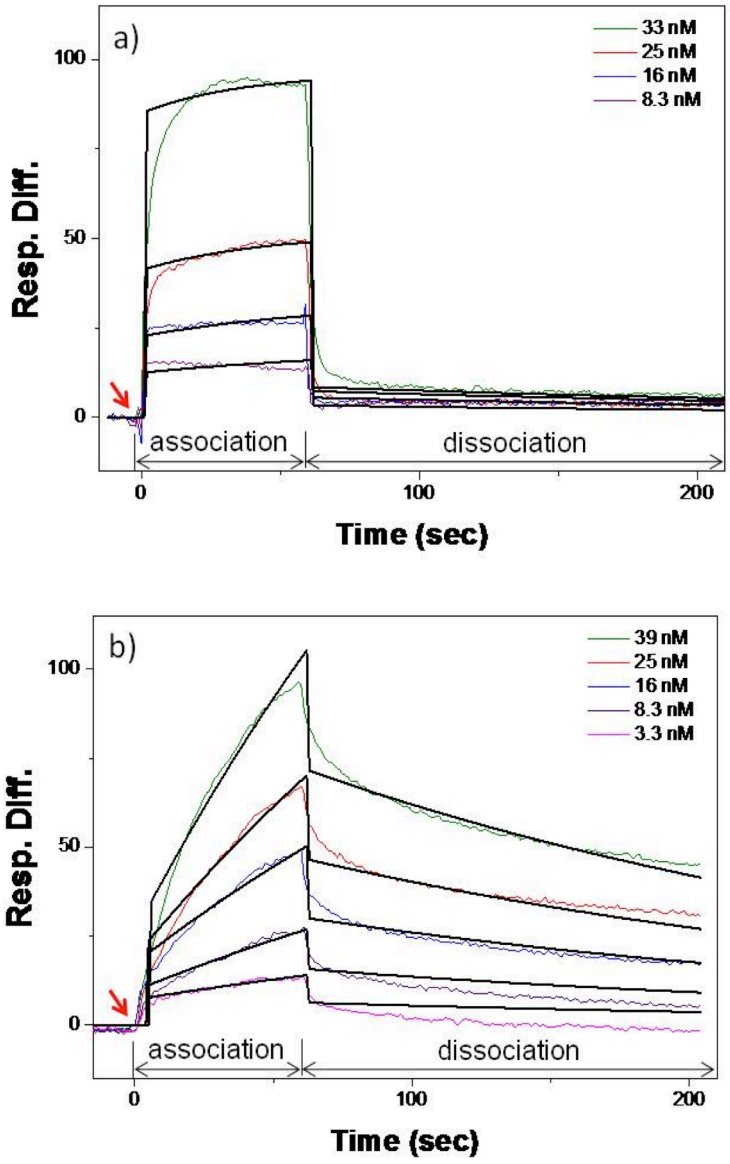

Figure 3.5. SPR sensorgrams showing the binding curves of (a) CD24 and (b) sLe^x with the immobilized E-selectin. The colored lines represent the raw data curves, and the solid black lines are simulated fitting curves using an 1:1 interaction model. The arrows indicate the injection time of the analytes.

3.3.1. Direct measurements of binding kinetics using SPR

For the first time to our knowledge, the binding kinetics of recombinant CD24 with E-selectin was quantitatively measured using a direct binding assay by BIAcore® X. A well-known ligand for E-selectin, sLe^x was also employed as a control. The BIAcore® sensorgrams illustrating the binding interactions between the E-selectin-immobilized sensor chips and CD24 or sLe^x are shown in **Fig. 3.5**, and all measured kinetic parameters are listed in **Table 3.1**. Note that concentrations of the analytes (CD24 and sLe^x) used for the SPR measurements were optimized to achieve similar levels of resonance unit (RU) (preferably lower than 100) between sensorgrams. The SPR measurements revealed that CD24 indeed bound to E-selectin. The association rate constant (k_a) and the dissociation rate constant (k_d) were 3.8×10^5 $M^{-1}s^{-1}$ and 1.6×10^{-3} s^{-1}, respectively, and the dissociation constant (K_D) of CD24 was 3.4 nM. The binding parameters k_a, k_d, and K_D of sLe^x were measured to be 7.9×10^4 $M^{-1}s^{-1}$, 5.6×10^{-3} s^{-1} and 78.3 nM, respectively. While the k_d values of CD24 and sLe^x were relatively similar, k_a of CD24 was

Table 3.1. Quantitatively measured kinetic parameters of binding of CD24 and sLe^x with E-selectin using SPR.

Kinetic Parameters[1]	**Ligands**	
	CD24	**sLe^x**
k_a ($\times 10^4$ $M^{-1}s^{-1}$)	37.9 ± 30.4	7.9 ± 2.6
k_d ($\times 10^{-3}$ s^{-1})	1.6 ± 1.3	5.6 ± 0.8
K_A ($\times 10^7$ M^{-1})	31.8 ± 6.5	1.4 ± 0.3
K_D (nM)	3.4 ± 0.7	78.3 ± 15.7

[1] k_a: association rate constant, k_d: dissociation rate constant, K_A: association constant, and K_D: dissociation constant. All the kinetic values were obtained by averaging three independent runs of SPR measurements, presented as averages ± standard deviations.

higher than those of sLe^x by an order of magnitude. Based on the ratio of the directly measured binding parameters, especially the dissociation constants, we have found that the binding affinity of CD24 with E-selectin is stronger than that of sLe^x by approximately 20 fold.

3.3.2. Cellular responses on selectin- and anti-EpCAM-functionalized surfaces

We then investigated how the measured binding parameters correlate with cell interactions with various proteins on surfaces under flow using a parallel plate flow chamber. As shown in our previous report, no interactions were observed between MCF-7 cells and P-selectin [20]. Although CD24 is known as a P-selectin ligand, it requires modification by mechanical enzymes to bind to P-selectin, which requires sLe^x decoration [22, 38]. This can explain the lack of interaction between sLe^x-deficient MCF-7 cells and P-selectin [20]. **Fig. 3.6** shows the surface interactions of MCF-7 cells with E-selectin and anti-EpCAM. The cell interactions with each of

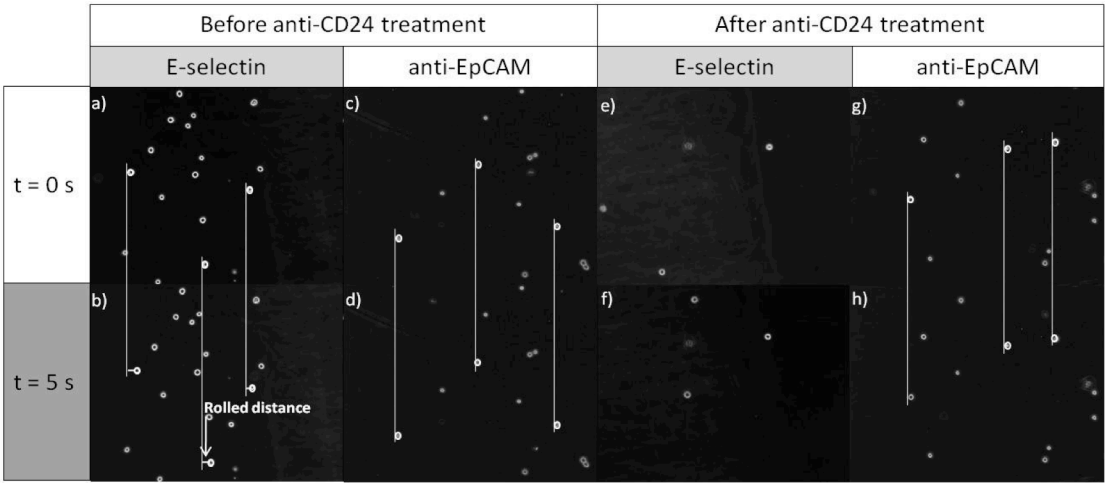

Figure 3.6. Time-course images of MCF-7 cells under shear stress of 0.08 dyn/cm^2 on E-selectin and anti-EpCAM-immobilized surfaces. Untreated MCF-7 cells exhibit the rolling behavior on the E-selectin-coated surface at a velocity of 2.76 ± 0.16 μm/sec (a and b) while being stationary bound on the anti-EpCAM-coated surface (c and d). Upon treatment with anti-CD24, the interaction of MCF-7 cells with E-selectin is disappeared (e and f) whereas the binding with anti-EpCAM is not affected (g and h). Flow direction is from left to right.

the individual proteins in **Fig. 3.6a-d** were compared to those of the anti-CD24-treated MCF-7 cells in **Fig. 3.6e-h**. Images of the cells on each surface were taken at t = 0 s (a randomly chosen time to begin recording during the flow experiment) and at t = 5 s to observe any dynamic cell response such as cell rolling. Untreated MCF-7 cells exhibited the rolling response on E-selectin and stationary adhesion on anti-EpCAM. The average rolling velocity of MCF-7 cells was 2.8 ± 0.2 μm/sec on E-selectin-immobilized slides at a wall shear stress of ~0.1 dyn/cm^2. Upon anti-CD24 treatment, the rolling behavior of MCF-7 cells on E-selectin was completely interrupted (**Fig. 3.6e and f**), while the responses of MCF-7 cells on anti-EpCAM remained the same (**Fig. 3.6g and h**), i.e. stationary binding with anti-EpCAM. The directly measured binding kinetics between CD24 and E-selectin using Biacore, along with the ceased rolling of MCF-7 cells upon anti-CD24 treatment, confirms that CD24 is a mediator for the MCF-7 cell rolling.

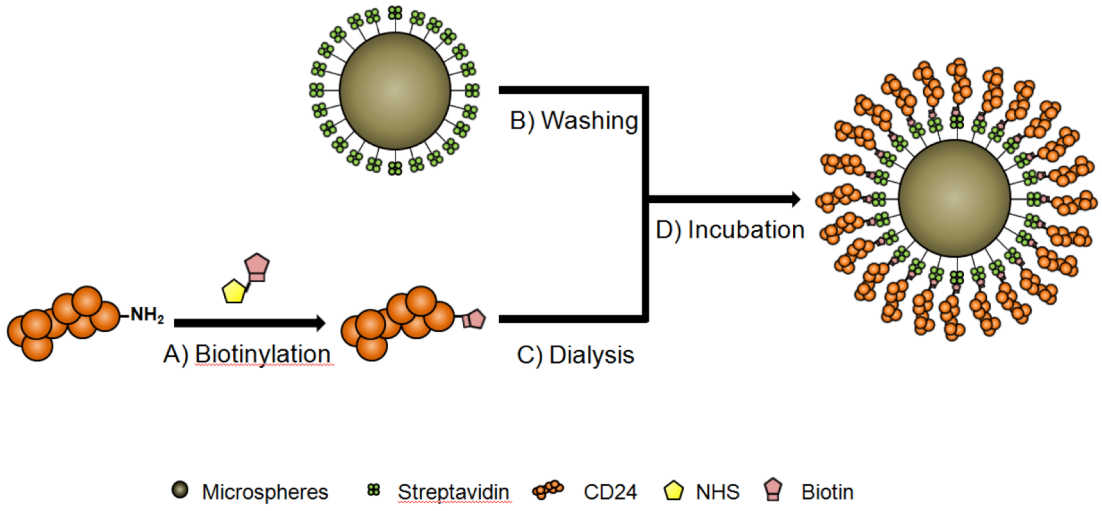

Figure 3.7. Preparation of CD24-coated microspheres. a) biotinylation of recombinant human CD24, b) pre-washing of streptavidin-coated microspheres, c) purification of the biotinylated CD24 using dialysis, and d) incubation of the biotinylated CD24 with streptavidin-coated microspheres.

3.3.3. Interactions of microspheres on the surfaces functionalized with E-selectin

To assess if CD24 is solely responsible for binding and rolling of the MCF-7 cells, CD24-coated microspheres were prepared for a flow-chamber experiment (**Fig. 3.7**). Microspheres functionalized with sLe^x were also prepared according to the previous report and used as a control group [35]. The coating of CD24 on microspheres (10 μm in diameter) was also confirmed using FACS following the same method described above, as shown in **Fig. 3.3**. The streptavidin-coated microspheres (negative control) showed the lowest fluorescence intensity, and the isotype control showed a slightly higher intensity than the negative control. A significantly higher intensity was observed from the CD24-coated microspheres, indicating that CD24 was successfully immobilized on the microsphere surfaces. Note that the streptavidin-immobilized microspheres (without CD24 or sLe^x) had no non-specific binding with immobilized E-selectin (**Fig. 3.4a and b**).

CD24- and sLe^x-coated microspheres exhibited different behaviors on the E-selectin-immobilized slides. As shown in **Fig. 3.8**, CD24-coated microspheres exhibited stationary binding to E-selectin, whereas sLe^x-coated microspheres exhibited the stable rolling response on E-selectin at a velocity of 0.4 μm/sec, which is consistent with the previous report [35]. The stationary adhesion of CD24 microspheres as opposed to the dynamic rolling of sLe^x microspheres can be explained by the significantly higher affinity between CD24 and E-selectin than sLe^x-based binding by ~20 fold, as measured by SPR. Additionally, in a Ca^{2+}-deficient PBS buffer, the CD24 and sLe^x-coated microspheres did not bind to E-selectin (**Fig. 3.4c and d**), indicating that the interaction of both CD24 and sLe^x with E-selectin is Ca^{2+} dependent.

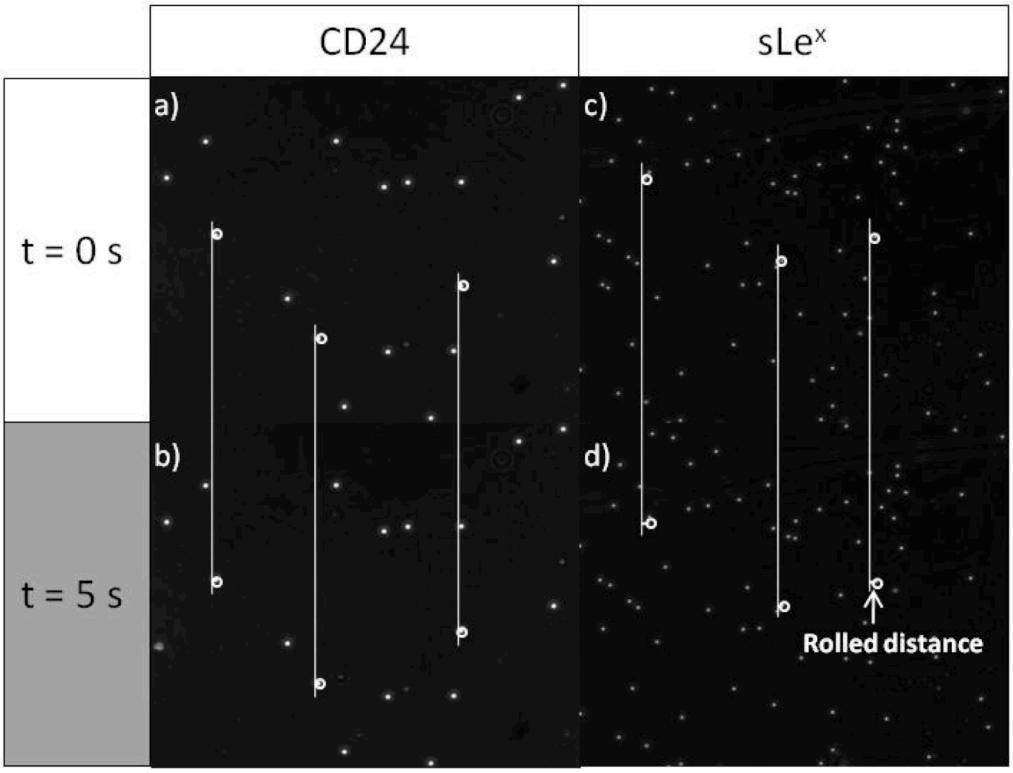

Figure 3.8. Time-course images of microspheres that are coated with (a and b) CD24 and (c and d) sLe^x under shear stress of 0.08 dyn/cm^2 on E-selectin-immobilized surfaces. CD24-coated microspheres are statically bound on E-selectin-immobilized surface, but sLe^x-coated microspheres exhibit the rolling behavior on E-selectin (0.44 ± 0.02 μm/sec). Flow direction is from left through right.

3.3.4. Actin filament dynamics for the cell rolling behavior

Our results so far still remain a question why CD24-coated microspheres bind statically (**Fig. 3.8**) unlike MCF-7 cells that exhibit rolling (**Fig. 3.6**) on the E-selectin-immobilized surface. This may be explained by the role of intracellular dynamics of the live cells. Given that actin filament dynamics are known to be involved in P-selectin-mediated rolling [39], we investigated the effect of the actin filaments on MCF-7 cell rolling. CytoD is a cell permeable inhibitor of actin polymerization, resulting in disruption of actin network organization [40], which alters the rolling response of neutrophiles on P-selectin to the stationary adhesion [39]. MCF-7 cells were incubated with various concentrations of cytoD ranging from 10 to 40 μM for 30 min and 60 min, and the rolling velocity ratios (the velocity of treated cells to that of untreated cells on E-selectin)

as a function of shear stress were measured. After treating the cells with cytoD at a concentration of 40 μM for 60 min, the rolling velocity was significantly reduced to less than half of that of untreated cells (**Fig. 3.9**), suggesting that actin filament dynamics play a role in the rolling process. Intracellular dynamics are known to be involved in various cellular interactions with adhesive molecules. Actin filament polymerization is one of the factors that affect cell morphology [33] and cellular behaviors (e.g. cell migration [41]) and intercellular interactions between cancer cells and endothelial cells [42]). In our experiments, cytoD-treated MCF-7 cells exhibited an increased adhesion, i.e. the decreased rolling velocities (**Fig. 3.9**). Therefore, actin

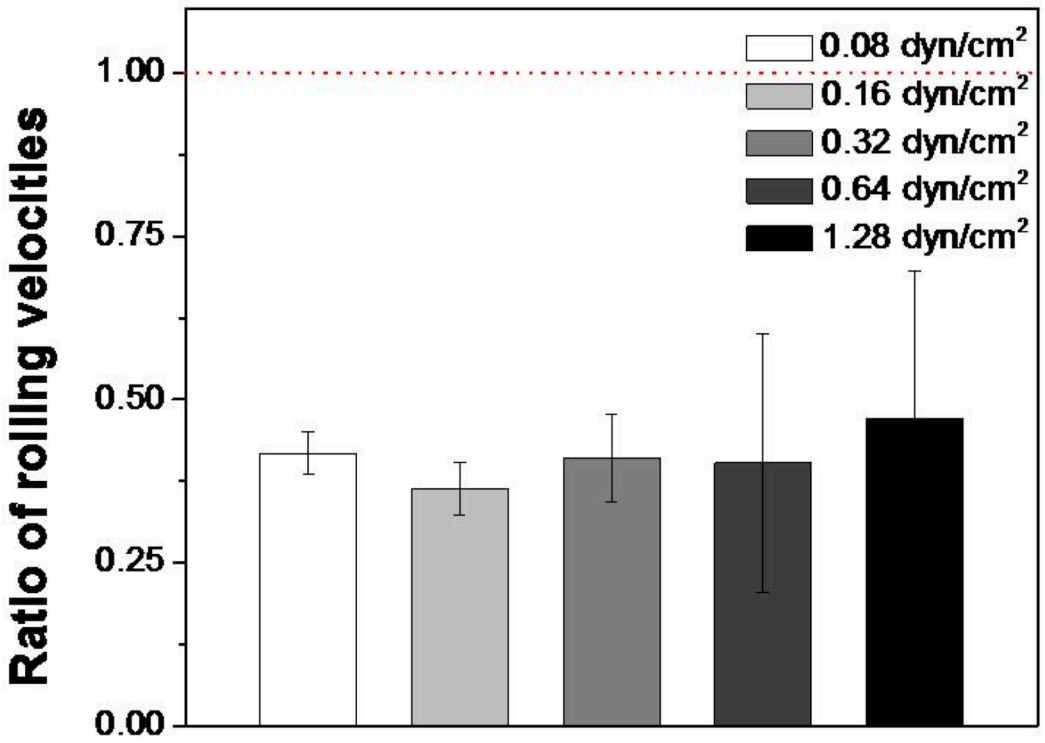

Figure 3.9. Ratios of rolling velocities of cytoD-treated MCF-7 cells to those of untreated cells on E-selectin-immobilized surfaces. MCF-7 cells were treated with 40 μM of cytoD for 30 min. The dotted red line (ratio 1) indicates the rolling velocity of the untreated MCF-7 cells. Note that the rolling velocities of the treated MCF-7 cells are significantly reduced in a shear stress independent manner. Error bars: standard error (n=120).

filament dynamics could be one factor that can control the intercellular interactions, which could explain the different behavior of the CD24-coated microspheres from MCF-7 cells with E-selectin. This can be further supported by the case of human colorectal carcinoma cells (HT-29), where it was reported that the adhesion between cells and the adhesive molecules became tight under dynamic condition after disruption of actin filaments [42].

3.4. SUMMARY

In summary, this chapter reports the specific interaction between CD24 and E-selectin, which is confirmed by: i) the direct measurements of the binding kinetics of CD24 by SPR (**Fig. 3.5**); ii) the observed interruption of rolling of MCF-7 cells upon treatment with anti-CD24 (**Fig. 3.6**); and iii) the specific binding of CD24-coated microspheres on E-selectin (**Fig. 3.8 and 3.9**). The identification of CD24 as a ligand for E-selectin will help to better understand the adhesion and invasion mechanisms of potentially metastatic cancer cells. For example, using CD24-mediated cell rolling on E-selectin-immobilized devices, CD24-positive and negative cancer cells may be separated without staining based on different binding and rolling behaviors that are reflected by CD24 expression. Further, in a similar way to several publications [43, 44], CD24- and sLe^x-coated microspheres may be utilized to inhibit E-selectin-mediated cell adhesion (cell migration antagonists), which can be potentially used as treatment of inflammatory diseases and metastatic cancer.

3.5. REFERENCES

1. Psaila, B. and D. Lyden, *The metastatic niche: adapting the foreign soil.* Nat Rev Cancer, 2009. **9**(4): p. 285-93.
2. Steeg, P.S., *Tumor metastasis: mechanistic insights and clinical challenges.* Nat Med, 2006. **12**(8): p. 895-904.
3. Kohler, S., et al., *E-/P-selectins and colon carcinoma metastasis: first in vivo evidence for their crucial role in a clinically relevant model of spontaneous metastasis formation in the lung.* Br J Cancer, 2009.
4. Miles, F.L., et al., *Stepping out of the flow: capillary extravasation in cancer metastasis.* Clin Exp Metastasis, 2008. **25**(4): p. 305-24.
5. McEver, R.P., *Selectins: novel receptors that mediate leukocyte adhesion during inflammation.* Thromb Haemost, 1991. **65**(3): p. 223-8.
6. Kansas, G.S., *Selectins and their ligands: current concepts and controversies.* Blood, 1996. **88**(9): p. 3259-87.
7. Shaker, O.G., et al., *Gene expression of E-selectin in tissue and its protein level in serum of breast cancer patients.* Tumori, 2006. **92**(6): p. 524-30.
8. Dimitroff, C.J., et al., *Rolling of human bone-metastatic prostate tumor cells on human bone marrow endothelium under shear flow is mediated by E-selectin.* Cancer Res, 2004. **64**(15): p. 5261-9.
9. Fang, X., et al., *CD24: from A to Z.* Cell Mol Immunol, 2010. **7**(2): p. 100-3.
10. Barthel, S.R., et al., *Targeting selectins and selectin ligands in inflammation and cancer.* Expert Opin Ther Targets, 2007. **11**(11): p. 1473-91.
11. Tozeren, A., et al., *E-selectin-mediated dynamic interactions of breast- and colon-cancer cells with endothelial-cell monolayers.* Int J Cancer, 1995. **60**(3): p. 426-31.

12. Steegmaier, M., et al., *The E-selectin-ligand ESL-1 is a variant of a receptor for fibroblast growth factor.* Nature, 1995. **373**(6515): p. 615-20.

13. Aeed, P.A., et al., *Partial characterization of the N-linked oligosaccharide structures on P-selectin glycoprotein ligand-1 (PSGL-1).* Cell Res, 2001. **11**(1): p. 28-36.

14. Zou, X., et al., *PSGL-1 derived from human neutrophils is a high-efficiency ligand for endothelium-expressed E-selectin under flow.* Am J Physiol Cell Physiol, 2005. **289**(2): p. C415-24.

15. Varki, N.M. and A. Varki, *Diversity in cell surface sialic acid presentations: implications for biology and disease.* Lab Invest, 2007. **87**(9): p. 851-7.

16. Thurin, M. and T. Kieber-Emmons, *SA-Lea and tumor metastasis: the old prediction and recent findings.* Hybrid Hybridomics, 2002. **21**(2): p. 111-6.

17. Matsumoto, M., et al., *CD43 collaborates with P-selectin glycoprotein ligand-1 to mediate E-selectin-dependent T cell migration into inflamed skin.* J Immunol, 2007. **178**(4): p. 2499-506.

18. Moser, M., et al., *Kindlin-3 is required for beta2 integrin-mediated leukocyte adhesion to endothelial cells.* Nat Med, 2009. **15**(3): p. 300-5.

19. Zen, K., et al., *CD44v4 is a major E-selectin ligand that mediates breast cancer cell transendothelial migration.* PLoS ONE, 2008. **3**(3): p. e1826.

20. Myung, J.H., et al., *Enhanced tumor cell isolation by a biomimetic combination of E-selectin and anti-EpCAM: implications for the effective separation of circulating tumor cells (CTCs).* Langmuir, 2010. **26**(11): p. 8589-96.

21. Aigner, S., et al., *CD24, a mucin-type glycoprotein, is a ligand for P-selectin on human tumor cells.* Blood, 1997. **89**(9): p. 3385-95.

22. Aigner, S., et al., *CD24 mediates rolling of breast carcinoma cells on P-selectin.* Faseb J, 1998. **12**(12): p. 1241-51.

23. Pirruccello, S.J. and T.W. LeBien, *The human B cell-associated antigen CD24 is a single chain sialoglycoprotein.* J Immunol, 1986. **136**(10): p. 3779-84.

24. Kristiansen, G., M. Sammar, and P. Altevogt, *Tumour biological aspects of CD24, a mucin-like adhesion molecule.* J Mol Histol, 2004. **35**(3): p. 255-62.

25. Lim, S.C., *CD24 and human carcinoma: tumor biological aspects.* Biomed Pharmacother, 2005. **59 Suppl 2**: p. S351-4.

26. Baumhoer, D., et al., *Expression of CD24, P-cadherin and S100A4 in tumors of the ampulla of Vater.* Mod Pathol, 2009. **22**(2): p. 306-13.

27. Kim, M.H., et al., *Response of human epithelial cells to culture surfaces with varied roughnesses prepared by immobilizing dendrimers with/without D-glucose display.* J Biosci Bioeng, 2007. **103**(2): p. 192-9.

28. Baumann, P., et al., *CD24 expression causes the acquisition of multiple cellular properties associated with tumor growth and metastasis.* Cancer Res, 2005. **65**(23): p. 10783-93.

29. Fogel, M., et al., *CD24 is a marker for human breast carcinoma.* Cancer Lett, 1999. **143**(1): p. 87-94.

30. Kim, J.B., et al., *CD24 cross-linking induces apoptosis in, and inhibits migration of, MCF-7 breast cancer cells.* BMC Cancer, 2008. **8**: p. 118.

31. Hong, S., et al., *The binding avidity of a nanoparticle-based multivalent targeted drug delivery platform.* Chem Biol, 2007. **14**(1): p. 107-15.

32. Nilsson, R. and H.O. Sjogren, *Antigen-independent binding of rat immunoglobulins in a radioimmunoassay. Solutions to an unusual background problem.* J Immunol Methods, 1984. **66**(1): p. 17-25.

33. Stevenson, B.R. and D.A. Begg, *Concentration-dependent effects of cytochalasin D on tight junctions and actin filaments in MDCK epithelial cells.* J Cell Sci, 1994. **107 (Pt 3)**: p. 367-75.

34. Hong, S., et al., *The Role of Ganglioside GM(1) in Cellular Internalization Mechanisms of Poly(amidoamine) Dendrimers.* Bioconjug Chem, 2009.

35. Hong, S., et al., *Covalent immobilization of p-selectin enhances cell rolling.* Langmuir, 2007. **23**(24): p. 12261-8.

36. Goldman, A.J., R.G. Cox, and H. Brenner, *Slow viscous motion of a sphere parallel to a plane wall--II Couette flow.* Chemical Engineering Science, 1967. **22**(4): p. 653-660.

37. Kim, H.J., et al., *Isolation of CD24(high) and CD24(low/-) cells from MCF-7: CD24 expression is positively related with proliferation, adhesion and invasion in MCF-7.* Cancer Lett, 2007. **258**(1): p. 98-108.

38. Lawrence, M.B., *Selectin-carbohydrate interactions in shear flow.* Curr Opin Chem Biol, 1999. **3**(6): p. 659-64.

39. Sheikh, S. and G.B. Nash, *Treatment of neutrophils with cytochalasins converts rolling to stationary adhesion on P-selectin.* J Cell Physiol, 1998. **174**(2): p. 206-16.

40. Schliwa, M., *Action of cytochalasin D on cytoskeletal networks.* J Cell Biol, 1982. **92**(1): p. 79-91.

41. Hayot, C., et al., *Characterization of the activities of actin-affecting drugs on tumor cell migration.* Toxicol Appl Pharmacol, 2006. **211**(1): p. 30-40.

42. Haier, J. and G.L. Nicolson, *Role of the cytoskeleton in adhesion stabilization of human colorectal carcinoma cells to extracellular matrix components under dynamic conditions of laminar flow.* Clin Exp Metastasis, 1999. **17**(8): p. 713-21.

43. Mackay, C.R., *Moving targets: cell migration inhibitors as new anti-inflammatory therapies.* Nat Immunol, 2008. **9**(9): p. 988-98.

44. Stahn, R., et al., *Multivalent sialyl Lewis x ligands of definite structures as inhibitors of E-selectin mediated cell adhesion.* Glycobiology, 1998. **8**(4): p. 311-19.

CHAPTER 4

DENDRIMER-MEDIATED MULTIVALENT BINDING FOR ENHANCED CAPTURE OF TUMOR CELLS

4.1. INTRODUCTION

Multivalent binding, the simultaneous binding of multiple ligands to multiple receptors, has played a central role in a number of pathological processes, including the attachment of viral, parasitic, mycoplasmal, and bacterial pathogens [1-3]. These biological activities have been extensively investigated to promote targeting of specific cell types [4-8], and biological multivalent inhibitors have yielded significant increases in binding avidities by 1-9 orders of magnitude [9-11]. In particular, nano-scale poly(amidoamine) (PAMAM) dendrimers have been reported to be an excellent mediator for facilitated multivalent effect due to their capability to pre-organize/orient ligands and easy deformability of the polymer chains [4].

PAMAM dendrimers have not been used only as a nanocarrier in a drug delivery system, but also as a scaffold to enhance the surface properties, such as stability and sensitivity, for DNA microarray and for cell culture *in vitro* [12-15]. For example, the PAMAM dendrimer-immobilized microarray mediates higher immobilization efficiency of amino-modified DNA-oligomers by 10-fold, up to 9-fold higher detection sensitivity of the target oligonucleotides from the solution, and a remarkable high stability during up to 10-time regeneration, than with other DNA microarrays [12]. The PAMAM dendrimer-immobilized surfaces also enhance the cell adhesion onto the treated surfaces, resulting to a promising scaffold to culture cells *in vitro* in tissue engineering [14]. However, no research that used dendrimer-immobilized surfaces to capture whole cells has been reported.

We hypothesized that the advantages of enhanced binding avidity through dendrimer-mediated multivalent effect could significantly improve detection of human disease-related rare cells (<0.1% subpopulation) such as circulating tumor cells (CTCs) in peripheral blood. Given the extreme rareness of CTCs (as few as one out of a billion hematologic cells), a very sensitive, specific detection is obviously necessary to achieve clinically significant CTC detection. Many efforts to increase sensitivity of CTC devices have been reported, mostly based upon engineering, such as topographical modifications [16, 17] and chaotic mixer fluidics [18, 19].

In this chapter, we have investigated a new approach to exploit naturally occurring processes using nanotechnology, i.e., biomimetic nanotechnology. To create a highly sensitive surface utilizing the multivalent effect, we have employed generation 7 (G7) PAMAM dendrimers and anti-epithelial-cell-adhesion-molecule (aEpCAM), as illustrated in **Fig. 4.1**. Note that aEpCAM is one of the most commonly used CTC capturing agents [16, 18, 20] as EpCAM is often expressed by CTCs but not by normal hematological cells [17, 21, 22]. G7 PAMAM dendrimers were chosen due to their adequate size (8-10 nm in diameter) and number of surface functional groups (512 theoretically) to accommodate multiple aEpCAM (around 5.5 nm in

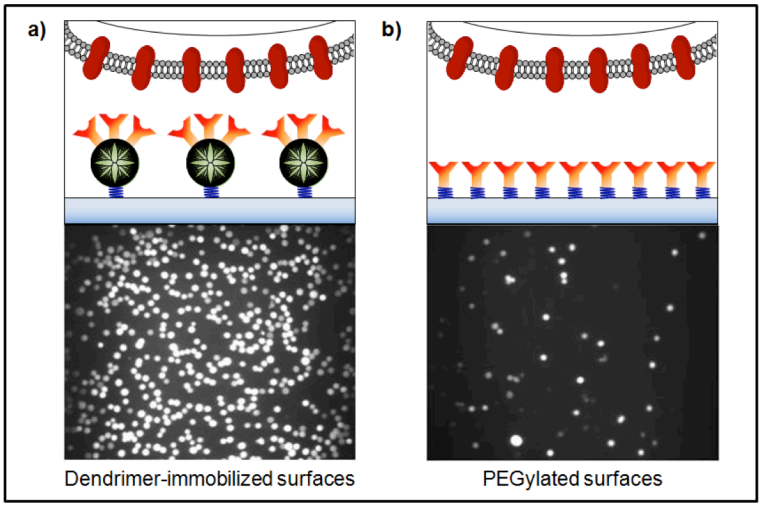

Figure 4.1. Schematic illustration and fluorescence images of tumor cell capture using aEpCAM on a) dendrimer (a)- and b) linear polymer-immobilized surfaces.

diameter of Fc region) per dendrimer, thereby enabling multivalent binding. In addition, another physiological process cell rolling mediated by E-selectin, mimicking the initial CTC recruiting process to the endothelia [23, 24], has been also implemented to our device to further enhance surface sensitivity and specificity towards tumor cells.

4.2. MATERIALS AND METHOD

4.2.1. Materials

PAMAM dendrimer (Generation 7, theoretical MW 116,488 Da), Deuterium Oxide (99.9 atom % D, D_2O), 1-ethyl-3-(3-dimethylaminopropyl) carbodiimide (EDC), and *N*-hydroxysuccinimide (NHS) were obtained from Sigma-Aldrich (St. Louis, MO) and used without further purification. All other chemicals, unless otherwise specified, were also purchased from Sigma-Aldrich and used without further purification.

4.2.2. Synthesis of G7 PAMAM Dendrimer Derivatives

The synthetic steps of dendrimer derivatives were performed using a slightly modified protocol from previous publications [4, 25], as illustrated in **Figure 4.2**.

4.2.2.1. Carboxylation of G7 PAMAM dendrimers

G7 PAMAM dendrimers (G7-$(NH_2)_{512}$) were first purified by ultracentrifugation using an Amicon® Ultra (MWCO = 50,000, Millipore, Billerica, MA) as described earlier [4, 25]. The purified G7 PAMAM dendrimers were partially carboxylated, in order to use the carboxylic ends and the remaining amine ends for aEpCAM conjugation and surface immobilization, respectively. Briefly, G7-$(NH_2)_{512}$ (56 mg, 0.48 μmol) were dissolved in 2 mL DMSO, and reacted with 24.6 mg succinic anhydride (245.6 μmol, 1:1 molar ratio) under vigorous stirring overnight. For completely carboxylated G7 dendrimers (G7-$(COOH)_{512}$), ten times excess molar ratio of

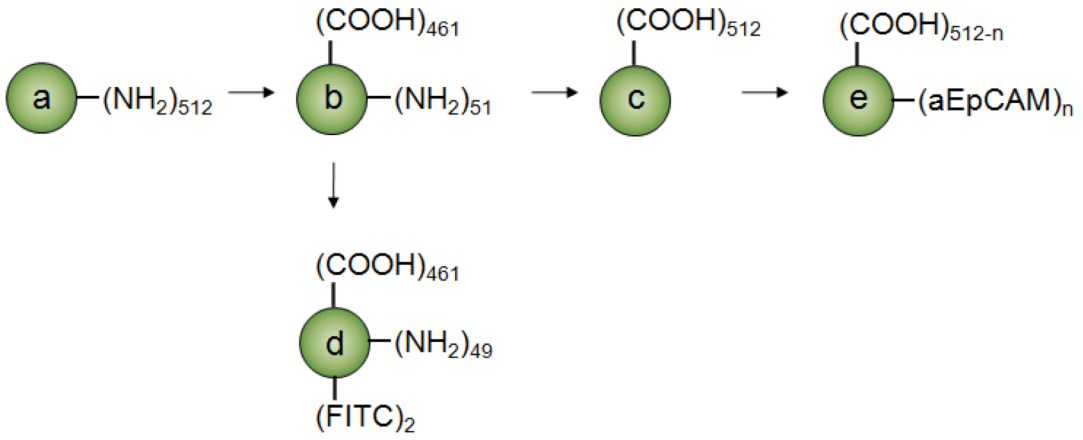

Figure 4.2. Surface modification and functionalization of G7 PAMAM dendrimers. a) starting G7 PAMAM dendrimer with primary amine end groups (G7-$(NH_2)_{512}$); b) partially carboxylated G7 PAMAM dendrimer (G7-$(COOH)_{461}$); c) completely carboxylated G7 PAMAM dendrimer (G7-$(COOH)_{512}$); d) G7-FITC conjugate (G7-$(COOH)_{461}$-$(FITC)_2$); and e) G7-aEpCAM conjugate (G7-$(COOH)_{512-n}$-$(aEpCAM)_n$, n = 2.8 or 4.9).

succinic anhydride (66 mg, 660 µmol) was added to G7-$(NH_2)_{512}$ (15 mg, 128.8 nmol) in 2 mL DMSO. The resulting G7-$(COOH)_{512}$ were dialyzed in deionized distilled (DDI) water for two days to remove the unreacted succinic anhydride as well as organic solvent, and obtained as powder by lyophilization (Labconco FreeZone 4.5 system (Kansas City, MO)). The partially carboxylated dendrimers (G7-$(COOH)_{461}$) were further reacted with fluorecein isothiocyanate (FITC) and aEpCAM as described in the following sections. The completely carboxylated dendrimers were used to make the dendrimer-aEpCAM conjugates for the subsequent SPR measurements.

4.2.2.2. Conjugation of fluorescein to dendrimers

To employ fluorescence-based techniques for confirmation of the dendrimer immobilization on the surfaces, fluorescein-conjugated dendrimers (G7-$(COOH)_{461}$-$(FITC)_2$) were synthesized through reaction between partially carboxylated dendrimers and FITC [6]. G7-

$(COOH)_{461}$ (24 mg, 0.2 μmol) were dissolved in 2 mL of DMSO, and reacted with 1.4 mg FITC (3.6 μmol) under vigorous stirring overnight. The FITC-conjugated dendrimers were recovered from DMSO solution via dialysis against DDI water for two days, followed by lyophilization.

4.2.3. Synthesis of Dendrimer-aEpCAM Conjugates

To measure binding kinetics of free aEpCAM and the dendrimer-aEpCAM conjugates using SPR, two dendrimer conjugates at different molar ratios of aEpCAM were prepared. The completely carboxylated dendrimers (0.01 mg, 86 pmol) were dissolved in 2 mL PBS buffer, and the carboxylic ends of the dendrimers were activated using EDC (920 ng, 4.3 nmol, 50 molar excess) and NHS (940 ng, 4.3 nmol, 50 molar excess) for 1 hr. The activated dendrimers were divided into two vials, and each was reacted with aEpCAM at 204 pmol (4.8 molar excess) and at 102 pmol (2.4 molar excess), respectively, under vigorous stirring overnight. The dendrimer-aEpCAM conjugates were purified by dialysis (Slide-A-Lyzer® mini dialysis units with 10,000 MWCO, Thermo scientific, Rockford, IL) in DDI water overnight and lyophilized [4, 25].

4.2.4. SPR Measurements of Free aEpCAM and the Dendrimer-aEpCAM Conjugates

Recombinant human EpCAM/TROP1 Fc chimera (EpCAM) was purchased from R&D systems (Minneapolis, MN). BIAcore® X instrument (GE Healthcare, Pittsburgh, PA) was used for quantitative and direct measurements of the binding kinetics of free aEpCAM and the dendrimer-aEpCAM conjugates to EpCAM at 25°C. EpCAMs were immobilized on CM5 sensor chips (GE Healthcare) using the amine coupling kit (GE Healthcare) as described earlier [26]. Briefly, 0.2 μL of EpCAM stock solution (1 mg/mL in PBS) was diluted in 149.8 μL of sodium acetate buffer (immobilization buffer, 10 mM, pH 5.0). The protein solution (40 μL) was then injected into the channel 2 of a sensor chip CM5 that was pre-activated by 70 μL of a 1:1 mixture of EDC and NHS. The remaining reactive ester residues were blocked by the injection of 70 μL

ethanolamine (pH 8.5). All protein immobilizations were carried out at a flow rate of 5 μL/min using HBS-EP buffer.

Prior to the binding assays between EpCAM and free aEpCAM or the dendrimer-aEpCAM conjugates, 80 μL of the completely carboxylated dendrimers (a negative control) in HBS-EP buffer at a concentration of 43 nM were injected into the two channels (channel 2 with EpCAM and channel 1 as reference) at a flow rate of 30 μL/min.

The binding kinetic parameters of the dendrimer-aEpCAM conjugates (G7-$(aEpCAM)_{2.8}$ and G7-$(aEpCAM)_{4.9}$) with surface-immobilized EpCAM were measured using BIAcore® X and compared to those of free aEpCAM using a similar protocol as we previously described [4, 26]. All SPR measurements were performed at 25 ºC. Free aEpCAM and the dendrimer-aEpCAM conjugates (G7-$(aEpCAM)_{2.8}$ and G7-$(aEpCAM)_{4.9}$) were diluted at a series of concentrations (6-170 μg/mL) using HBS-EP buffer. As described above, 80 μL of free aEpCAM or dendrimer-aEpCAM conjugates were injected into the two channels at a flow rate of 30 μL/min at 25 °C. After obtaining the binding curves, the sensor chip surface was regenerated using Glycin-HCl (10 mM, pH 2.0 or pH 2.5) buffer for further experiments. All sensorgrams were recorded from the start of the injection to the end of the dissociation phase, and were shifted to adjust the baseline resonance level.

4.2.5. Preparation of Dendrimer-aEpCAM-immobilized Surfaces

Three different types of surfaces were functionalized by conjugation with aEpCAM: i) epoxy-functionalized surfaces; ii) PEGylated surfaces; and iii) G7 PAMAM dendrimer-immobilized surfaces. Briefly, an epoxy-functionalized glass slide ((SuperEpoxy2®, TeleChem International, Inc (Sunnyvale, CA)) was defined as 5 mm (L) × 5 mm (W) by a polydimethylsiloxane (PDMS) gasket, followed by direct conjugation with aEpCAM [23]. For PEGylated surface, the epoxy surface defined by PDMS were incubated with PEG (NH_2-

$(PEG)_{5000}$-COOH, Nektar Therapeutics (Huntsville, AL)) at a concentration of 0.5 μg/mL in DDI water, followed by conjugation with aEpCAM after activation using 1:1 mixture of 1-ethyl-3-(3-dimethylaminopropyl) carbodiimide (EDC) and *N*-hydroxysuccinimide (NHS) for 1 hr. The dendrimer-coated surfaces were prepared on the PEGylated surfaces. After activation of carboxylic termini of PEG using 1:1 mixture of EDC/NHS, partially carboxylated G7 PAMAM dendrimers (50 μM in PBS buffer (pH 9.0)) were immobilized on the surface [17]. The dendrimers immobilized on the surface were then activated using EDC/NHS, followed by conjugation with aEpCAM. For aEpCAM conjugation on all surfaces, a concentration of 5 μg/mL in PBS and overnight incubation were used. For investigation on the combination effect of cell rolling and multivalent effect, all three EpCAM-coated surfaces were further treated with 5 μg/mL of E-selectin (R&D system) in PBS for 4 hrs. All surface functionalization reactions were carried out at room temperature with constant gentle shaking. The volumes of all reagent solutions were fixed at 40 μL, and the surfaces between each step were washed with DDI water three times to remove the extra reagents from the surfaces. Potential non-specific binding on the surfaces was blocked by 1% (w/v) BSA solution. The functionalized surfaces were immediately used for subsequent experiments or stored at 4 ºC no longer than 1 week before use.

4.2.6. Characterization of Dendrimer-aEpCAM-immobilized Surfaces

The immobilization of dendrimers and aEpCAM on the surface was confirmed by fluorescence intensity analysis using fluorescein-conjugated dendrimers and monoclonal human EpCAM-allophycocyanin (aEpCAM-APC) and X-ray photoelectron spectroscopy (XPS).

Surface immobilization of dendrimers and free aEpCAM was confirmed by fluorescence intensity analysis. A general process of the surface characterization was described in our previous report [23]. The presence of dendrimers on the surface was confirmed by observing green fluorescence from FITC-conjugated dendrimers. Monoclonal human EpCAM-

Allophycocyanin (aEpCAM-APC, red fluorescence) was used instead of non-fluorescent aEpCAM to visualize the immobilized aEpCAM by fluorescence. All slides were then covered using Vectashield® mounting medium (Vector laboratories, Inc., Burlingame, CA), and air bubbles in the mounting medium were gently removed by applying pressure to the cover slides. The fluorescence images were taken using an Olympus IX70 inverted microscope using a 10× objective and filters for FITC (450 nm excitation and 535 nm emission) and APC (560 nm excitation and 645 nm emission). For each image, 5 regions of equal size were randomly selected, and the total pixel intensity values within these regions were acquired using ImageJ (NIH).

The functionalized surfaces were characterized using XPS as described in our previous report [23]. Axis 165 X-ray photoelectron spectrometer (Kratos Analytical, Manchester, U.K.) equipped with a monochromatic AlKα source (hv = 1486.6 eV, 150W) and a hemispherical analyzer was used. The % mass concentrations were obtained from high-resolution spectra of the C 1s, O 1s, N 1s, and S 2p regions at an X-ray irradiating angle of 30° with pass energy of 80 eV and a step size of 0.5 eV, carried on 5 scans per spectrum.

4.2.6. Cell culture and Cell treatment

All cell lines were purchased from ATCC (Manassas, VA). MCF-7 cells were cultured in DMEM media supplemented with 10% (v/v) FBS and 1% (v/v) penicillin/streptomycin (P/S) in a humidified incubator at 37 °C and 5% CO_2. HL-60 cells were grown in IMDM media supplemented with 20% (v/v) FBS and 1% (v/v) P/S under same conditions of incubation for MCF-7 cells. MDA-MB-231 and MDA-MB-361 cells were cultured in Leibovitz's L-15 media supplemented with 1% (v/v) P/S and 10 or 20% (v/v) FBS, respectively, in a humidified incubator at 37 °C without CO_2. Prior to the various cell experiments, 5 mL of cell suspensions at a concentration of 10^6 cells/mL were seeded into 25cm^2 T flask one day before the experiment. The seeded cells were treated with 4 μM Calcein AM in PBS in the incubator for 30 min to

fluorescently label viable cells for cell experiments. The Calcein AM-labeled cells were trypsinized to create cell suspensions at a concentration of 10^6 cells/mL in PBS. The final suspensions were kept on ice throughout the subsequent cell experiments.

4.2.6. Cell adhesion on the functionalized surfaces under static agitation

A dendrimer-immobilized surface and a PEGylated surface were located vertically within one PDMS gasket (15 mm (L) × 10 mm (W), **Fig. 4.1**), and treated with aEpCAM simultaneously under the same condition. The defined surfaces were then incubated with cell suspensions (250 μL of 10^6 cells/mL in PBS buffer) at 37 ºC, under 5% CO_2 for MCF-7 and 0% CO_2 for MDA-MB-361 and 231 cells, for 10 min. For the regression assay, 10-1000 of Calcein AM-labeled MDA-MB-361 cells in 40 μL of PBS buffer with HL-60 cells (0 or 10^7 cells per each surface) were applied on each functionalized surface defined by a PDMS gasket (5 mm (L) × 5 mm (W)). After removing non-adhered cells, the surfaces were placed on a petri dish with grid, and 30 sequential images of each functionalized surface were taken under a fluorescent light (ex. 490 nm/em. 520 nm) to count the numbers of the bound tumor cells. To observe the binding stability between the cells and the surfaces, the cells adhered on the surfaces were counted at 0, 1, 2, 5, 10 and 30 min time points during static agitation using a plate shaker at 600 rpm at room temperature.

All cells on the surface were monitored and the images were recorded at 10X magnification using an Olympus IX70 inverted microscope equipped with a fluorescence illuminator (IX 70-S1F2, Olympus America, Inc., Center Valley, PA) and a CCD camera (QImaging Retiga 1300B, Olympus America, Inc.). The cells bound on the surfaces in the images were counted using ImageJ (NIH). The measured recovery yields of the dendrimer-immobilized surfaces were statistically analyzed by comparing to those of the PEGylated surfaces

using one-factor ANOVA (SPSS software, Chicago, IL) with 95% simultaneous confidence intervals.

4.2.7. Surface Characterization after E-selectin Treatment by Immunostaining

Surface functionalization by E-selectin and non-fluorescent aEpCAM was confirmed using monoclonal anti-E-selectin-fluorescein (aE-selectin-fluorescein, green fluorescence, R&D system). A general process of the surface characterization is described in our previous report [23], and again in the section 4.2.6 (Characterization of Dendrimer-aEpCAM-immobilized Surfaces). The fluorescence intensities of the surfaces were summarized with images after normalization using the intensities of a positive control (E-selectin-immobilized epoxy functionalized surfaces).

4.2.8. Flow chamber experiments for cell binding strength comparison under flow

All three functionalized surfaces, i.e., epoxy-functionalized, PEGylated, and dendrimer-immobilized surfaces (defined by a 5 mm (L) × 5 mm (W) PDMS gasket for each), were prepared on one glass slide, followed by aEpCAM conjugation using the same condition as above. The functionalized glass slide along with a gasket (30 mm (L) × 10mm (W) × 0.25 mm (D)) was assembled into a flow chamber [23]. Calcein AM-labeled cell suspensions (all three cell lines) at a concentration of 10^5 cells/mL were injected at a flow rate of 50 μL/min (0.08 dyn/cm^2) using a syringe pump (New Era Pump Systems Inc., Farmingdale, NY). The numbers of the bound cells on the functionalized surfaces were counted under fluorescence after the injection step consisting of forward flow (injection) for 5 min, backward flow (withdrawal) for 5 min, and PBS washing for 1 min. To observe the differences in cell binding stability among the surfaces, the numbers of the remaining cells on the surfaces were monitored after 5 min washing at a flow rate of 500 μL/min (0.8 dyn/cm^2).

4.3. RESULTS AND DISCUSSION

4.3.1. Characterization of dendrimer derivatives

Chemical structures of all dendrimer derivatives were confirmed by ^{1}H NMR in D_2O using

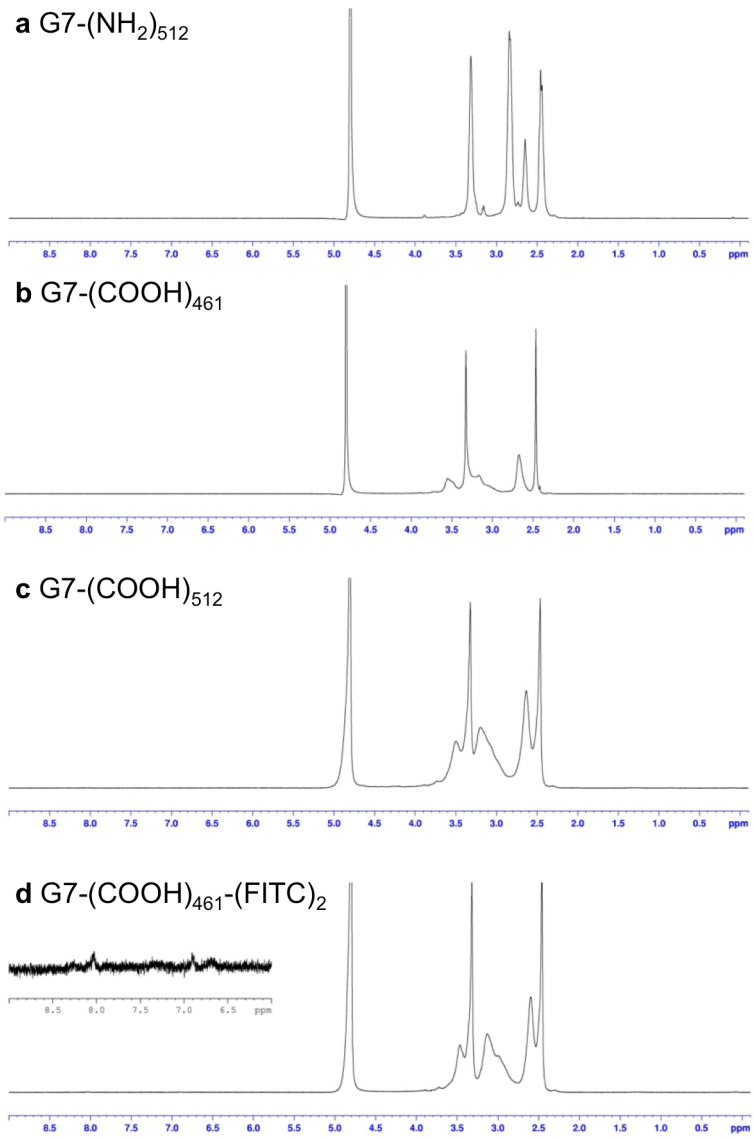

Figure 4.3. ^{1}H NMR spectra of various dendrimer derivatives. a) starting G7 PAMAM dendrimer with primary amine end groups (G7-$(NH_2)_{512}$); b) partially carboxylated G7 PAMAM dendrimer (G7-$(COOH)_{461}$); c) completely carboxylated G7 PAMAM dendrimer (G7-$(COOH)_{512}$); and d) G7-FITC conjugate (G7-$(COOH)_{461}$-$(FITC)_2$). Inset spectrum is the enlarged characteristic peaks of FITC.

a 400 MHz Bruker DPX-400 spectrometer (Bruker BioSpin Corp., Billerica, MA) as shown in **Fig. 4.3**. The number of FITC molecules per dendrimer was calculated by fitting the fluorescence intensity measurements of the dendrimer-FITC conjugates to a standard curve of free FITC solution in DMSO using a SpectraMAX GeminiXS microplate spectrofluorometer (Molecular Devices, Sunnyvale, CA) as described earlier [4, 27]. From ^{1}H NMR and fluorescence measurement of fluorescein, it was confirmed that approximately two fluorescein molecules were conjugated per dendrimer (G7-$(COOH)_{461}$-$(FITC)_2$). In addition, particle size (diameter, nm) and surface charge (zeta potential, mV) of the dendrimer derivatives were measured by quasi-elastic laser light scattering using Nicomp 380 Zeta Potential/Particle Sizer (Particle Sizing Systems, Santa Barbara, CA) as summarized in **Table 4.1**. As the degree of carboxylation increased, the surface charge of the dendrimer derivatives became more negative in aqueous solution.

Table 4.1. Size and zeta potential of the dendrimer derivatives.

	Size (nm)	**ζ potential (mV)**
G7-$(NH_2)_{512}$	8.0 ± 0.7	13.6 ± 1.3
G7-$(COOH)_{461}$	8.9 ± 1.8	-6.6 ± 3.5
G7-$(COOH)_{512}$	6.8 ± 0.9	-7.4 ± 2.2
G7-$(COOH)_{461}$-$(FITC)_2$	10.4 ± 1.7	-18.8 ± 1.9

Date presented as average ± standard deviation (n = 3).

4.3.2. Characterization of dendrimer derivatives

A series of free aEpCAM solutions (50, 100, 250, and 500 μg/mL) in HBS-EP buffer (a running buffer for the SPR mesurement, GE Healthcare, Pittsburgh, PA) was prepared and used to create a standard curve for the UV/Vis measurements. The standard solutions and the recovered dendrimer-aEpCAM conjugates (0.25 mL) in HBS-EP were characterized using a NanoDrop 1000 Spectrophotometer (Thermo Scientific, Wilmington, DE). The completely carboxylated dendrimers (43 nM) showed no absorption at 220 nm (**Fig. 4.4**), which was used as

an indicator of the presence of aEpCAM. Based on the linear curve of free aEpCAM at 220 nm, the numbers of the conjugated aEpCAM molecules per dendrimer were calculated to be 2.8 and 4.9 molecules in each conjugate (G7-(aEpCAM)$_{2.8}$ and G7-(aEpCAM)$_{4.9}$, respectively) (**Fig. 4.4**). The dendrimer-aEpCAM conjugates were immediately used or stored at -20 ºC for the subsequent SPR measurements.

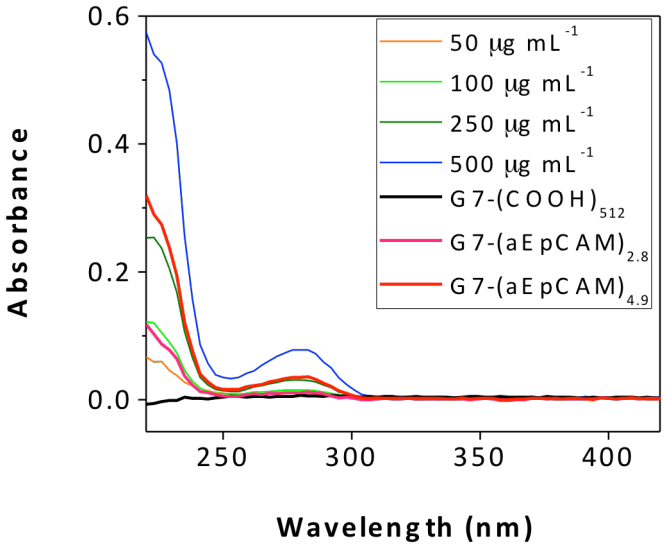

Figure 4.4. UV spectra of free aEpCAM solutions, completely carboxylated dendrimers, and dendrimer-aEpCAM conjugates. The amount of aEpCAM in each sample was determined by UV absorption at 220 nm.

4.2.3. SPR Measurements of Free aEpCAM and the Dendrimer-aEpCAM Conjugates

To investigate the dendrimer-mediated multivalent binding, we directly measured the binding behaviors of the G7-aEpCAM conjugates using surface plasmon resonance (SPR). G7 PAMAM dendrimers were carboxylated and conjugated with aEpCAM, which was confirmed by ^{1}H NMR and size/zeta potential analyses (**Fig. 4.3** and **Table 4.1**). The UV analysis revealed that 2.8 and 4.9 aEpCAM molecules were conjugated per dendrimer, resulting in G7-(aEpCAM)$_{2.8}$ and G7-(aEpCAM)$_{4.9}$, respectively. The binding parameters of the G7-aEpCAM conjugates to EpCAM-immobilized sensor chips were recorded and compared to those of free aEpCAM. CM5

sensor chips with an immobilized shift of around 2,000 resonance units (RU, approximately 2 ng/mm of surface presentation) were used for subsequent binding analyses (**Fig. 4.5**). The protein-immobilized sensor chips were rinsed with HBS-EP buffer until a stable baseline was obtained, prior to the injection of analytes. The completely carboxylated dendrimers without aEpCAM conjugation (a negative control) showed no noticeable binding as shown in **Fig. 4.6**, indicating that there are no non-specific interactions between the carboxylated dendrimers and EpCAM immobilized on sensor chips (**Fig. 4.6**). The carboxylated G7 PAMAM dendrimers without aEpCAM showed no non-specific binding, assuring that the observed binding events of the G7-aEpCAM conjugates are results of specific EpCAM-aEpCAM interactions.

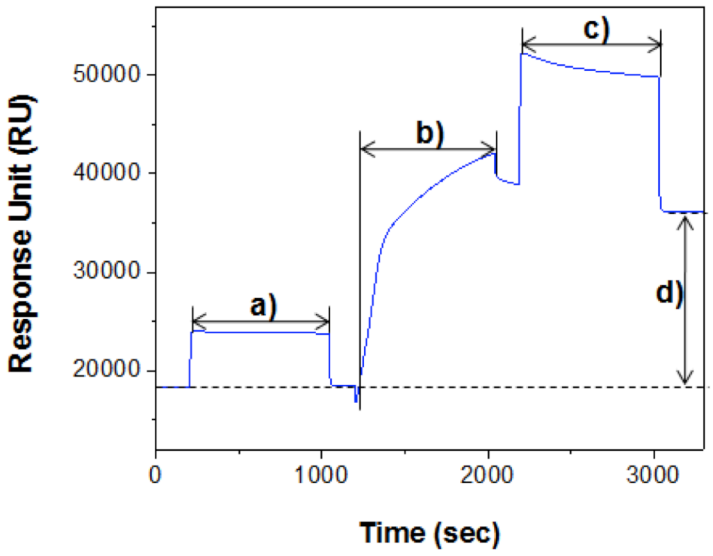

Figure 4.5. A representative SPR sensorgram of EpCAM immobilization on a CM5 sensor chip. The amount of immobilized protein on the sensor chip was determined by the difference in resonance unit before and after immobilization of EpCAM (d)). The sensor chips with immobilized shift of around 2000 RU were used for subsequent binding analyses. The immobilization process was performed by three steps; a) activation of CM5 sensor chip using a mixture of EDC and NHS; b) injection and binding of EpCAM; and c) removal of loosely bound EpCAM and deactivation of remaining reactive ester residues on the sensor chip using ethanolamine.

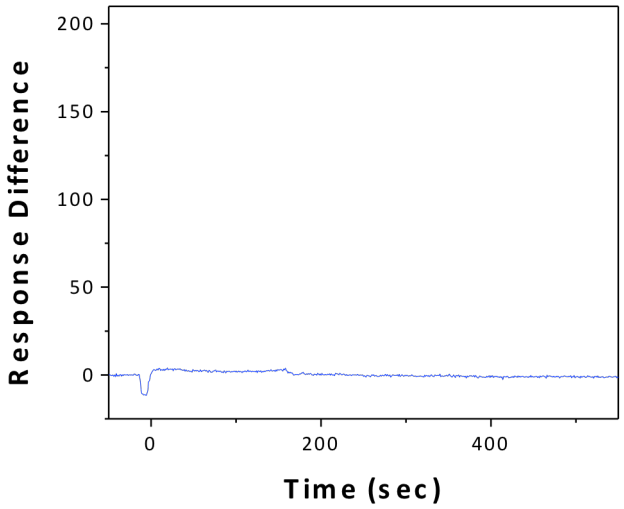

Figure 4.6. A binding sensorgram of completely carboxylated G7 dendrimers. The completely carboxylated G7 dendrimers without aEpCAM do not exhibit any non-specific binding with an EpCAM-immobilized sensor chip.

The SPR sensorgrams (**Fig. 4.7**) were used to obtain the quantitative binding kinetic parameters, such as association rate constant (k_a) and dissociation rate constant (k_d) (**Table 4.2**). All sensorgrams shown in **Fig. 4.7** represent the response differences, i.e., the responses from channel 2 (with EpCAM) subtracted by those from channel 1 (reference), to confirm that the observed binding is a result of the specific interactions. The colored lines represent the raw data curves, and the solid black lines are simulated fitting curves using an 1:1 interaction model provided by the BIAevaluation software (**Fig. 4.7**). Dissociation constants (K_D) were calculated from the measured k_a and k_d ($K_D = k_d/k_a = 1/K_A$), where a lower value of K_D corresponds to a stronger binding strength. Based on the simulated fitting curves (Chi^2 value < 3.0), all binding kinetics parameters, including K_a and K_d, were obtained (**Table 4.2**).

As listed in **Table 4.2**, the dendrimer conjugates show significantly lower K_D values than free aEpCAM. The changes in the dissociation constants can be expressed by the multivalency parameter β [2, 4].

$$\beta K_{N}^{multi} = K^{mono} \qquad \text{[Eq. (1)]}$$

In Equation (1), K^{mono} is the dissociation constant of free aEpCAM (K^{mono} = 7.3 × 10^{-7} M), and N is the number of ligands (2.8 and 4.9) per dendrimer. The dissociation constants of the conjugates with multiple aEpCAMs, K_N^{Multi}, were measured to be $K_{2.8}^{Multi}$ = 3.5 × 10^{-8} M and $K_{4.9}^{Multi}$ = 5.8 × 10^{-13} M, providing the β values of 21.01 and 1.26 × 10^{6}, respectively. The phenomenal increase in binding avidity of G7-$(aEpCAM)_{4.9}$ by approximately a million-fold is largely due to the exponential decrease in k_d, which is typical for multivalent binding [4].

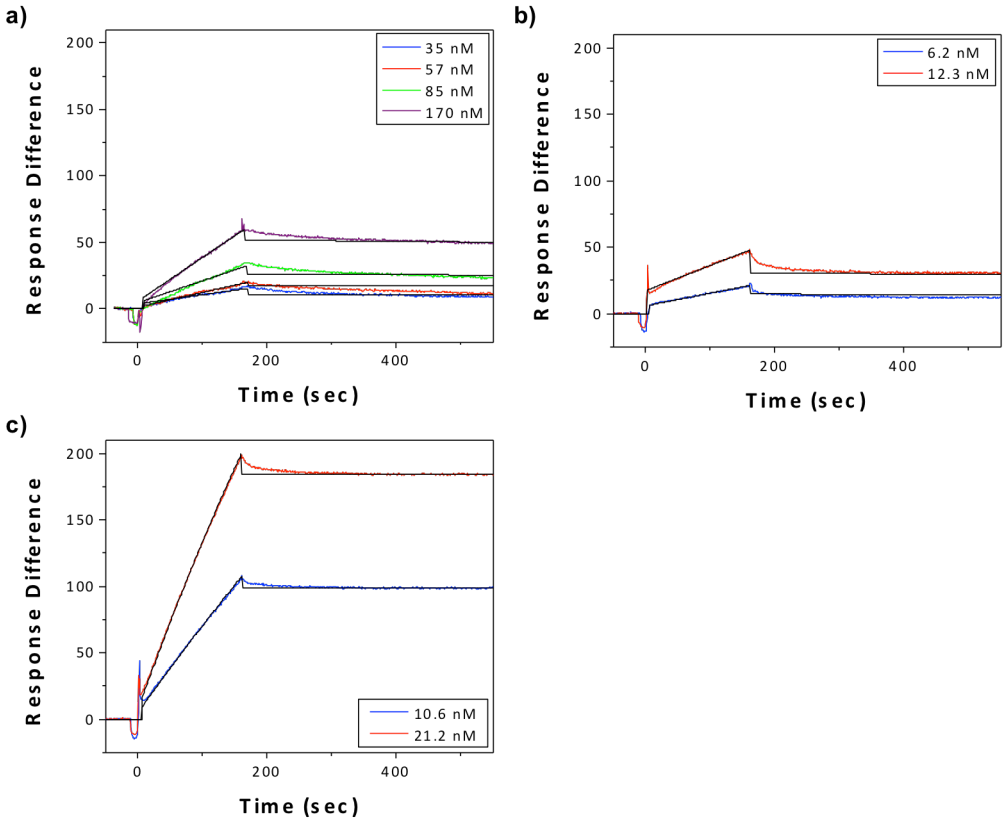

Figure 4.7. SPR sensorgrams of aEpCAM and dendrimer-aEpCAM conjugates using EpCAM-immobilized sensor chips. a) free aEpCAM; b) G7-$(aEpCAM)_{2.8}$; and c) G7-$(aEpCAM)_{4.9}$.

Table 4.2. Kinetic parameters for binding of free aEpCAM and the G7-aEpCAM conjugates to EpCAM measured by SPR

	Kinetic parameters				$\beta^{[a]}$
	k_a (Ms^{-1})	k_d (s^{-1})	K_A (M^{-1})	K_D (M)	
Free aEpCAM	131	1.0×10^{-4}	1.4×10^{6}	7.3×10^{-7}	-
G7-(aEpCAM)$_{2.8}$	5.2×10^{4}	1.3×10^{-4}	2.8×10^{8}	3.5×10^{-8}	21.0
G7-(aEpCAM)$_{4.9}$	1.2×10^{5}	7.3×10^{-8}	1.8×10^{12}	5.8×10^{-13}	1.3×10^{6}

All kinetic values were obtained by averaging at least three independent runs of SPR measurements. [a]The multivalency parameter β.

4.3.4. Characterization of Dendrimer-aEpCAM-immobilized Surfaces

The immobilization of dendrimers and aEpCAM on the surface was confirmed by fluorescence intensity analysis using fluorescein-conjugated dendrimers and monoclonal human EpCAM-allophycocyanin (aEpCAM-APC) and X-ray photoelectron spectroscopy (XPS).

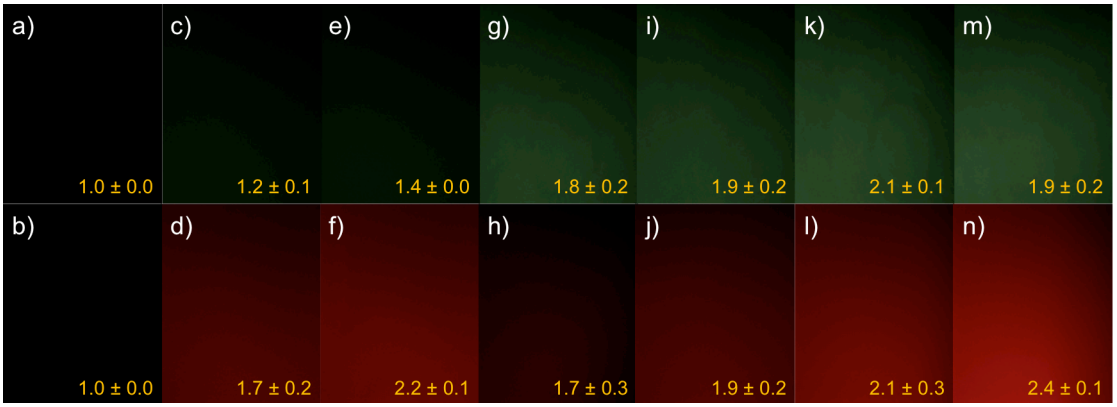

Figure 4.8. Surface characterization using fluorescence intensity analysis. Fluorescence images of functionalized surfaces treated with a) and b) IgG; c) and d) FITC-dendrimer; e) and f) aEpCAM-PEG; and g) and h) aEpCAM and FITC-dendrimer. Note that green and red fluorescences come from fluorescein-conjugated dendrimer and aEpCAM-APC, respectively. Immunostaining results of surfaces show that dendrimer and aEpCAM are immobilized onto the glass substrate as designed. Note that all the fluorescence intensities are normalized based on the intensities measured on the control surfaces with IgG. Error bars: standard deviation (n=15).

Surface immobilization of dendrimers and free aEpCAM was confirmed by fluorescence intensity analysis, as shown in **Fig. 4.8**. The epoxy-functionalized glass slide treated with IgG was used as a negative control, and the intensities obtained from all functionalized slides were normalized by the average intensity values of the negative control to make all numbers semi-quantitative. The measured fluorescence intensities of each fluorophore dictate the surface functionalization, thus dendrimer-immobilized surface is a good platform to immobilize more aEpCAM (2 fold greater than other substrates) on the surface.

The immobilization of aEpCAM and dendrimer was quantitatively confirmed by an increase in carbon and nitrogen compositions and decreased silicon detection in the underlying glass substrate, as measured by XPS analysis (**Table 4.3**). Because PEG and dendrimer both have amine termini, nitrogen compositions of the surfaces were slightly increased after PEGylation and dendrimer immobilization, before aEpCAM treatment. The measured nitrogen content corresponds to the degree of protein coverage on the glass surface, which is confirmed by the significant increase in nitrogen and decrease in silicon compositions when aEpCAM was immobilized.

Table 4.3. Surface characterization using XPS. Atomic compositions of surfaces functionalized with aEpCAM were measured by XPS.

Mass concentration %	Untreated	PEG	Dendrimer	PEG-aEpCAM	Dendrimer-EpCAM
C(%)	11.3	26.0	27.7	39.1	41.6
O(%)	59.7	54.2	51.8	40.9	38.2
N(%)	0.0	0.4	0.9	4.2	4.7
Si(%)	29.0	19.4	19.5	15.8	15.5

4.3.5. Tumor Cell Adhesion of Various Functionalized Surfaces under Static Conditions

To translate the multivalent binding benefit to enhanced tumor cell capture on surfaces, aEpCAM was covalently immobilized to G7 PAMAM dendrimer-coated surfaces and using a similar method described earlier [4]. The cell adhesion of the dendrimer surfaces was compared to that of the linear polymer poly(ethylene glycol) (PEG)-immobilized (PEGylated) surfaces. Three breast cancer cell lines, MDA-MB-361, MCF-7, and MDA-MB-231 cells were employed as CTC models. The comparison analysis using the cancer cells (**Fig. 4.9a**) showed that the dendrimer-immobilized surfaces induced substantially more cells to be bound than the PEGylated surfaces for all three cell lines.

We also observed that dendrimer-coated surfaces accommodate more aEpCAM to be immobilized than the PEGylated surfaces do, even under the identical protein immobilization condition. This is an additional advantage of using dendrimers. However, it is possible that the

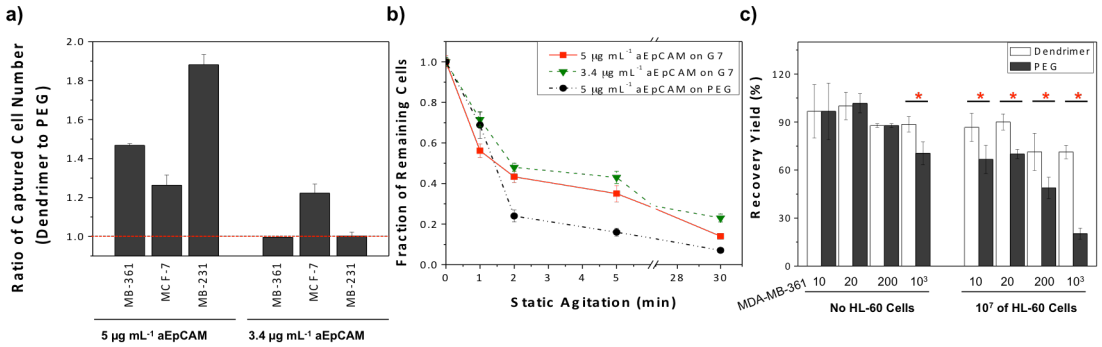

Figure 4.9. Enhanced cell adhesion and binding stability on the dendirmer-coated surfaces under static conditions. a) The ratios of the numbers of the bound cancer cells on the dendrimer-immobilized surfaces to those on the PEGylated surfaces. Error bars: standard error ($n > 3$). b) Dissociation kinetics of MDA-MB-361 cells on the dendrimer-immobilized surfaces and the PEGylated surfaces. The dendrimer-immobilized surfaces significantly increase the fraction of remaining cells on the surfaces upon static agitation as compared to the PEGylated surfaces even after reducing the amount of aEpCAM added. Error bars: standard error ($n=3$). c) Recovery yields of the captured MDA-MB-361 cells using various numbers (10, 20, 200, and 1,000) of the cells spiked with and without HL-60 cells. Significant improvements of the dendrimer surfaces were observed when either 10^3 of cancer cells were applied or the cells were mixed with HL-60 cells (10^7 cells per surface). Error bars: standard error ($n=3$). Asterisks indicate $p < 0.05$.

observed enhancement in tumor cell capturing is simply due to the increased amount of aEpCAM present on the dendrimer-coated surfaces rather than the multivalent binding. To investigate this, a reduced concentration (from 5.0 to 3.4 μg/mL) of aEpCAM was applied onto the dendrimer-immobilized surfaces to match the surface density of aEpCAM on the PEGylated surfaces where 5.0 μg/mL of aEpCAM was added. Although the number of the captured cells on the dendrimer-coated surfaces was reduced, the dendrimer-coated surfaces still exhibit similar or higher initial capture efficiencies than the PEGylated surface (**Fig. 4.9a**, the right three bars). More importantly, the dendrimer surfaces show markedly decreased dissociation rate constants of the surface binding of the tumor cells (up to 3.6-fold) and the enhanced binding stability upon agitation (up to 15.2-fold), compared to the PEGylated surface counterparts (**section 4.2.5**). These results indicate that the multivalent binding effect mediated by dendrimers is the major factor that enhances the cancer cell capture efficiency and the surface binding strength of the tumor cells.

The cell-bound surfaces were then agitated to show the stability of the cell binding on each surface. The number of remaining cells was normalized based on the initial cell number attached to each surface before agitation. **Fig. 4.9b** shows greater numbers of the bound cancer cells (MDA-MB-361 cells) remained on the dendrimer-immobilized surface upon agitation than those on the PEGylated surface. To quantitatively analyze the multivalent effect in the cell adhesion experiments, the dissociation rate constant of the cell-surface complexes were calculated by nonlinear curve fitting using the following exponential dissociation Equation (2) [28].

$$Y = Y_p + Ae^{-kd \times T} \qquad \text{[Eq. (2)]}$$

Where Y is the number of remaining cells on a surface at T, Y_p is the number of the surface-bound cells after reaching a plateau, A is the difference between the number of cells at 0 min and at the plateau, and T is time. The plateau is defined as the region where no more cells are being detached from the surfaces. Although the dissociation rate constants vary between the

Table 4.4. Dissociation rate constants of cell-surface complexes. Dissociation rate constants were obtained by nonlinear fitting (exponential decay function formulated by Equation (2)) using the average number (n=3) of cells remaining on each surface during static agitation. The dissociation rate constants of all cancer cell lines on the dendrimer-immobilized surfaces were lower than those on the PEGylated surfaces.

Cancer cell type	Dissociation rate constant (k_d [min^{-1}])		
	Dendrimer-immobilized	PEGylated	Fold decreased
MDA-MB-361	0.2	1.0	4.6
MCF-7	0.2	0.8	5.2
MDA-MB-231	2.3	2.6	1.1

Table 4.5. Ratios of the association rate constants of cell-surface complexes. Based on the average number (n=3) of the bound cells on the each surface before static agitation, ratios of association rate constants were calculated using Equation (4). The ratios were higher than 1.5 in all cancer cell lines, indicating that the binding rates of cells on the dendrimer-immobilized surfaces are faster than those on the PEGylated surfaces.

Cancer cell type	Ratio of association rate constants (k_a of dendrimer-immobilized surface / k_a of PEGylated surface)
MDA-MB-361	1.6
MCF-7	1.8
MDA-MB-231	1.6
HL-60	1.1

cell types, it is obvious that all cancer cells exhibit the significantly slower dissociation rates (up to 5.2 fold for MCF-7 cells) from the dendrimer-immobilized surfaces than those from the PEGylated surfaces (**Table 4.4**). Association rates were also calculated using an equation (3-4) published by Motulsky et al [29]. The dendrimer-immobilized surfaces induce the slow dissociation and the enhanced association of the cancer cells.

Association rates were also calculated using an equation published by Motulsky et al [29]. As for association, despite the difficulty to quantitatively calculate the association rate constant

between cells and each surface, the relative ratio of the association rate constants between the surfaces with cells can be calculated by modifying the exponential association Equation (3) [29].

$$Y = Ymax\,(1 - e^{-ka \times T}) \quad \text{[Eq. (3)]}$$

Where Y is the number of bound cells before agitation, Y_{max} is the number of applied cells on surface, and T is time. Further, Equation (3) can be modified in terms of association rate constant shown in Equation (4).

$$k_a = \{\ln(Y_{max} - Y) - \ln(Y_{max})\} / T \quad \text{[Eq. (4)]}$$

Based on Equation (4), the relative ratio of the association rate constants on the dendrimer-immobilized and on the PEGylated surfaces could be calculated.

As shown in **Fig. 4.10**, the ratios of the bound cell numbers on the dendrimer-immobilized surfaces to those of the PEGylated surfaces were consistently higher than 1, over 30 min of static agitation, indicating that the multivalent effect mediated by dendrimers enhance cell adhesion to the surface. Although the dissociation rate constants vary between cell types in **Table 4.4**, it is obvious that all cancer cells exhibit significantly slower dissociation rates from the dendrimer-immobilized surfaces than those from the PEGylated surfaces. Before agitation, the dendrimer immobilized surface enhanced the association, whereas the PEGylated did not, giving the ratio higher than 1 (**Table 4.5**). Compared to the control surfaces, the dendrimer-immobilized surfaces induce more stable binding of cancer cells, which is likely due to the multivalent effect mediated by the dendrimers. The dendrimer-immobilized surfaces induce the slow dissociation and the enhanced association of the cancer cells.

To further evaluate the tumor cell adhesion under various conditions, we performed a series of regression assays using calcein AM-labeled MDA-MB-361 cells spiked with 10^7 HL-60 cells (**Fig. 4.9c**). Human leukemia HL-60 cells were used as a control leukocyte model, and the

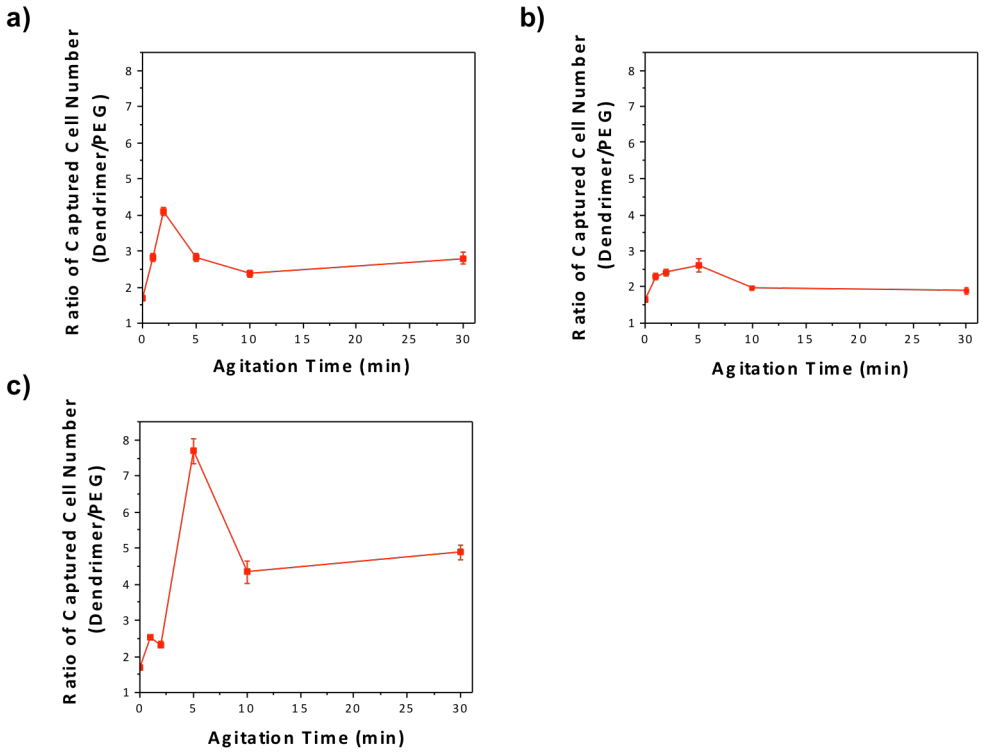

Figure 4.10. Enhanced binding stability by multivalent effect in static conditions. Enhanced binding stability on the dendrimer-aEpCAM conjugate-immobilized surfaces was observed using a) MDA-MB-361; b) MCF-7; and c) MDA-MB-231. The numbers of the bound cancer cells during static agitation were higher on the dendrimer-aEpCAM conjugate-immobilized surfaces, compared to those on the PEGylated surface without dendrimers. Non-specific binding on both surfaces of HL-60, a leukocyte model in this investigation, was negligible. Error bars: standard error (n=3).

numbers of the spiked cancer cells and HL-60 cells in the mixtures were decided to simulate the clinical samples roughly 1 CTC per 10^3-10^6 leukocytes [31]. Although the recovery yield (the number of the cells being captured divided by the number of the cells that were originally spiked) of the both surfaces was generally decreased with an increase in the number of the applied cells, the recovery yield of the dendrimer-immobilized surfaces (at least over 70% regardless of the presence of HL-60 cells) were remarkably greater than those on the PEGylated surfaces. In contrast, the recovery yield of the PEGylated surfaces was rapidly dropped from ~80% to ~20% when the cell mixtures were applied. These results further support that the dendrimer-

immobilized surfaces are superior to the linear polymer-functionalized surfaces in terms of the detection sensitivity from the cell mixtures.

4.3.6. Surface Characterization after E-selectin Treatment by Immunostaining

The fluorescence intensities of the surfaces were summarized with images after normalization using the intensities of a positive control (E-selectin-immobilized epoxy functionalized surfaces, **Fig. 4.11**). In the epoxy functionalized surfaces and PEGylated surfaces, the green fluorescence intensity was lower than the dendrimer-immobilized surfaces when equal amount of E-selectin solution was applied onto various surfaces. The dendrimer-immobilized surface showed similar fluorescence intensity as the positive control, indicating that dendrimer-immobilized surface is a good platform to attach more E-selectin on the surface.

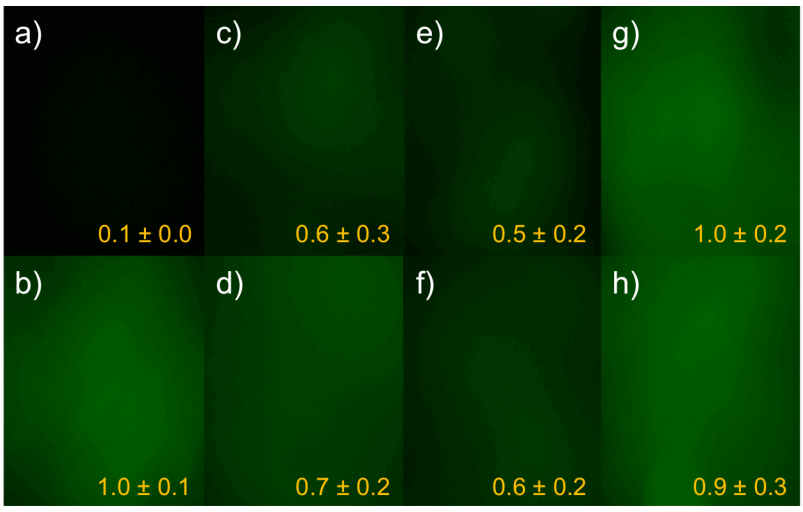

Figure 4.11. Surface characterization after E-selectin treatment using immunostaining. Fluorescence images of functionalized surfaces treated with a) untreated surface; b) positive control (only E-selectin treated surface); c) IgG and d) aEpCAM-immobilized Epoxy functionalized surfaces; e) IgG and f) aEpCAM-immobilized PEGylated surfaces; and g) IgG and h) aEpCAM-immobilized dendrimer surfaces. Note that green fluorescence comes from aE-selectin-fluorescein. Immunostaining results of surfaces showed that dendrimer-immobilized substrate has higher fluorescence intensities than other substrates, indicating that dendrimer-immobilized surface is a good platform to hold more E-selectin. Error bars: standard deviation (n=15).

4.3.7. Tumor Cell Capture of Various Functionalized Surfaces under Dynamic Conditions

The dendrimer-mediated cell capture was further assessed under dynamic conditions (under flow) by comparing three substrates (epoxy functionalized, PEGylated, and dendrimer-immobilized) using a parallel-plate flow chamber [23]. **Fig. 4.12** demonstrates that more cells were being captured on the dendrimer-coated surface than on the control surfaces by 1.5-3 fold,

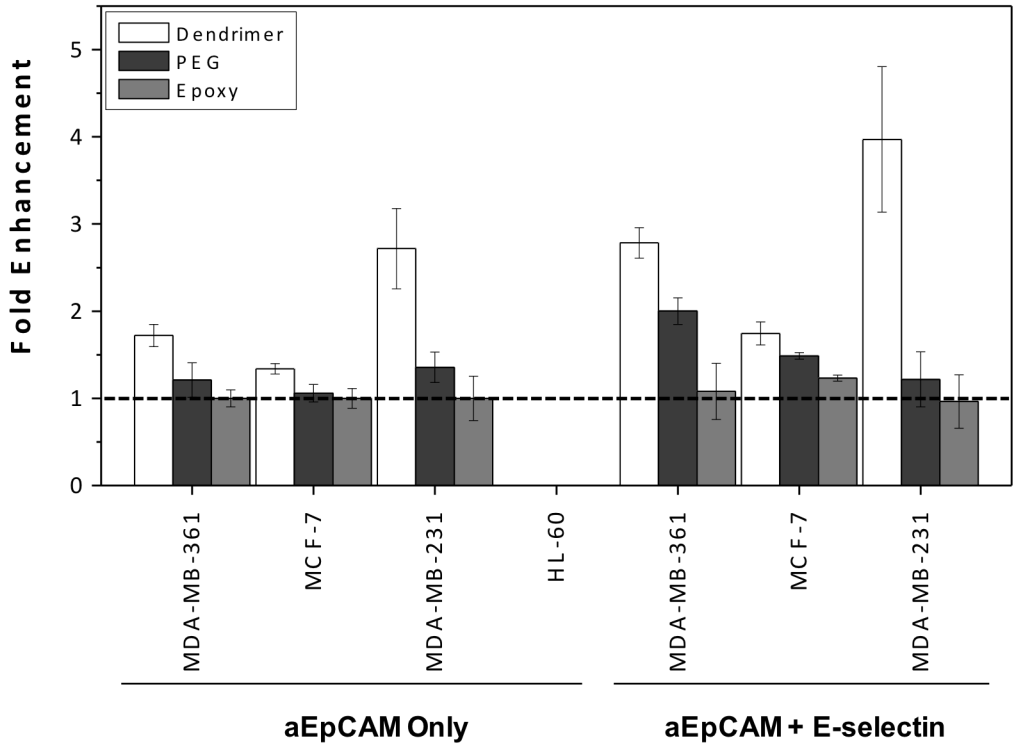

Figure 4.12. Enhanced selective capture of tumor cells by multivalent effect on the dendrimer-immobilized surfaces. Three substrates, epoxy-functionalized, PEGylated and dendrimer-immobilized surfaces, were treated only with aEpCAM (left) or with both aEpCAM and E-selectin (right). All numbers of the bound cancer cells on the surfaces were measured after cell suspension injection (at 0.08 dyn/cm^2 of shear stress) before PBS washing (at 0.8 dyn/cm^2 of shear stress), and normalized using the number of each cell line on epoxy-functionalized surfaces without E-selectin treatment. Regardless of E-selectin treatment, the dendrimer-immobilized surfaces enhanced the cancer cell binding (1.6–4.0 fold), compared to that on other surfaces without dendrimer immobilization. Regardless of the surface type, all E-selectin treated surfaces (right) showed higher capture of cancer cells under flow than surfaces without E-selectin treatment (left). The capture efficiency of the dendrimer-immobilized surface (up to 4-fold (MDA-MB-231)) was significantly increased by a combination of rolling (E-selectin) and stationary binding (aEpCAM). Error bars: standard error (n=3).

indicating that the cell capture on the dendrimer-immobilized surfaces is enhanced under static as well as dynamic conditions. Non-specific interactions between the HL-60 cells and all three surfaces were negligible under flow, although minimal non-specific captures on the surfaces were observed under static conditions.

Fig. 4.13a shows fold enhancements in capture efficiency of the three surfaces after a harsh washing step (washing with PBS for 5 min at a flow rate of 500 μL/min (0.8 dyn/cm^2)). Compared to the epoxy-functionalized surface where aEpCAM was immobilized without a polymer linker (PEG or dendrimer), PEGylated surface exhibited slightly improved capture

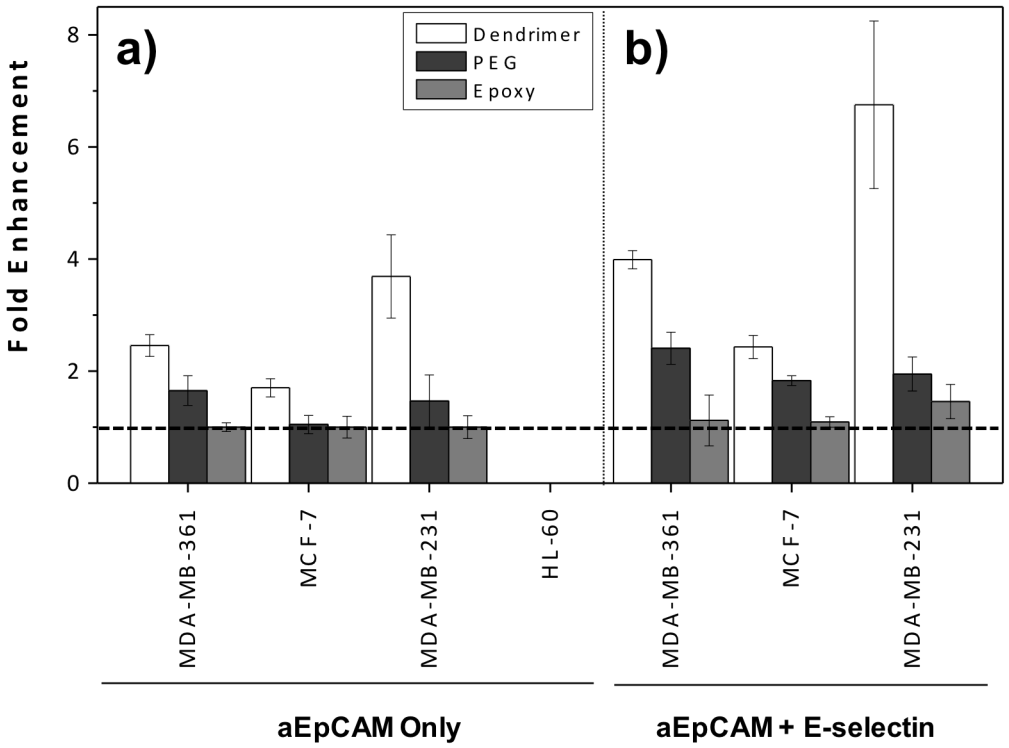

Figure 4.13. Enhanced cell binding stability by combination of multivalent binding and cell rolling under flow. Three substrates, epoxy-functionalized, PEGylated, and dendrimer-immobilized surfaces, treated with aEpCAM alone (a) or with both aEpCAM and E-selectin (b) were compared in terms of capture efficiency. The captured cancer cells on the surfaces were counted after injection of cell suspensions and washing with PBS at a shear stress of 0.8 dyn cm^{-2}, followed by normalization based on the number of each cell line on the epoxy-functionalized surfaces without E-selectin. Up to 7-fold enhancement in the capture efficiency by the dendrimer-immobilized surface was achieved through combination of rolling (E-selectin) and multivalent binding (aEpCAM). Error bars: standard error (n=3).

efficiency (1.1-1.7 fold). More importantly, a significantly enhanced capture efficiency was observed on the surface with dendrimers (1.7-3.7 fold, **Fig. 4.13a**), further supporting that dendrimers indeed mediated the multivalent binding effect in cell capture.

In previous chapter 2, the biomimetic combination of dynamic rolling (E-selectin) and stationary binding (aEpCAM) showed substantially enhanced capture efficiency (over 3-fold enhancement), as compared to a surface functionalized solely with aEpCAM [23]. To utilize the biomimetic effect, the three types of the aEpCAM-immobilized surfaces were treated with E-selectin and characterized by immunostaining using monoclonal anti-E-selectin-fluorescein (Section 4.3.6). The capture efficiencies of all three surfaces after addition of E-selectin were significantly improved than those treated only with aEpCAM (**Fig. 4.12**), indicating that additional cell rolling mediated by E-selectin synergistically cooperates with stationary binding through aEpCAM. In particular, the dendrimer-immobilized surface showed, after adding E-selectin, remarkably higher capture efficiency of cancer cells up to 7-fold, as shown in **Fig. 4.12b** in the case of MDA-MB-231 cells. Note that the fold enhancement was increased from up to 4-fold (**Fig. 4.12**) to up to 7-fold (**Fig. 4.13**) after washing at a shear stress of 0.8 dyn/cm^2, demonstrating the enhanced binding stability by the dendrimer-mediated multivalent effect.

4.3.7. Dendrimer, a multivalent binding-mediator

The dramatic enhancement in tumor cell capturing of the dendrimer surfaces is a result of the combined effect of multivalent binding and efficient protein immobilization, likely due to the spherical architecture of dendrimers. Obviously, dendrimers can provide more functional groups available to protein immobilization than linear polymers. However, it is noteworthy to discuss why the same level of the multivalent binding was not observed in the linear polymer-coated surfaces. To induce the multivalent binding effect efficiently, the selection of scaffolds and linkers is crucial [32]. Three-dimensional structure of the dendrimer organizes the ligands into a small region of space, as compared to what can be obtained when the ligands are conjugated to a

similar molecular weight linear polymer [4, 33]. This geometric advantage likely reduces the energy of deformation (entropy) of ligands on dendrimer surface to bind with their receptors, facilitating the localized multivalent binding. Furthermore, it has been known that the carboxylated dendrimer has good accessibility of target cells to the immobilized targeting ligands on the dendrimer surface [6], and reduces denaturation of the ligands during immobilization [34].

4.4. SUMMARY

Taken together, the significantly increased binding avidity of the G7-aEpCAM conjugates measured by SPR, along with the enhanced binding stability of the tumor cells on the dendrimer-functionalized surfaces, supports our hypothesis that the dendrimer-mediated multivalent binding effect can be exploited in cell capture on engineered surfaces. Additionally, we have shown that the combination of the two-biomimetic approaches, i.e., multivalent binding and cell rolling, substantially enhances the tumor cell detection. The results demonstrate that the combination of nanotechnology and biomimicry has a great potential to be applied for highly sensitive detection of rare tumor cells from blood.

4.5. REFERENCES

1. Lee, R.T. and Y.C. Lee, *Affinity enhancement by multivalent lectin-carbohydrate interaction.* Glycoconj J, 2000. **17**(7-9): p. 543-51.
2. Mammen, M., S.K. Choi, and G.M. Whitesides, *Polyvalent interactions in biological systems: Implications for design and use of multivalent ligands and inhibitors.* Angew Chem Int Ed Engl, 1998. **37**(20): p. 2755-2794.
3. Mourez, M., et al., *Designing a polyvalent inhibitor of anthrax toxin.* Nat Biotechnol, 2001. **19**(10): p. 958-61.
4. Hong, S., et al., *The binding avidity of a nanoparticle-based multivalent targeted drug delivery platform.* Chem Biol, 2007. **14**(1): p. 107-15.
5. Kiessling, L.L. and N.L. Pohl, *Strength in numbers: non-natural polyvalent carbohydrate derivatives.* Chem Biol, 1996. **3**(2): p. 71-7.
6. Quintana, A., et al., *Design and function of a dendrimer-based therapeutic nanodevice targeted to tumor cells through the folate receptor.* Pharm Res, 2002. **19**(9): p. 1310-6.
7. Peer, D., et al., *Nanocarriers as an emerging platform for cancer therapy.* Nat Nanotechnol, 2007. **2**(12): p. 751-60.
8. Weissleder, R., et al., *Cell-specific targeting of nanoparticles by multivalent attachment of small molecules.* Nat Biotechnol, 2005. **23**(11): p. 1418-23.
9. Christensen, T., et al., *Additivity and the physical basis of multivalency effects: a thermodynamic investigation of the calcium EDTA interaction.* J Am Chem Soc, 2003. **125**(24): p. 7357-66.
10. Gestwicki, J.E., et al., *Selective immobilization of multivalent ligands for surface plasmon resonance and fluorescence microscopy.* Anal Biochem, 2002. **305**(2): p. 149-55.
11. Kitov, P.I. and D.R. Bundle, *On the nature of the multivalency effect: a thermodynamic model.* J Am Chem Soc, 2003. **125**(52): p. 16271-84.

12. Benters, R., et al., *DNA microarrays with PAMAM dendritic linker systems.* Nucleic Acids Res, 2002. **30**(2): p. E10.

13. Le Berre, V., et al., *Dendrimeric coating of glass slides for sensitive DNA microarrays analysis.* Nucleic Acids Res, 2003. **31**(16): p. e88.

14. Kawase, M., et al., *Immobilization of ligand-modified polyamidoamine dendrimer for cultivation of hepatoma cells.* Artif Organs, 2000. **24**(1): p. 18-22.

15. Kim, M.H., et al., *Response of human epithelial cells to culture surfaces with varied roughnesses prepared by immobilizing dendrimers with/without D-glucose display.* J Biosci Bioeng, 2007. **103**(2): p. 192-9.

16. Nagrath, S., et al., *Isolation of rare circulating tumour cells in cancer patients by microchip technology.* Nature, 2007. **450**(7173): p. 1235-9.

17. Wang, S., et al., *Three-dimensional nanostructured substrates toward efficient capture of circulating tumor cells.* Angew Chem Int Ed Engl, 2009. **48**(47): p. 8970-3.

18. Stott, S.L., et al., *Isolation of circulating tumor cells using a microvortex-generating herringbone-chip.* Proc Natl Acad Sci U S A, 2010. **107**(43): p. 18392-7.

19. Wang, S., et al., *Highly efficient capture of circulating tumor cells by using nanostructured silicon substrates with integrated chaotic micromixers.* Angew Chem Int Ed Engl, 2011. **50**(13): p. 3084-8.

20. He, W., et al., *In vivo quantitation of rare circulating tumor cells by multiphoton intravital flow cytometry.* Proc Natl Acad Sci U S A, 2007. **104**(28): p. 11760-5.

21. Momburg, F., et al., *Immunohistochemical study of the expression of a Mr 34,000 human epithelium-specific surface glycoprotein in normal and malignant tissues.* Cancer Res, 1987. **47**(11): p. 2883-91.

22. Allard, W.J., et al., *Tumor cells circulate in the peripheral blood of all major carcinomas but not in healthy subjects or patients with nonmalignant diseases.* Clin Cancer Res, 2004. **10**(20): p. 6897-904.

23. Myung, J.H., et al., *Enhanced tumor cell isolation by a biomimetic combination of E-selectin and anti-EpCAM: implications for the effective separation of circulating tumor cells (CTCs).* Langmuir, 2010. **26**(11): p. 8589-96.

24. Dimitroff, C.J., et al., *Rolling of human bone-metastatic prostate tumor cells on human bone marrow endothelium under shear flow is mediated by E-selectin.* Cancer Res, 2004. **64**(15): p. 5261-9.

25. Hong, S., et al., *The Role of Ganglioside GM(1) in Cellular Internalization Mechanisms of Poly(amidoamine) Dendrimers.* Bioconjug Chem, 2009.

26. Myung, J.H., et al., *Direct measurements on CD24-mediated rolling of human breast cancer MCF-7 cells on E-selectin.* Anal Chem, 2011. **83**(3): p. 1078-83.

27. Sunoqrot, S., et al., *Kinetically controlled cellular interactions of polymer-polymer and polymer-liposome nanohybrid systems.* Bioconjug Chem, 2011. **22**(3): p. 466-74.

28. Motulsky, H.J. and R.E. Brown, *Detecting outliers when fitting data with nonlinear regression - a new method based on robust nonlinear regression and the false discovery rate.* BMC Bioinformatics, 2006. **7**: p. 123.

29. Motulsky, H.J. and R.R. Neubig, *Analyzing binding data.* Curr Protoc Neurosci, 2010. **Chapter 7**: p. Unit 7 5.

30. Owens, D.E., 3rd and N.A. Peppas, *Opsonization, biodistribution, and pharmacokinetics of polymeric nanoparticles.* Int J Pharm, 2006. **307**(1): p. 93-102.

31. Sieuwerts, A.M., et al., *Anti-epithelial cell adhesion molecule antibodies and the detection of circulating normal-like breast tumor cells.* J Natl Cancer Inst, 2009. **101**(1): p. 61-6.

32. Lindhorst, T., *Artificial Multivalent Sugar Ligands to Understand and Manipulate Carbohydrate-Protein Interactions*, in *Host-Guest Chemistry*, S. Penadés, Editor 2002, Springer Berlin / Heidelberg. p. 201-235.

33. Reuter, J.D., et al., *Inhibition of viral adhesion and infection by sialic-acid-conjugated dendritic polymers.* Bioconjug Chem, 1999. **10**(2): p. 271-8.

34. Ajikumar, P.K., et al., *Carboxyl-terminated dendrimer-coated bioactive interface for protein microarray: high-sensitivity detection of antigen in complex biological samples.* Langmuir, 2007. **23**(10): p. 5670-7.

CHAPTER 5.

A NOVEL MULTIFUNCTIONAL PLATFORM USING A BIOMIMETIC COMBINATION OF CELL ROLLING AND MULTIVALENT BINDING FOR HIGHLY SENSITIVE TUMOR CELL CAPTURE

5.1. INTRODUCTION

CTCs are one of the exceedingly rare cells related to human diseases (one CTC in the background of one million to one billion blood cells in cancer patient blood) [1]. It is known that the quantification of CTCs in blood well correlates with cancer progress and metastasis [2], thus provides an effective tool for diagnosis and prognosis of cancer metastasis [3, 4]. CTCs can be detected by antibodies that have specific affinities for tumor cell surface markers that are overexpressed on the surface of cancer cells, and not on normal hematological cells. Currently, there are several tumor cell markers targeted; epithelial cell adhesion molecule (EpCAM) [3, 4], human epidermal growth factor receptor-2 (HER2) [5, 6], and prostate specific antigen (PSA) [7, 8].

Although the current CTC detection methods based on a single antibody against one cancer cell marker have shown promising results, several clinical challenges are encountered due to the highly heterogeneous nature of cancer cells. Due to various cancer cell surface markers and its expression levels, it is extremely difficult to effectively detect CTCs with one universally expressed marker [9]. Although most of epithelial cancer cell universally express EpCAM, a number of CTCs lose their epithelial cell nature upon epithelial-mesenchymal transition (EMT, in exchange for expressing stem cell-like phenotypes) [10]. Because the expression of EpCAM is down-regulated during EMT, the detection using anti-EpCAM would be less efficient to target the CTCs that are released from the primary tumor cells after EMT [10]. However, there are

FDA-approved CTC detection methods using other cell surface markers, such as HER2 and PSA. HerceptTest, an immunohistochemistry using anti-HER2 after tissue-based biopsy, is FDA-approved diagnostic method for breast cancers [11]. Because HER2 is overexpressed only on 20-30% of breast and prostate cancers, the detection method based only on the anti-HER2 have vast variations of detection and less effective than fluorescence in situ hybridization alone [12, 13]. Serum PSA is detected by RT-PCR-based assay in AdnaTest ProstateCancerSelect, but is limited due to PSA mRNA expression in some other organs and normal blood [8, 14]. For the personalized immunotherapy and diagnosis of the cancer properties, more accurate and sensitive diagnostic tools for screening multiple cancer cell surface markers need to be developed.

Herein, a novel multifunctional surface platform with multiple antibodies and two biomimetic approaches (i.e. E-selectin for cell recruitment and multivalent binding effect through surface nanotechnology) is designed to detect the rare CTCs at great sensitivity and selectivity, as illustrated in **Fig. 5.1**. To prove the multifunctional concepts, we focused on three cancer-specific

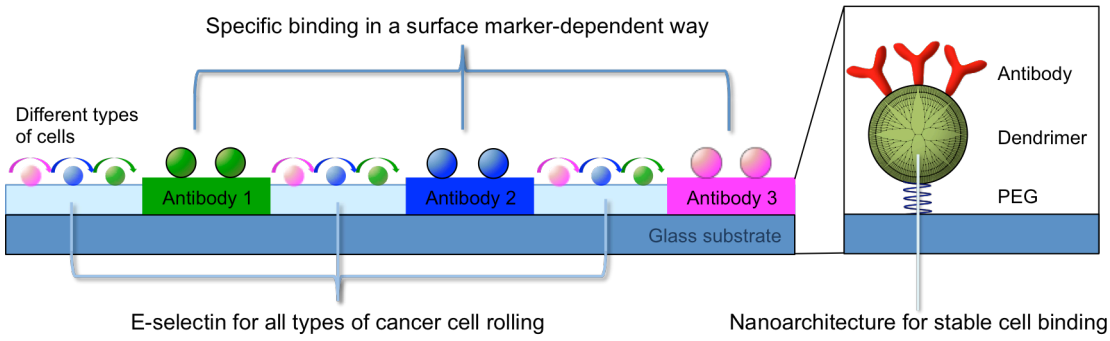

Figure 5.1. A schematic illustration of the multifunctional surfaces for simultaneous detection of multiple cell surface markers. The multifunctional surfaces are composed of several antibodies against multiple cell surface markers, E-selectin for cell rolling on the surface, and dendrimer-mediated nanoarchitecture for multivalent binding effect. Based on the specific binding between surface markers and their antibodies, different types of cancer cells can be separated and enriched in a surface marker-dependent way.

biomarkers, i.e., EpCAM, HER2, and PSA, to target and capture CTCs [15][16][17]. The antibodies against three model biomarkers were immobilized separately on surfaces micropatterned using a gasket. To enhance the capture efficiency (directly related to detection sensitivity) on the antibody-immobilized stripes, the surface was treated with adhesive proteins such as E-selectin to recruit the cells under flow onto the surface like a landing-induced road [16]. Surface nanoarchitecture of dendrimers can mediate multivalent binding effect to enhance the binding specificity and stability between cancer cells and the antibodies [17]. The specific interactions between the optimized surfaces and *in vitro* cell lines including prostate cancer (MDA-PCa-2b) and breast cancer (MDA-MB-361 and MCF-7) cell lines were validated in terms of cell capture efficiency. The enhanced sensitivity and specificity of the functionalized surfaces after incorporation of cell rolling and multivalent binding were feasible to facilitate the continuous sorting of the targeted cancer cells from human blood.

5.2. MATERIALS AND METHOD

5.2.1. Materials

Anti-human epithelial-cell-adhesion-molecule (EpCAM)/TROP1 antibody (anti-EpCAM), anti-human epidermal growth factor receptor-2 (HER2)/TROP1 antibody (anti-HER2), anti-human prostate specific antigen /TROP1 antibody (anti-PSA) [7], and recombinant human E-selectin (E-selectin) were all purchased from R&D systems (Minneapolis, MN). The epoxy-functionalized glass surfaces (SuperEpoxy2®) were purchased from TeleChem International, Inc (Sunnyvale, CA). PAMAM dendrimers (generation 7), bovine serum albumin (BSA), Calcein AM, and all other chemicals were obtained from Sigma-Aldrich (St. Louis, MO), unless otherwise specified, and used without further purification.

5.2.2. Surface functionalization by immobilization of adhesive proteins

A polydimethylsiloxane (PDMS) gasket was used to define the area of an epoxy functionalized glass slides, as portrayed in **Fig. 5.3**. Three different types of surfaces were functionalized by conjugation with each antibody: i) epoxy-functionalized glass surfaces; ii) PEGylated surfaces; and iii) G7 PAMAM dendrimer-immobilized surfaces. The surface functionalization was followed as previously reported [17]. For all antibody conjugation reactions, the antibody solutions of anti-EpCAM, anti-HER2 at a concentration of 5 μg/mL, and anti-PSA at a concentration of 10 μg/mL in PBS buffer were applied on the defined surfaces. The antibody-immobilized stripes were marked using FITC-conjugated BSA treatment (1 mg/mL in PBS) for 1 hour. After the micropatterned PDMS gasket was removed, the surface with the antibody stripes was covered with E-selectin at a concentration of 5 μg/mL in PBS buffer for 4 hours. The volumes of all reagent solutions except E-selectin were fixed at 20 μL. All incubation processes were carried at room temperature with constant gentle shaking, and the surfaces between steps were washed with PBS buffer three times to remove the chemical residues from the surfaces. Potential non-specific binding of both protein-coated and uncoated regions was blocked by a final incubation with 1% (w/v) BSA or 1 μg/mL methoxy PEG-NH_2 (Nektar Therapeutics, Huntsville, AL) solution. The functionalized surfaces were kept in 4°C of refrigerator and the experiments using the surfaces were performed within 24 hours.

5.2.3. Characterization of the functionalized surfaces by X-ray photoelectron spectroscopy (XPS)

The surfaces were characterized as described in our previous publication [16, 18]. In brief, Axis 165 X-ray photoelectron spectrometer (Kratos Analytical, Manchester, U.K.) equipped with a monochromatic AlKα source (hv = 1486.6 eV, 150W) and a hemispherical analyzer were used. The % mass concentrations were obtained from high-resolution spectra of the C 1s, O 1s, N 1s,

and S 2p regions at an X-ray irradiating angle of 30° at 80 eV of energy and a step size of 0.5 eV, carried on 5 scans per each spectrum.

5.2.4. Cellular response observation of each cell line on the antibody- and E-selectin-immobilized surfaces under flow

MDA-MB-361 cells were cultured in Leibovitz's L-15 media (Gibco, Invitrogen, Grand Island, NY) that were supplemented with 1% (v/v) Penicillin/Streptavidin (P/S) and 20% (v/v) FBS in a 37°C humidified atmosphere containing 100% air and 0% CO_2. MCF-7 cells were cultured in DMEM media (Cellgro, Mediatech, Manassas, VA) that were supplemented with 10% (v/v) FBS and 1% (v/v) penicillin/streptomycin (P/S). MDA-PCa-2b cells and HL-60 cells were cultured in BRFF-HPC1 media (AthenaES, Baltimore, MD) and IMDM media (Gibco), respectively, supplemented with 20% FBS and 1% (v/v) P/S. All cell lines were purchased from ATCC (Manassas, VA). All of cancer cell lines except MDA-MB-361 cells cultured in a 37°C humidified incubator containing 95% air and 5% CO_2.

A typical flow chamber experiment was performed as the previous researches [16]. In short, a glass slide functionalized by protein immobilization, a gasket (30 mm (L) × 10mm (W) × 0.25 mm (D), Glycotech, Gaithersburg, MD), and a rectangular parallel plate flow chamber (Glycotech) were assembled in line under vacuum. To observe cellular interactions with the biofunctionalized surfaces, individual cell lines (MDA-PCa-2b, MDA-MB-361, MCF-7, and HL-60) at a concentration between 10^6-10^7 cells/mL in the completed media were injected into the flow chamber at a shear stress of 0.08 dyn/cm^2 using a syringe pump (New Era pump Systems Inc., Farmingdale, NY). Note that, in this flow chamber, 50 μL/min of flow rate is correspondent to 0.08 dyn/cm^2 of a wall shear stress, 8 s^{-1} of a wall shear rate, and 20 μm/sec of near-wall non-adherent cell velocity according to the Goldman equation [19]. Cellular response of each cell line was monitored using a parallel flow chamber against each antibody-immobilized surface, and

recorded using an Olympus IX70 microscope (IX 70-S1F2, Olympus America, Inc., Center Valley, PA) attached with a CCD camera (QImaging Retiga 1300B, Olympus America, Inc.).

5.2.5. Fluorescence labeling for viable cells

Cells, except HL-60 cells, at a concentration of 1×10^6 cells/mL (5 mL) were seeded onto 25cm^2 T flask one day before the experiment. To label the viable cells with fluorescence, the MDA-PCa-2b, MDA-MB-361, and MCF-7 cells were treated with 4 μM Calcein AM, 5 μM Alive cell track It Blue (AAT Bioquest, Inc., Sunnyvale, CA) or Calcein Blue AM (Sigma-Aldrich), and 5 μM Alive cell track It Red (AAT Bioquest, Inc.), respectively, at 37°C in the dark for 30 min (**Fig. 5.2**). The labeled cells were trypsinized to make their suspension at a designed concentration in the completed cell culture media or the whole blood withdrawn from healthy donor. The final suspensions were kept on ice throughout the subsequent cell rolling experiments.

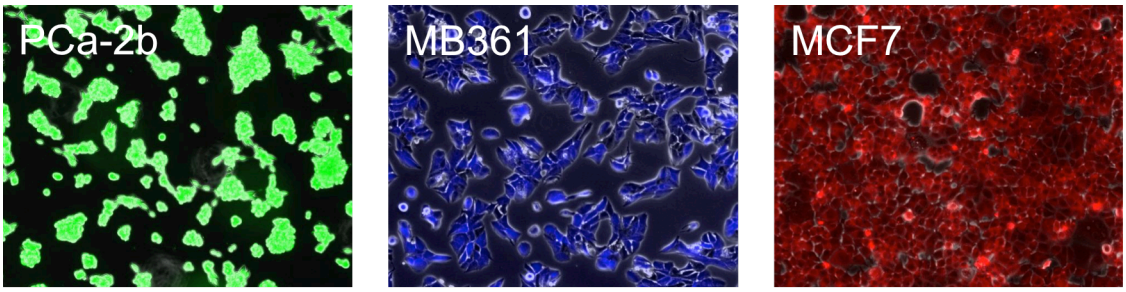

Figure 5.2. Fluorescence-labeled cancer cell models. MDA-PCa-2b, MDA-MB-361, and MCF-7 cells were stained with Calcein AM (green), Alive cell track It Blue or Calcein Blue AM (blue), and Alive cell track It Red [red], respectively.

5.2.6. Optimization of the surface micropatterning

A polydimethylsiloxane (PDMS) gasket was used to define the area of an epoxy functionalized glass slides, as portrayed in **Fig. 5.3**. Epoxy-functionalized glass surfaces were functionalized by conjugation with each antibody as previously reported [16]. For all antibody conjugation reactions, the solutions of anti-EpCAM at a concentration of 5 μg/mL in PBS buffer were applied on the defined surfaces. The antibody-immobilized stripes were marked using FITC-conjugated BSA (1 mg/mL in PBS) for 1 hour. After the PDMS gasket was removed, the surfaces with the antibody stripes were covered with 200 μL of E-selectin at a concentration of 5 μg/mL in PBS buffer for 4 hours. The volumes of all reagent solutions except E-selectin were fixed at 20 μL. All incubation processes were carried at room temperature with constant gentle shaking, and the surfaces between steps were washed with PBS buffer three times to remove the

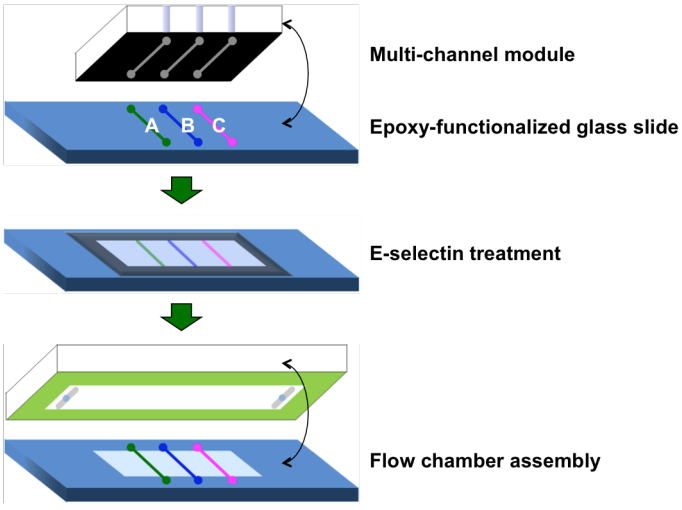

Figure 5.3. A schematic illustration of micropatterning surface using a PDMS gasket. Multiple antibodies against cancer cell surface markers were immobilized on the epoxy-functionalized glass slide using the PDMS gasket (a). The antibody-treated surfaces were back-filled with E-selectin to enhance the cell capture efficiency (b). After the micropatterned surfaces were treated with 1% (w/v) BSA solution to prevent potential non-specific binding, the flow chamber-based experiments using the surfaces were performed within 24 hours (c).

chemical residues from the surfaces. Potential non-specific binding of both protein-coated and uncoated regions was blocked by a final incubation with 1% (w/v) BSA solution. The functionalized surfaces were kept in 4°C of refrigerator and the experiments using the surfaces were performed within 24 hours.

5.2.7. Measurement of Capture Efficiency using Flow Chamber

A typical flow chamber experiment was performed as the previous researches [16]. A glass slide functionalized by protein immobilization, a gasket (30 mm (L) × 10mm (W) × 0.25 mm (D), Glycotech, Gaithersburg, MD), and a rectangular parallel plate flow chamber (Glycotech) were assembled in line under vacuum. Suspensions of fluorescence-labeled cancer cells (MDA-PCa-2b, MDA-MB-361, MCF-7, and HL-60) were injected into the flow chamber using a syringe pump (New Era pump Systems Inc., Farmingdale, NY). The number of captured cells on the antibody-immobilized stripe defined using FITC-BSA treatment was counted using the images taken after one cycle, consisting of forward flow (pushing) for 5 min and backward flow (withdrawing) for 5 min at 50 μL/min (0.08 dyn/cm^2). The surface was washed using PBS for 10 min at 200 μL/min (0.32 dyn/cm^2). To remove the leukocyte cells from the E-selectin-regions, the surface was washed using EGTA/Mg^{2+} in PBS for 3 min at 200 μL/min (0.32 dyn/cm^2) [20]. As the known number of cancer cells was perfused into the flow chamber, the number of captured cells per antibody-stripe could be translated into the capture efficiency (%). All cells on the surface were monitored using an Olympus IX70 inverted microscope (IX 70-S1F2, Olympus America, Inc., Center Valley, PA) with fluorescence light and images were recorded using a 10× objective and a CCD camera (QImaging Retiga 1300B, Olympus America, Inc.). The number of cells on the surfaces was measured, based on the images taken in repetitive observations using ImageJ (NIH).

Cellular responses of each cell line on the interphases between antibody- and E-selectin-stripes under flow were observed under flow. Note that the FITC-BSA-labeled antibody-stripes did not appeared in the images taken under natural light. Cancer cell suspensions in the completed cell culture media (MDA-PCa-2b, MDA-MB-361, and MCF-7) at 10^6 cells/mL were injected into the flow chamber. We monitored cellular responses of the cancer cells on the interphases during PBS washing at a shear stress of 0.32 dyn/cm^2. All cells on the surface were monitored using an Olympus IX70 inverted microscope with fluorescence light and images were recorded using a 4× objective and a CCD camera.

5.2.8. Enhanced capture efficiency on G7 dendrimer-immobilized surfaces

Three different types of surfaces were functionalized by conjugation with each antibody: i) epoxy-functionalized glass surfaces; ii) PEGylated surfaces; and iii) G7 PAMAM dendrimer-immobilized surfaces. The surface functionalization was followed from our previous work [17]. Briefly, epoxy-functionalized glass slides were directly conjugated with antibody solutions. For PEGylated surface, the epoxy-functionalized slides were incubated with PEG (NH_2-$(PEG)_{5000}$-COOH) at a concentration of 0.5 μg/mL in DDI water for 4 hrs, followed by conjugation with antibody solutions after EDC/NHS activation. The dendrimer-surface nanoarchitectures were prepared on the PEGylated slides. After activation of carboxylic termini of PEG using 1:1 mixture of EDC/NHS, partially carboxylated G7 PAMAM dendrimers (50 μM in PBS buffer (pH 9.0)) were immobilized on the surface. The dendrimers immobilized on the surface were then activated using EDC/NHS, followed by conjugation with antibody solutions. After the antibody immobilization, the surfaces were covered with E-selectin at a concentration of 5 μg/mL in PBS buffer for 4 hours. All antibody conjugation reactions were incubated overnight at a concentration of 5 μg/mL (except anti-PSA at 10 μg/mL) for all other antibodies. All surface functionalization reactions were carried out at room temperature. Potential non-specific binding

of both protein-coated and uncoated regions was blocked by a final incubation with 1% (w/v) BSA. The volumes of all reagent solutions were fixed at 40 μL for non-patterned surface or 20 μL for the micropatterned surface, respectively. The surfaces between each step were washed with DDI water or PBS buffer three times to remove the residues from the surfaces.

To compare the surface types for cancer cell capture, MDA-PCa-2b cells, all three cell surface marker-expressed cells, were used. MDA-PCa-2b cell suspensions (10^5 cells/mL in completed cell culture media) were injected into flow chamber at 0.08 dyn/cm^2 of shear stress for one cycle. The surfaces were washed with PBS buffer for 10 minutes at a shear stress of 0.32 dyn/cm^2. The captured cancer cells on the surfaces were counted, followed by normalization using the cell number on epoxy-functionalized surfaces without E-selectin treatment.

5.2.9. Blood sample preparation using Ficoll-Paque Plus

Cancer cell-spiked blood samples were prepared as follows. Cells at a concentration of 1 × 10^6 cells/mL (5 mL) were seeded onto 25cm^2 T flask one day before the experiment. Alive MDA-PCa-2b, MDA-MB-361, and MCF-7 cells were labeled with fluorescence dyes as described in Section 5.2.5. The labeled cells were detached from the surface using TrypLE™ Express (Gibco BRL, Grand Island, NY, USA) to make suspension at a concentration of 1 × 10^5 cells/mL in the whole blood withdrawn from healthy donor. The withdrawn blood was kept in 4°C of refrigerator and the experiments using the whole human blood from healthy donors was performed within 48 hrs. On a round bottom-tube, a sequence of the following solutions was loaded without mixing as the instruction of vendor, in order: 3 mL of Ficoll-Paque Plus (Stemcell Technologies Inc., Vancouver, Canada), and 3mL of the cancer cell-spiked whole blood diluted with 3mL of PBS buffer. The PBS buffer for blood dilution was included with 2% FBS and 95 USP unit heparin. The round bottom-tube was centrifuged at 20 °C for 20 minutes at 1,500 g with brake function off. The upper plasma layer was removed without disturbing the plasma-

Ficoll interphase. Three milliliter of mononuclear cell layer at the plasma-Ficoll interphase (buffy coat) was transferred into a new round bottom tube without disturbing erythrocyte/granulocyte pellets in the bottom layer. The buffy coat including cancer cells was washed twice with the FBS/heparin-included PBS buffer for 10 minutes at 2,000 rpm with brake function on. The recovered cells were suspended with 3 mL of the completed cell culture media. The cell suspension was injected into the flow chamber as described in Section 5.2.7.

To capture the tumor cells from blood samples, multifunctional surfaces with multiple antibodies were prepared using a PDMS gasket. All functionalization using the dendrimers, E-selectin, and antibodies were same as described in Section 5.2.8. Potential non-specific binding of both protein-coated and uncoated regions was blocked by a final incubation with 1 μg/mL methoxy PEG-NH_2 (Nektar Therapeutics) solution.

5.3. RESULTS

5.3.1. Characterization of the functionalized surfaces by X-ray photoelectron spectroscopy (XPS)

Prior to the investigation of the multifunctional surface, cellular responses of CTC model cells were examined on the protein-immobilized surfaces. The proteins such as antibodies and E-selectin can be immobilized on epoxy-functionalized surfaces by simple chemical reaction, as reported in our earlier study [16]. Surface functionalization by protein immobilization was confirmed by XPS, as summarized in **Tables 5.1**. The immobilization of anti-EpCAM, anti-HER2 and anti-PSA was quantitatively confirmed by an increase in carbon and nitrogen compositions, subsequently decrease in silicon detection in the underlying glass substrate, as measured by XPS analysis (**Table 5.1**). All surfaces immobilized with proteins had a high degree of coverage, as evidenced by the lack of visible underlying silicon. The measured nitrogen

content likely corresponds to the degree of protein coverage on the glass surface as the nitrogen composition increased when the total amount of proteins immobilized was increased.

Table 5.1. Measured atomic compositions of functionalized slides by XPS

(mass conc. %)	Control	anti-PSA	anti-HER2	anti-EpCAM
C 1s	28.1	34.6	41.8	42.2
N 1s	0.5	5.4	5.8	5.3
O 1s	55.2	47.0	40.0	39.7
Si 2p	16.2	13.0	12.4	12.8
(C+N)/(O+Si) ratio	0.4	0.7	0.9	0.9

5.3.2. Cellular Responses on the Protein-immobilized Surfaces

On the surfaces prepared with antibodies and E-selectin separately, all cell lines exhibited stable rolling on E-selectin-immobilized slides at a variety of different velocities (0.09-6.45 μm/sec) under 0.08 dyn/cm^2 of shear stress (**Fig. 5.4**). However, all cell lines, excluding leukocyte model HL-60 cells, were stationary binding on the antibody-immobilized surfaces, and the bindings on the surface were dependent on the surface markers of the cells (**Fig. 5.4**).

Cellular responses of all cancer cell models and HL-60 on each antibody-immobilized surface were monitored under flow. Each set of **Fig. 5.4** shows the cellular responses of each cancer cell line on anti-PSA, anti-HER2, and anti-EpCAM-coated surfaces at t = 0 s (a randomly-picked starting recording time during the flow experiment) and 10 s (10 sec after the starting time), respectively. MDA-PCa-2b cells were stationary binding on all of three antibody-immobilized surfaces under flow (**Fig. 5.4a**). Although MDA-MB-361 cells have no binding affinity to the anti-PSA-immobilized surface, the cells were stationary binding on other two

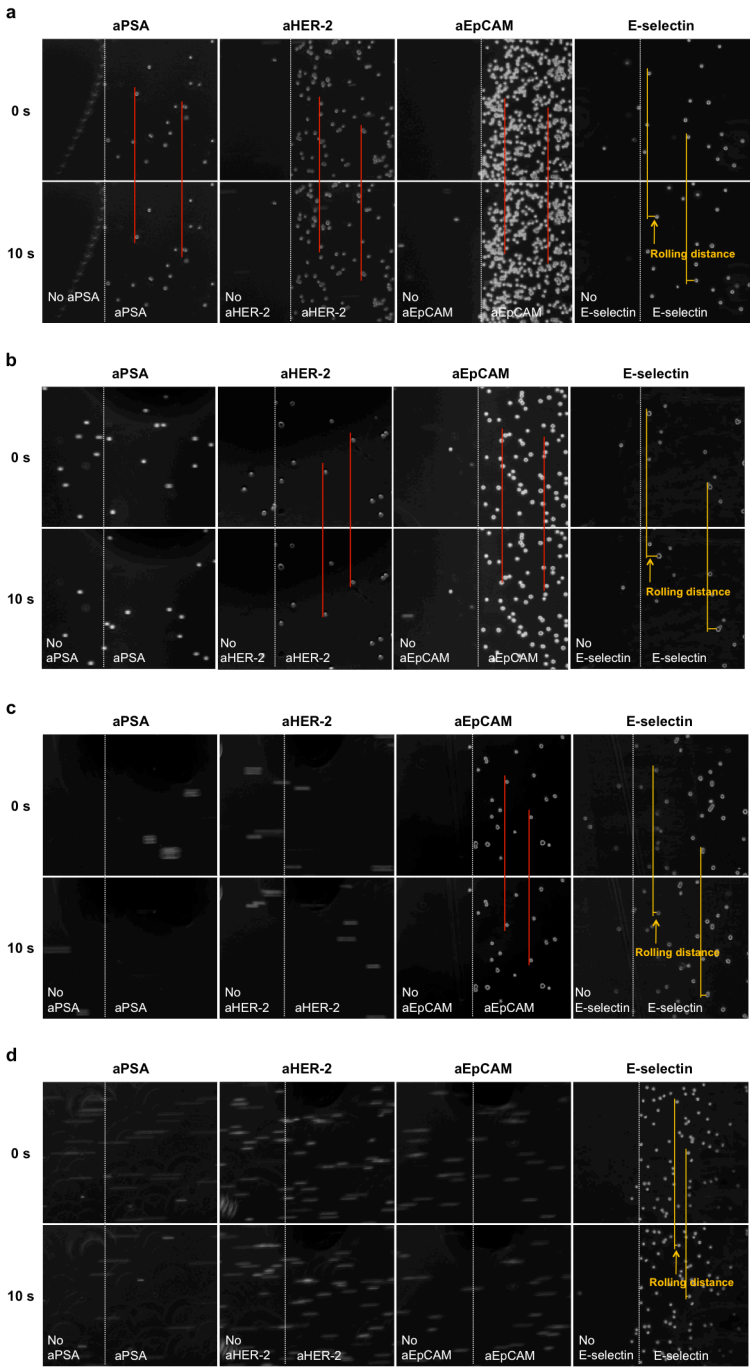

Figure 5.4. Time-course images of four different cell lines under a shear stress of 0.08 dyn/cm^2 on protein-immobilized surfaces. Each cell line, MDA-PCa-2b (a), MDA-MB-361 (b), and MCF-7 (c), showed the stationary binding on the antibody-immobilized surfaces in cell surface marker-dependent ways. However, no interaction on the antibody-immobilized surfaces was observed with HL-60 cells (d). All cell lines, including HL-60 cells, were observed to be rolling under flow on E-selectin-immobilized surface. Rolling velocities of MDA-PCa-2b, MDA-MB-361, MCF-7, and HL-60 cells were 3.13 ± 0.23 μm/sec, 6.45 ± 0.41 μm/sec, 3.22 ± 0.24 μm/sec, and 0.09 ± 0.07 μm/sec, respectively. Flow directions of three sets were from left through right.

surfaces, anti-HER2 and anti-EpCAM-immobilized surfaces (**Fig. 5.4b**). MCF-7 cells were stationary binding only on anti-EpCAM-immobilized surface, not on other surfaces functionalized with anti-PSA and anti-HER2 (**Fig. 5.4c**). Unlike other cancer cell lines, HL-60 cells exhibited no interaction with any antibody-immobilized slides, traveling the flow path in the chamber at the speed of free stream velocity (**Fig. 5.4d**).

On E-selectin-immobilized surface, cellular responses of all cancer cell models and HL-60 were monitored under flow. E-selectin, an adhesive protein involved in the cell rolling of leukocyte and cancer cells on the endothelium during leukocyte homing and cancer metastasis, has shown the cell recruitment effect from flow and the biomimetic effect for cancer cell capture [16, 21]. All cell lines including HL-60 cells exhibited stable rolling on E-selectin-immobilized slides, but the rolling velocities for each cell line varied under 0.08 dyn/cm^2 of shear stress (**Fig. 5.4**). The average rolling velocities of MDA-PCa-2b, MDA-MB-361, and MCF-7 cells on E-selectin-immobilized slides were 3.13 ± 0.23 μm/sec, 6.45 ± 0.41 μm/sec, and 3.22 ± 0.24 μm/sec, respectively. Generally, the rolling velocities of cancer cell lines were faster than those of HL-60 (0.09 ± 0.07 μm/sec) on E-selectin-immobilized surfaces.

5.3.3. Surface Micropatterning

Multiple antibodies can be patterned and miniaturized on one substrate to capture the cancer cells from flow efficiently. Multiple antibodies were immobilized on the epoxy surface using a polydimethylsiloxane (PDMS) gasket that had accurately fabricated channels for protein-immobilized stripes, and the prepared surface is defined as a micropatterned surface (**Fig. 5.5**). The feasibility of PDMS gaskets to define the area for antibody immobilization was confirmed using FITC-conjugated BSA. As the channel width in PDMS gasket was increased, the width of FITC-BSA stripes with green fluorescence was proportionally increased (**Fig. 5.5**).

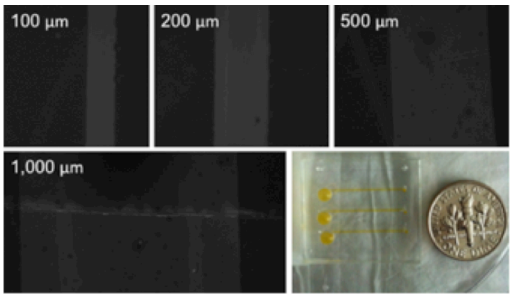

Figure 5.5. Characterization of the surface micropatterning using FITC-BSA solution. The representative images were taken under a fluorescence microscope at 10X magnification. In the case of the representative image with 1,000 μm, it is a merged image of two pictures because it was hard to take by one shot.

The effect of the surface patterning with E-selectin and anti-EpCAM was examined by a quantitative analysis using MDA-MB-361 cells. For surface micropatterning, PDMS gaskets with four channel widths ranging from 100 μm to 1,000 μm were selected. The surface patterning parameters such as widths of antibody and E-selectin-immobilized stripes were optimized to maximize the cell capture. The number of captured cells at different parameters were normalized as follows: for **Fig. 5.6a**, 100 μm channel width and 2 mm distance between channels; for **Fig. 5.6b**, 500 μm channel width and 1 mm distance between channels without E-selectin treatment. As the E-selectin stripe between antibody-stripes was fixed at a width of 2 mm, the MDA-MB-361 cells captured on the anti-EpCAM-immobilized stripes were increased as the width of the stripe increased, irrespective of E-selectin treatment (**Fig. 5.6a**). When the width of the anti-EpCAM-immobilized stripes was fixed at 500 μm, the capture efficiency on the anti-EpCAM- stripes was decreased if the E-selectin-stripes were wider than 2 mm (**Fig. 5.6b**). Both **Fig. 5.6a and b** using the anti-EpCAM/E-selectin-micropatterned surfaces (μAE) demonstrated a statistically significant enhancement (up to 147 fold) in MDA-MB-361 capture, as compared to the results using the surfaces with anti-EpCAM only (μA). It clearly showed the biomimetic effect of E-selectin-mediated cell rolling for cancer cell capture. Based on these results, the

widths of the anti-EpCAM and E-selectin stripes on the micropatterned surfaces were fixed at 500 μm and 2 mm, respectively, demonstrated a statistically significant enhancement (up to ~147-fold) in capture efficiency (**Fig. 5.6**).

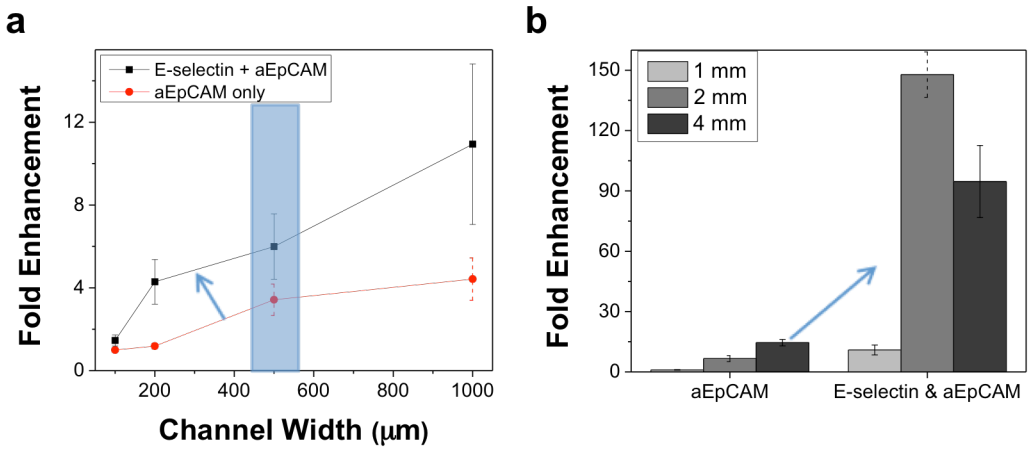

Figure 5.6. Optimization of the surface micropatterning parameters using MDA-MB-361 and anti-EpCAM. The MDA-MB-361 cell capture at the fixed E-selectin width exhibited proportional increase as the channel width increased (a). When the width of the aEpCAM-stripes was fixed at 500 μm, the maximum MDA-MB-361 cell capture was at 2 mm of the E-selectin-immobilized stripes. Error bars: standard error (n=6).

5.3.4. Cellular Responses using the Micropatterned Surfaces

The micropatterned surfaces with multiple antibodies can be used to capture the target cancer cells efficiently, as well as to differentiate the cells according to their surface markers. As we observed using antibody-immobilized surfaces in **Fig. 5.4**, each cell line had different cellular responses on the micropatterned surfaces (surface marker-dependent binding, **Fig. 5.7**). Regardless of E-selectin treatment on the surface, MDA-PCa-2b was binding with all three antibody-stripes (**Fig. 5.7a**), and MDA-MB-361 was binding with both anti-HER2 and anti-EpCAM stripes simultaneously (**Fig. 5.7b**). In the absence of E-selectin, MCF-7 cells were only

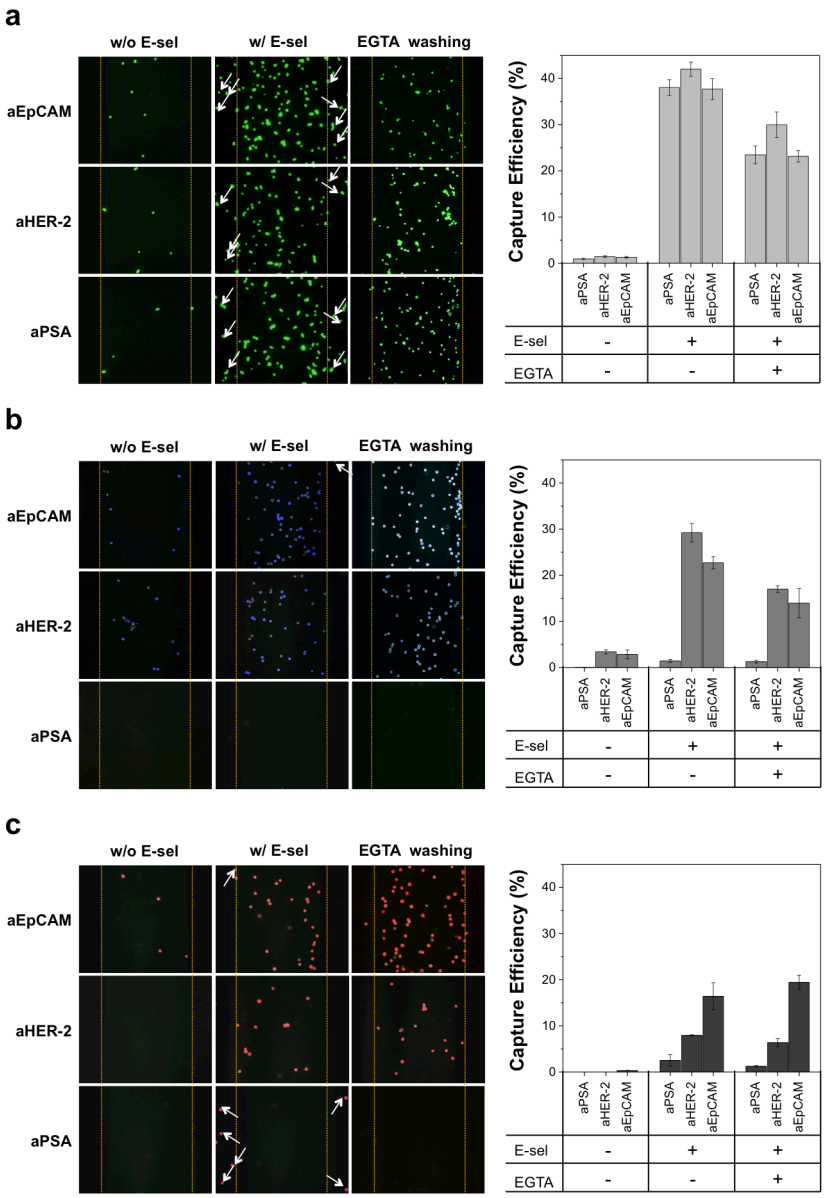

Figure 5.7. Representative images and capture efficiencies of three cell lines, MDA-PCa-2b (a), MDA-MB-361 (b), and MCF-7 (c), on the multifunctional surfaces. Before E-selectin treatment, MDA-PCa-2b cells were binding with all three antibodies (a), but other two cell lines were partially binding; MDA-MB-361 cells (b) on two antibodies, anti-HER2 and anti-EpCAM; MCF-7 cells (c) only on one anti-EpCAM, respectively. After E-selectin treatment, the capture efficiency on the surface was significantly increased, and MCF-7 cells showed the additional binding on anti-HER2-immobilized stripe (c). The cells indicated by the white arrows are those bound to E-selectin-coated region, which reduced the clarity of the patterns. These cells were easily removed upon EGTA/Mg^{2+}-included PBS buffer washing. The capture efficiency was calculated based on the ratio between the bound cell number and the number of the cells injected into the flow chamber per antibody-stripe. The presence of E-selectin and EGTA-washing is expressed as '+' in the figures. Error bars: standard error (n=6).

binding on the anti-EpCAM stripes under the same flow condition. Interestingly, although MCF-7 cells are known to have relatively low HER2 expression [22], the binding affinity of MCF-7 cells on the anti-HER2-immobilized stripes was observed after E-selectin treatment proving that E-selectin plays key role in recruiting cancer cells (**Fig. 5.7c**). E-selectin-mediated cell binding on the surface could not only recruit the cells under flow, but also raise the potential issues for detection specificity because of E-selectin binding affinity of leukocytes in blood [23]. We can control the E-selectin-mediated leukocyte binding by washing the surface with ethylene glycol tetraacetic acid (EGTA, Ca^{2+} chelator)-included PBS buffer because the interaction between E-selectin and cells are calcium^{2+}-dependent (**Fig. 5.7**) [20].

The sequential responses of rolling and capturing on the interphase between E-selectin and antibody-immobilized stripes were observed under flow. As shown in **Fig. 5.8**, all of the cell lines were rolling on the region that functionalized only with E-selectin (the right-hand side of the images), following the flow direction (from right to left). When the rolling cells under flow reached the adjacent antibody-immobilized regions (the left-hand side of the images), the cells were stationary binding in cell surface marker-dependent ways, as shown in **Fig. 5.8**. If the targeted cancer cells have binding affinities to the immobilized antibody, we observed that the cancer cells were accumulated on the boundary of E-selectin and antibody (e.g. MCF-7 cell accumulation on the boundary of anti-EpCAM and E-selectin in **Fig. 5.8c**). The biomimetic effect from E-selectin treatment enhanced the surface detection sensitivity as MCF-7 cell binding on the aHER2-E-selectin-treated interphase (**Fig. 5.8c**).

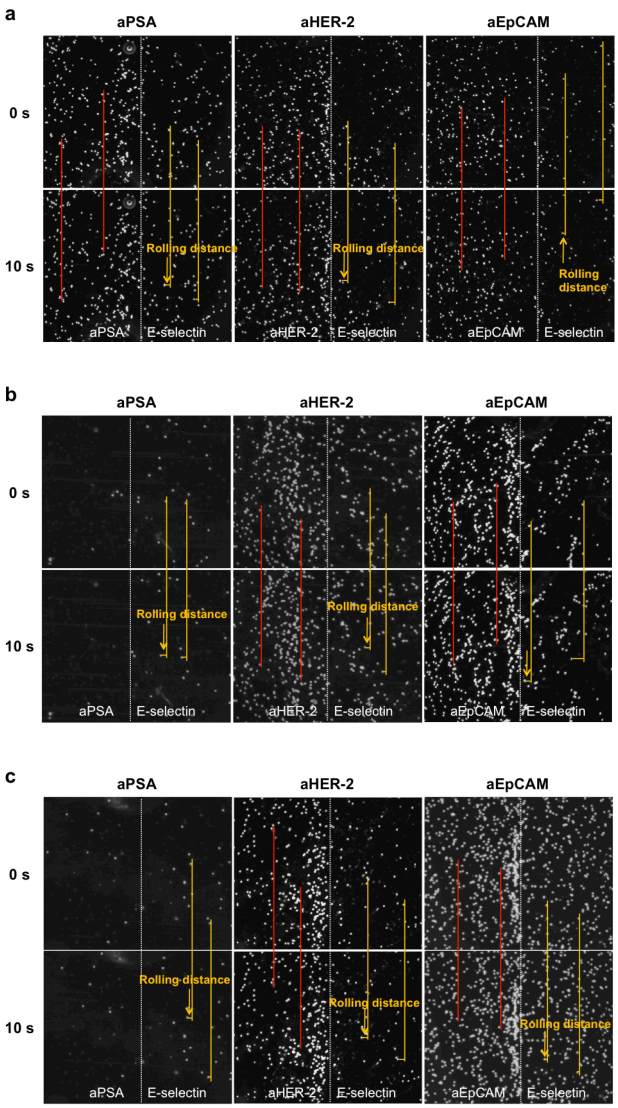

Figure 5.8. Time-course images of three cell lines under shear stress of 0.32 dyn/cm^2 on the surface interphases functionalized with antibodies and E-selectin. All cells exhibited the rolling behavior on the E-selectin-coated surface, but the stationary binding on the antibody-coated surface in cell surface marker-dependent ways. Flow directions of three sets were from right through left.

5.3.5. Cell Separation using the Micropatterned Surfaces

The surface patterning of E-selectin and multiple antibodies can be used to separate the mixture of various cancer cells as their surface markers (**Fig. 5.9**). When we mixed the three different types of cell lines at 1:1:1 ratio (v/v/v), the cells were enriched and differentiated by the

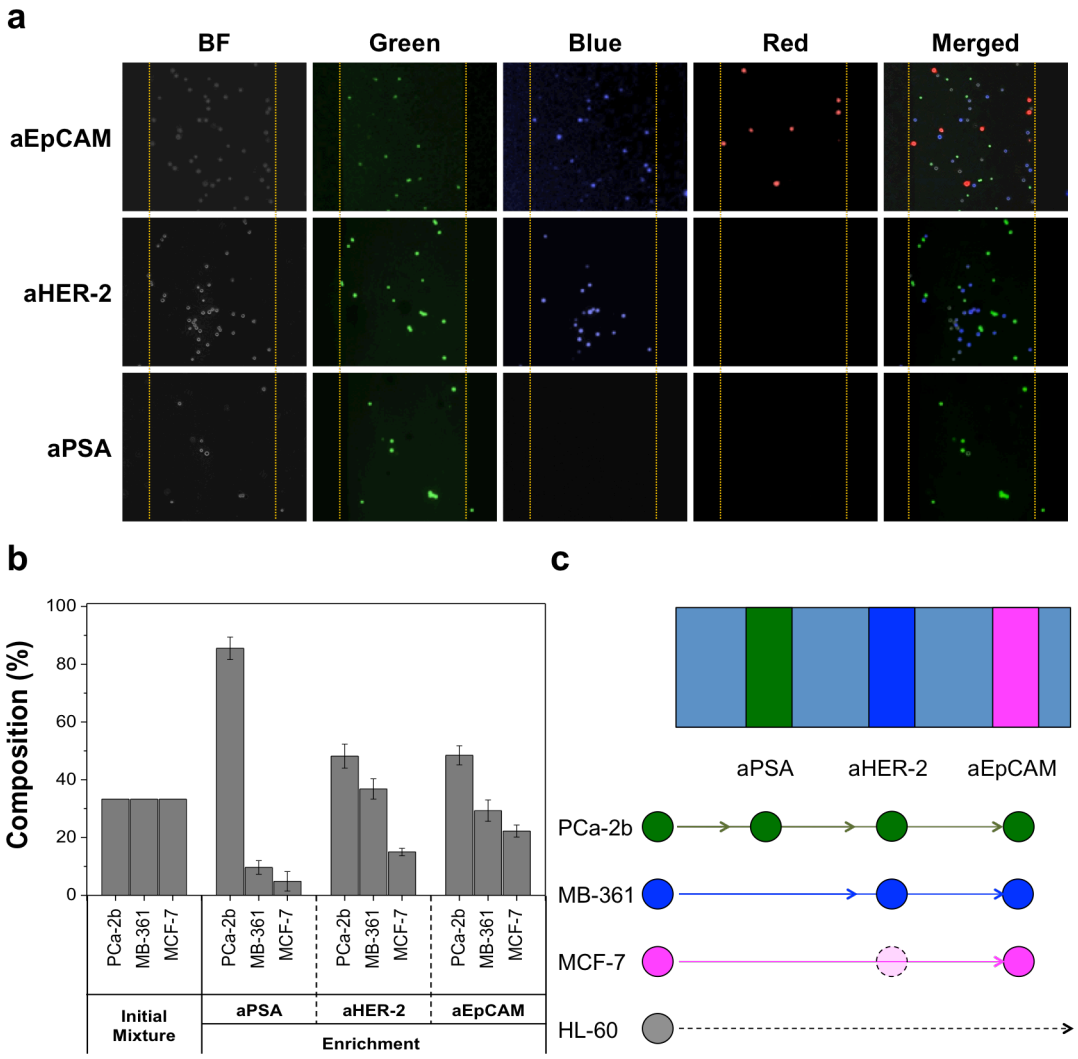

Figure 5.9. Effective cell separation from cell mixture in cell surface marker-dependent ways. a) In heterogeneous cell mixture of three cancer cells, the individual cell line can be distinguished by different fluorescence colors: Calcein AM-labeled MDA-PCa-2b (green), Alive cell tracker Blue-labeled MDA-MB-361 (blue), and Alive cell tracker Red-labeled MCF-7 [red]. The bindings of all three cell lines on the multifunctional surfaces were cell surface marker-specific as observed from those of the individual cell line on the surfaces. The representative image taken under bright field is marked as BF in the figure. b) Composition (%) of each cell line in the initial cell mixture and the bound cells on each antibody stripe were quantitatively measured. The composition percentage in the bound cells on each antibody, especially MDA-PCa-2b cells on anti-PSA stripes, showed clearly the surface marker-dependent cell enrichment. Representative images and composition percentages were obtained after injection of mixture of the three cell populations (1:1:1) onto the multifunctional surfaces of antibodies and E-selectin. Error bars: standard error (n=6). c) A schematic illustration summarizes the results of cell separation from the mixture. The transparent circle for MCF-7 cell on anti-HER2 surface represented the enriched MCF-7 cells after E-selectin treatment. HL-60 cells are represented other hematological cells.

specific binding affinities of the cell lines to the different antibodies on the surface (**Fig. 5.9a**). Although EpCAM on cell surface have binding affinities against anti-EpCAM, the composition percentage of three cell lines from their mixture on the anti-EpCAM-stripe were not as similar as their initial mixing ratios (0.33, **Fig. 5.9b**). Based on the different composition percentage, we can tell that the cell surface marker density of each cell line affects the capturing efficiency on the antibody-stripes. The biomimetic approach (i.e., E-selectin for cell recruitment) also affected the detection sensitivity, as well as cell separating ratios (**Fig. 5.9b** and **Fig. 5.10**). In particular, the separated group composition on anti-HER2-stripes was significantly changed after E-selectin incorporation, because of the enhanced surface sensitivity for MCF-7 cells (**Fig. 5.7c**).

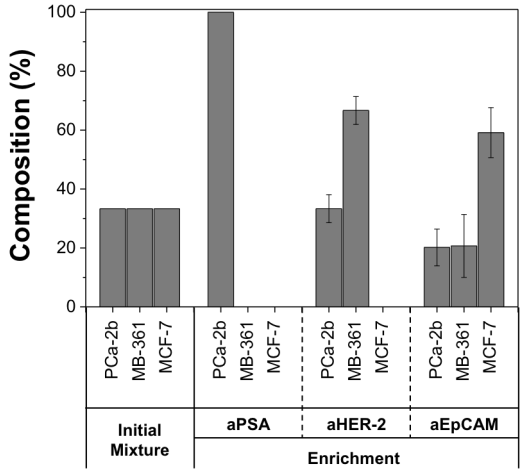

Figure 5.10. Cell separation and enrichment from cell mixture in cell surface marker-dependent ways. Composition (%) of each cell line in the initial cell mixture and the bound cells on each antibody stripe without E-selectin were quantitatively measured. The surface marker-dependent cell enrichment was achieved in the bound cells on each antibody, especially MDA-PCa-2b cells on anti-PSA stripes. Images and composition percentages were obtained after injection of mixture of the three cell populations (1:1:1) onto the multifunctional surfaces of antibodies only, without E-selectin treatment.

5.3.6. Dendrimer-mediated Multivalent Binding Effect for the Micropatterned Surface

The surface efficiency to capture and differentiate various cancer cells using multiple antibodies can be improved by multivalent binding effect using dendrimer nanotechnology. When surface nanoarchitecture of polyamidoamine (PAMAM) dendrimers in our previous works, the dendrimer-mediated multivalent binding can be leveraged to develop a sensitive device for CTC detection [17]. However, because the enhancement of detection sensitivity were measured using the surface functionalized with anti-EpCAM in the previous work, other effects such as micropatterning and antibody types need to be confirmed to develop the multifunctional surfaces. The multifunctional surface is defined as the multiple antibody-immobilized, micropatterned surfaces with E-selectin and dendrimers for two biomimetic approaches.

The biomimetic combination of cell rolling and multivalent binding on the non-patterned surfaces enhanced cell detection under flow. The surfaces modified using dendrimer

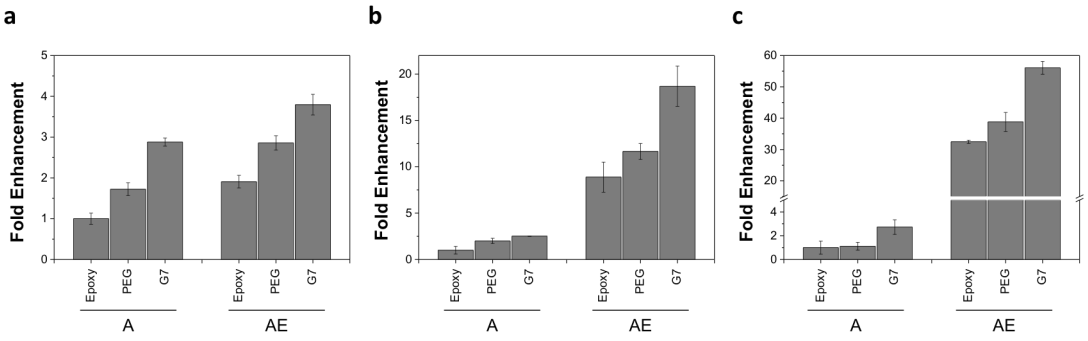

Figure 5.11. Enhanced cell detection by multivalent effect and combination effect of rolling, under dynamic conditions. Three substrates, epoxy-functionalized, PEGylated, and dendrimer-immobilized surfaces without micropatterning, treated with antibodies alone (A) or with both antibodies and E-selectin (AE) are compared in terms of capture efficiency. The captured cancer cells on the surfaces were normalized using the cell number on epoxy-functionalized surfaces without E-selectin treatment. MDA-PCa-2b cell suspension at 10^5 cells/mL in completed media was used. The dendrimer-immobilized surfaces with E-selectin enhance the cancer cell detection (4 fold for anti-EpCAM (a), 17 fold for anti-HER2 (b), and 56 fold for anti-PSA (c)) with greater binding stability, compared to that on the surfaces without dendrimers. Irrespective of the surface type, all of the E-selectin treated surfaces (AE) show higher capture efficiencies of cancer cells under flow than surfaces without E-selectin (A). Error bars: standard error (n=3).

nanotechnology generally captured more cancer cells under flow than the epoxy-functionalized surfaces up to 3 fold (**Fig. 5.11**). The cell capture efficiency was enhanced by a combination effect of cell rolling and multivalent binding effect on dendrimer-incorporated surfaces: 4 fold for anti-EpCAM (**a, in Fig. 5.11**), 17 fold for anti-HER2 (**b**), and 56 fold for anti-PSA (**c**)) with greater binding stability, compared to that on the surfaces without dendrimers.

The biomimetic combination of cell rolling and multivalent binding on the micropatterned surfaces enhanced cell detection under flow. The micropatterned surfaces modified using dendrimer nanotechnology generally captured more cancer cells under flow than the epoxy-functionalized surfaces up to 4 fold (**Fig. 5.12**). The cell capture efficiency was enhanced by a combination effect of cell rolling and multivalent binding effect on dendrimer-incorporated surfaces: 14 fold for anti-EpCAM (**a in Fig. 5.12**), 33 fold for anti-HER2 (**b**), and 39 fold for anti-PSA (**c**)) with greater binding stability, compared to that on the surfaces without

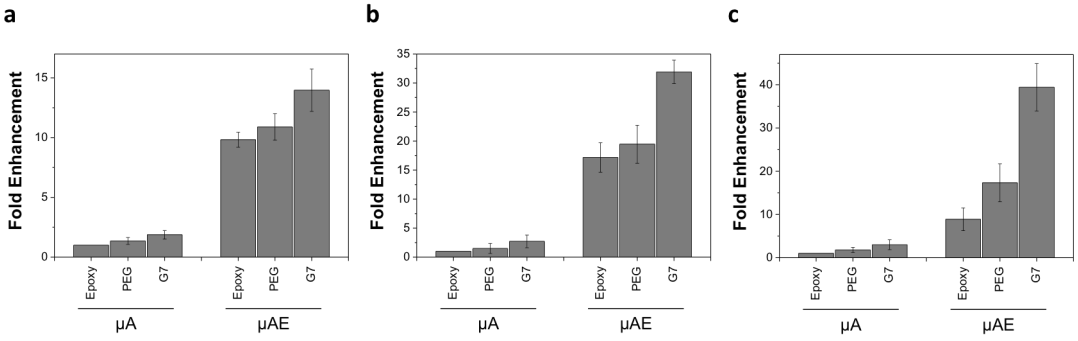

Figure 5.12. Enhanced capture efficiencies by combination effects of rolling, multivalent binding, and micropatterning. Three substrates (epoxy-, PEG-, and dendrimer-substrates) on the micropatterned surfaces, treated with antibodies alone (μA) or with both antibodies and E-selectin (μAE) were compared in terms of capture efficiency. The captured cancer cells on the surfaces were normalized using the cell number on epoxy-functionalized surfaces without E-selectin treatment. MDA-PCa-2b cell suspension at 10^5 cells/mL in completed media was used. The dendrimer-**immobilized** surfaces with E-selectin enhance the cancer cell detection (14 fold for anti-EpCAM (a), 33 fold for anti-HER2 (b), and 39 fold for anti-PSA (c)) with greater binding stability, compared to that on the micropatterned surfaces without dendrimers. Irrespective of the surface type, all of the E-selectin treated surfaces (μAE) show higher capture efficiencies of cancer cells under flow than surfaces without E-selectin (μA). Error bars: standard error (n=3).

dendrimers. At 4X magnification under natural light, the clear patterned stripes through the combination effect of cell rolling and multivalent binding were observed (**Fig. 5.13**).

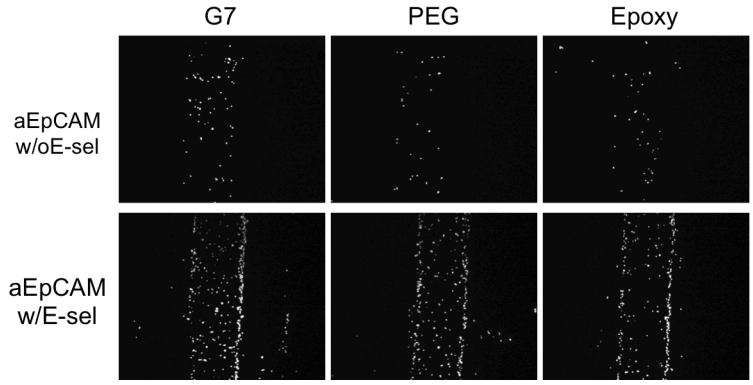

Figure 5.13. Enhanced capture efficiencies by combination effects of rolling, multivalent binding, and micropatterning. The patterned stripes with E-selectin, dendrimers, and antibodies were observed clearly at 4X magnification under natural light.

Irrespective of micropatterning, immobilized antibody type, and cancer cell lines, the dendrimer-mediated surface nanotechnology showed the enhanced capture efficiencies under flow (**Fig. 5.11 and 5.12**). Although the dendrimer nanotechnology itself enhanced the antibody-based capture efficiency (~ 2 fold enhancement), the combination effects of cell rolling and multivalent binding (μAG_7E) were the most effective compared to any single biomimetic approach (μAE and μAG_7) and only antibody-based capture (μA, **Fig. 5.14a-d**). In addition, the enhanced surface sensitivity can be seen from the clear micropatterned stripes at low magnification without further analysis or treatment, which showed the potential to be developed as a detecting kit (**Fig. 5.13**).

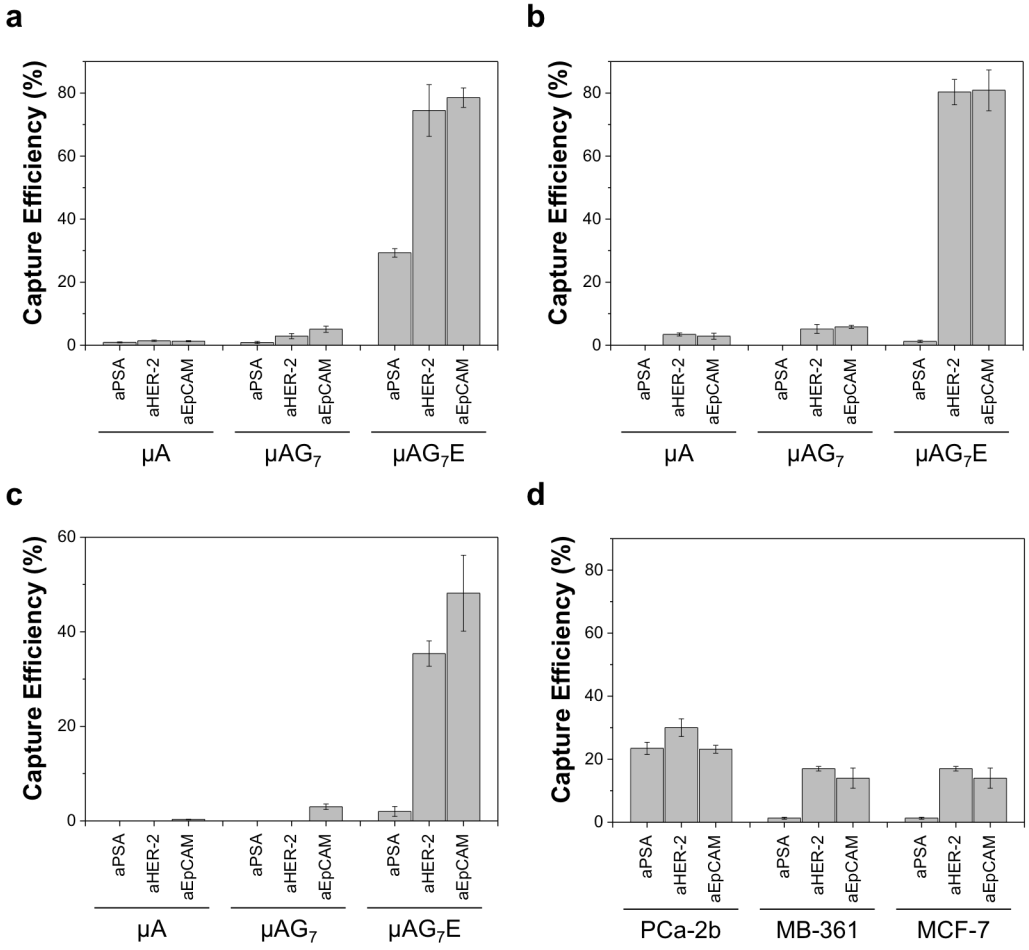

Figure 5.14. Enhanced capture efficiency on the multifunctional surfaces by dendrimer-mediated multivalent binding effect. Capture efficiencies of MDA-PCa-2b (a), MDA-MB-361 (b), and MCF-7 (c) MDA-MB-361 cell lines on the multifunctional surface were summarized. Compared to the antibody on the micropatterned surface (μA), the dendrimer-incorporated surfaces (μG_7A and μG_7AE), especially after E-selectin treatment (μG_7AE), showed the enhanced cell capture efficiencies. Although the binding specificity of the surfaces were slightly decreased after E-selectin treatment, the binding sensitivity and stability were significantly enhanced by multifunctionalized surface using E-selectin and dendrimer nanotechnology. The calculated capture efficiency was based on the captured cell number and the number of the cells injected into the flow chamber per antibody-stripe. Error bars: standard error (n=4).

5.3.7. Blood sample preparation using Ficoll-Paque Plus

The multifunctional surfaces with a combination of cell rolling and multivalent binding effect captured the targeted cancer cells successfully from blood samples. The cancer cells spiked into blood were recovered using Ficoll-Paque Plus, and the recovery yields of three cancer cell lines from blood ranged between 10-20% (**Fig. 5.15**).

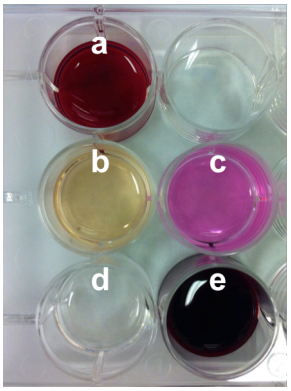

Figure 5.15. Blood separation using Ficoll-Paque Plus. Cancer cell-spiked whole blood withdrawn from healthy donors (a) was separated into plasma (b), buffy coat with MCF-7 cells (c), Ficoll solution (d), and erythrocytes (e). The mononuclear cells including cancer cells and leukocytes were collected into buffy coat layer (c), and the recovery yield of all cancer cells in buffy coat from whole blood was between 10-20%.

5.3.7. Tumor Cell Capture from Blood Samples

The multifunctional surfaces that enhance detection sensitivity can be used to detect CTCs in clinical samples. To check the tumor cell binding in clinically relevant conditions, the CTC model cells were spiked into human blood withdrawn from healthy donors, and treated for analysis as described in Section 5.3.7. As the cancer cells and hematological cells were monitored during PBS washing under flow on the multifunctional surfaces, the rolling responses of the fluorescence-labeled cancer cells and natural leukocytes in blood on E-selectin-stripes were observed. However, leukocytes rolling on the E-selectin-treated surfaces can be removed by washing with EGTA-buffer, thus highly pure population of the captured cells were observed

(between 50%-90% purity, **Fig. 5.16a**). Cancer cells from blood samples showed the surface marker-dependent binding as the cell suspension in *in vitro* cell culture media (**Fig. 5.16b and Fig. 5.17**).

Based on the recovery yield of the cancer cells from blood samples using Ficoll-Paque Plus, the capture efficiency of the cancer cells recovered from whole blood samples were calculated. The capture efficiency of the multifunctional surface (μAG$_7$E, up to 80%) was significantly higher than that of the micropatterned surface only with antibodies (μA, up to 8%) under the same conditions (**Fig. 5.15**). The E-selectin treatment was significantly enhanced

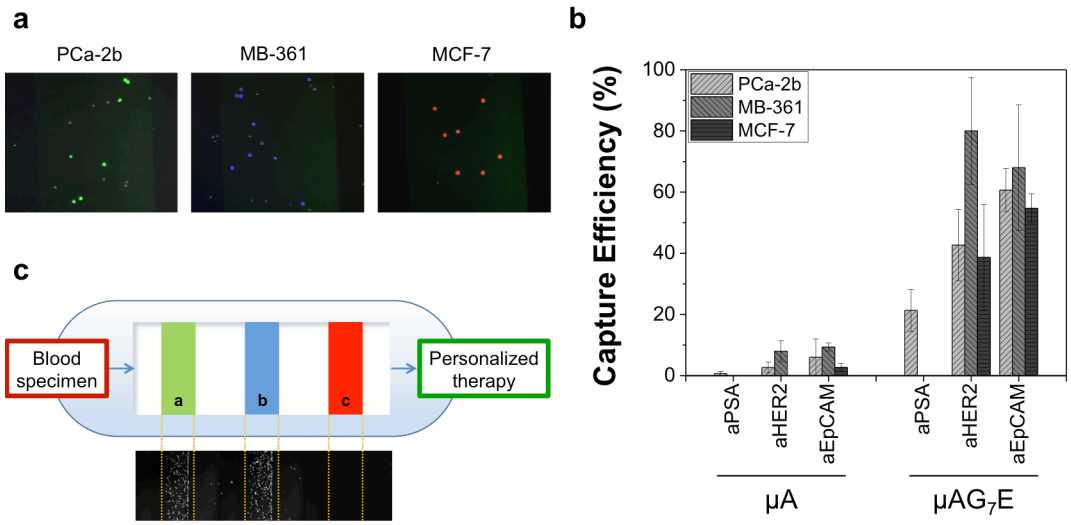

Figure 5.16. Effective cell capture from cancer cell-spiked blood specimens. a) A set of representative images of the captured cells from blood samples on multifunctional stripes with anti-EpCAM showed. The individual cancer cell line in blood specimens can be distinguished by different fluorescence colors: green-labeled MDA-PCa-2b, blue-labeled MDA-MB-361, and red-labeled MCF-7. A few of cells on the images without fluorescence colors are hematological cells from blood, and the purity of the captured cells on the multifunctional surfaces was higher than 50%. b) Detection sensitivity of the multifunctional surfaces (μAG7E) was significantly higher up to 20 fold than that of the surfaces with only antibody stripes (μA). The surface marker-dependent bindings of cancer cell models were also observed. c) The enhanced capture efficiency on the multifunctional surfaces can be developed as a diagnostic platform for rare CTC without analytical assistances of complicated imagining tools. The additional information about cell surface markers with high sensitivity can be used as personalized cancer therapy. Error bars: standard error (n=4).

the surface capture efficiency, irrespective of the dendrimer functionalization. However, the synergetic effect of cell rolling and multivalent binding (μAG_7E) was most effective in cancer cell capture. All the capture efficiencies were enhanced mostly via the combination effects of two biomimetic approaches up to 12 fold, compared to that of antibody-stripes without E-selectin and dendrimers (μA, **Fig. 5.16b and Fig. 5.17**). Based on these results, we can conclude that the E-selectin can induce the rolling of both leukocyte and cancer cells and the antibody stripe can sort out the targeted cancer cells successfully in blood samples. The cell surface marker-specific binding of cancer cells on the multifunctional surfaces with biomimetic approaches can develop to a visualized kit as a pregnant detection kit (**Fig. 5.16c**).

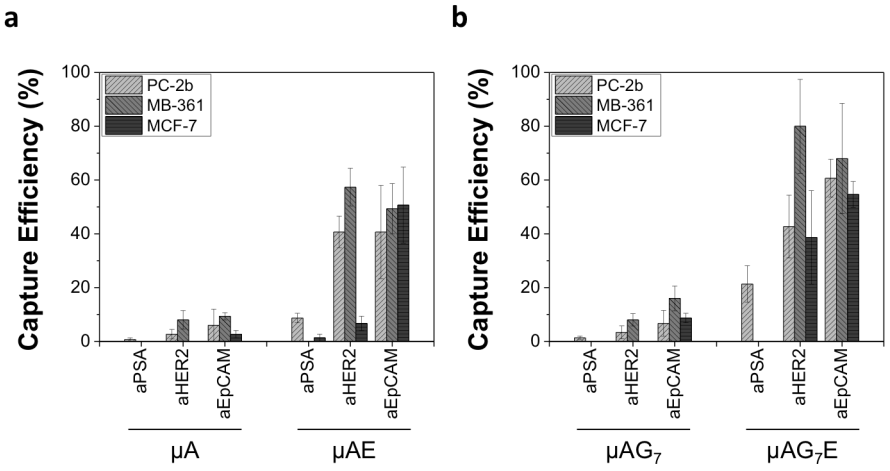

Figure 5.17. Effective cell capture from cancer cell-spiked blood specimens. a) Detection sensitivity of the micropatterned surfaces with E-selectin (μAE) was significantly higher up to 5 fold than that of the surfaces with only antibody stripes (μA). b) Detection sensitivity of the multifunctional surfaces with E-selectin (μAG7E) was significantly higher up to 8 fold than that of the dendrimer-immobilized surfaces with antibody (μAG_7). The surface marker-dependent bindings of cancer cell models were also observed. Error bars: standard error (n=4).

5.4. DISCUSSION

The surface micropatterning with E-selectin and antibodies has great potential to maximize the detection sensitivity from blood samples. First, high specificity, and fast association and dissociation rate constants between E-selectin and its ligands on the cells can facilitate the recruitment of the selected cells from flow onto the surface successfully [16, 21]. Selected cells with E-selectin binding affinity such as cancer cells and leukocytes are binding on the functionalized surfaces, hence the targeted cells can be isolated first from blood samples or cell mixtures on the surface. Secondly, under flow in the presence of Ca^{2+}, we observed the accumulation of the cancer cells on the boundary between antibody- and E-selectin-stripes as shown in **Fig. 5.8**. The sequential rolling and stationary binding of the cells on the boundary were recorded under flow, which is clearly explaining the cell accumulation mechanism on the antibody-stripes. A clear evidence of the enhanced surface capturing efficiency is stationary binding of MCF-7 cells on the aHER2-stripes of the multifunctional surfaces as MCF-7 cells have relatively low expression of HER2 [22].

The combination of biomimetic approaches is important to enhance the detection specificity. E-selectin treatment enhanced the binding affinity of the non-targeted cells, e.g. MDA-MB-361 and MCF-7 binding on anti-PSA stripes (**Fig. 5.9b-c**). However, those non-targeted binding mediated by E-selectin is minimized by the EGTA-included PBS buffer washing, and by the increased density of antibodies immobilized on the dendrimer nanoarchitecture (**Fig. 5.14**). Compared to the other detection methods (purity between 1-20%) [3, 4], the multifunctional surfaces with biomimetic approaches also showed clearly the enhanced detection specificity from blood samples with higher purity (up to 90%, **Fig. 5.16**).

Using this novel multifunctional surface, we can identify multiple surface markers simultaneously by one single injection without cell labeling. This is a proof of concept study to make a multifunctional platform for label-free diagnostic tools (**Fig. 5.16c**). Upon success with

our initial study for EpCAM, HER2, and PSA, the modularity of our device allow for easy incorporation of more surface markers, such as CD24/44, CD146, carcinoembryonic antigen (CEA) and others as needed. Although the expression of one surface biomarker is down-regulated during metastasis, the other antibody-stripes and E-selectin-mediated cancer cell recruitment will be still useful to detect the metastatic cancer cells. In addition to the potential use of this device as a diagnostic tool by collecting CTCs from whole blood under continuous flow without labeling or damaging the CTCs, the advantages of this device include the ability to filter CTCs from bloodstream as a metastatic cancer treatment tool.

Screening of the multiple cancer markers could give us more genetic information such as genetic regulation. For example, the expression of one surface marker is correlated to the other surface marker post-expression in cancer cells. The HER2 expression confers androgen-independent growth to the prostate cancer cell line *in vitro* through the activation of the androgen receptor in a ligand-independent way [24]. The active androgen receptor could affect the transcription of its known down-stream target, PSA, and eventually induce the prostate cancer metastasis [24]. Simultaneous screening of HER2 and PSA using the multifunctional surface could be used to monitor the progress of prostate cancer. The genetic information obtained using the designed multifunctional surfaces also could be used to provide his/her personalized treatment for individual cancer patient, which can further enhance the therapeutic efficiency of metastatic cancer patients. If we use antibodies against the organ-specific antigens (e.g. PSA majorly expressed in human prostate), the cellular responses of the CTCs on the antibodies against tissue-specific cancer markers can be used an indicator of their origins.

5.5. SUMMARY

Taken together, the significantly increased sensitivity and specificity of the multifunctional surface for cancer cell capture were achieved by two biomimetic approaches: cell rolling on E-selectin and stable binding through nanotechnology-induced multivalent binding. The biomimetic surface showed the remarkably enhanced capture efficiency of the tumor cells, along with the increased purity of the captured cell population from cancer cells in culture media as well as in human blood. Additionally, we have shown that the surface micropatterning with multiple antibodies and E-selectin showed the separation effect of cancer cells as the cell surface markers. Our results clearly demonstrate that the combined nanotechnology and biomimicry have a great potential to be applied for highly sensitive detection of rare tumor cells from blood.

5.6. REFERENCES

1. Ashworth, T.R., *A case of cancer in which cells similar to those in the tumors were seen in the blood after death.* Aus Med J, 1869. **15**: p. 146-149.

2. Cristofanilli, M., et al., *Circulating tumor cells, disease progression, and survival in metastatic breast cancer.* N Engl J Med, 2004. **351**(8): p. 781-91.

3. Nagrath, S., et al., *Isolation of rare circulating tumour cells in cancer patients by microchip technology.* Nature, 2007. **450**(7173): p. 1235-9.

4. Stott, S.L., et al., *Isolation of circulating tumor cells using a microvortex-generating herringbone-chip.* Proc Natl Acad Sci U S A, 2010. **107**(43): p. 18392-7.

5. Xiao, Y., et al., *Anti-HER2 IgY antibody-functionalized single-walled carbon nanotubes for detection and selective destruction of breast cancer cells.* BMC Cancer, 2009. **9**: p. 351.

6. Thierry, B., et al., *Herceptin functionalized microfluidic polydimethylsiloxane devices for the capture of human epidermal growth factor receptor 2 positive circulating breast cancer cells.* Biomicrofluidics, 2010. **4**(3): p. 32205.

7. Psaila, B. and D. Lyden, *The metastatic niche: adapting the foreign soil.* Nat Rev Cancer, 2009. **9**(4): p. 285-93.

8. Thalmann, G.N., et al., *LNCaP progression model of human prostate cancer: androgen-independence and osseous metastasis.* Prostate, 2000. **44**(2): p. 91-103 Jul 1;44(2).

9. Osta, W.A., et al., *EpCAM is overexpressed in breast cancer and is a potential target for breast cancer gene therapy.* Cancer Res, 2004. **64**(16): p. 5818-24.

10. Sieuwerts, A.M., et al., *Anti-epithelial cell adhesion molecule antibodies and the detection of circulating normal-like breast tumor cells.* J Natl Cancer Inst, 2009. **101**(1): p. 61-6.

11. Jacobs, T.W., et al., *Specificity of HercepTest in determining HER-2/neu status of breast cancers using the united states food and drug administration-approved scoring system.* J Clin Oncol, 1999. **17**(7): p. 1983-1987.

12. Pauletti, G., et al., *Assessment of methods for tissue-based detection of the HER-2/neu alteration in human breast cancer: A direct comparison of fluorescence in situ hybridization and immunohistochemistry.* J Clin Oncol, 2000. **18**(21): p. 3651-3664.

13. Elkin, E.B., et al., *HER-2 testing and trastuzumab therapy for metastatic breast cancer: a cost-effectiveness analysis.* J Clin Oncol, 2004. **22**(5): p. 854-63.

14. Smith, M.R., S. Biggar, and M. Hussain, *Prostate-specific antigen messenger RNA is expressed in non-prostate cells: implications for detection of micrometastases.* Cancer Res, 1995. **55**(12): p. 2640-4.

15. Navone, N.M., et al., *Establishment of two human prostate cancer cell lines derived from a single bone metastasis.* Clin Cancer Res, 1997. **3**(12 Pt 1): p. 2493-500.

16. Myung, J.H., et al., *Enhanced tumor cell isolation by a biomimetic combination of E-selectin and anti-EpCAM: implications for the effective separation of circulating tumor cells (CTCs).* Langmuir, 2010. **26**(11): p. 8589-96.

17. Myung, J.H., et al., *Dendrimer-mediated multivalent binding for the enhanced capture of tumor cells.* Angew Chem Int Ed Engl, 2011. **50**(49): p. 11769-72.

18. Hong, S., et al., *Covalent immobilization of p-selectin enhances cell rolling.* Langmuir, 2007. **23**(24): p. 12261-8.

19. Goldman, A.J., R.G. Cox, and H. Brenner, *Slow viscous motion of a sphere parallel to a plane wall--II Couette flow.* Chemical Engineering Science, 1967. **22**(4): p. 653-660.

20. Launiere, C., et al., *Channel Surface Patterning of Alternating Biomimetic Protein Combinations for Enhanced Microfluidic Tumor Cell Isolation.* Anal Chem, 2012. **84**(9): p. 4022-8.

21. Myung, J.H., et al., *Direct measurements on CD24-mediated rolling of human breast cancer MCF-7 cells on E-selectin.* Anal Chem, 2011. **83**(3): p. 1078-83.

22. Rusnak, D.W., et al., *The effects of the novel, reversible epidermal growth factor Receptor/ErbB-2 tyrosine kinase inhibitor, GW2016, on the growth of human normal and tumor-derived cell lines in vitro and in vivo.* Molecular Cancer Therapeutics, 2001. **1**(2): p. 85-94.

23. Bevilacqua, M.P., et al., *Endothelial Leukocyte Adhesion Molecule-1 - an Inducible Receptor for Neutrophils Related to Complement Regulatory Proteins and Lectins.* Science, 1989. **243**(4895): p. 1160-1165.

24. Signoretti, S., et al., *Her-2-neu expression and progression toward androgen independence in human prostate cancer.* J Natl Cancer Inst, 2000. **92**(23): p. 1918-25.

CHAPTER 6

CONCLUSIONS AND OUTLOOK

Selective detection of CTCs is of significant clinical importance for the clinical diagnosis and prognosis of cancer metastasis. However, largely due to the extremely low number of CTCs (as low as one in 10^6-10^9 hematologic cells) in the blood of patients, effective detection and separation of the rare cells remain a tremendous challenge.

The preceding chapters 2, 4, and 5 in this dissertation focus on biomimetic approaches such as E-selectin-mediated cell rolling and dendrimer-mediated multivalent binding effects to enhance the sensitivity and specificity of anti-EpCAM-based CTC detection. Cell rolling is known to play a key role in physiological processes such as recruitment of leukocytes to sites of inflammation and selectin-mediated CTC metastasis. As a few surface markers such as EpCAM, HER-2, and PSA are expressed on CTCs but not on normal hematologic cells, substrates immobilized with antibodies against the surface markers specifically isolate the CTCs. The interaction between CTCs and anti-EpCAM can be enhanced by multivalent binding effect using PAMAM dendrimer immobilization on the substrates.

The findings in this dissertation regarding cancer cell binding with adhesive proteins such as selectin and anti-EpCAM can be summarized as follows:

- The biomimetic surfaces functionalized with P-/E-selectin and anti-EpCAM induce different responses of HL-60 (used as a model of leukocytes in this study) and other models of CTCs (breast cancer-MCF-7, MDA-MB-361, and MDA-MB-231 cells, and prostate cancer-MDA-PCa-2b cells).
- HL-60 and other tumor cells showed different degrees of interaction with P-/E-selectin and anti-EpCAM at a shear stress of 0.32 dyn/cm^2: All cell lines including HL-60 cells showed

interactions with E-selectin; Only HL-60 cells, not other tumor cells, were rolling on the P-selectin-immobilized surfaces; All tumor cells except HL-60 cells interacted with anti-EpCAM-coated surfaces, forming stationary binding.

- The combination of the rolling (E-selectin) and stationary binding (anti-EpCAM) resulted in substantially enhanced separation capacity and capture efficiency (more than 3-fold enhancement), as compared to a surface functionalized solely with anti-EpCAM which has been commonly used for CTC capture.

A novel surface engineering approach to exploiting the strong multivalent binding for sensitive detection of tumor cells was investigated in chapter 4. The findings in this dissertation regarding cancer cell binding through multivalent binding effect can be summarized as follows:

- A direct, quantitative analysis using SPR revealed that the dendrimer conjugates exhibited a dramatically enhanced binding avidity by 10^6-fold, compared to free aEpCAM.
- Surface immobilization of the dendrimer-aEpCAM conjugates resulted in a significantly enhanced tumor cell detection with greater stability than the surfaces with the linear PEG-aEpCAM conjugates.

Based on these findings, a multifunctional surface through a combination of E-selectin-mediated cell rolling and dendrimer-mediated multivalent binding effect has been developed. Multiple antibodies directed to cancer cell-specific surface markers such as EpCAM, HER2, and PSA, were also incorporated on the multifunctional surfaces. The biomimetic combination of E-selectin, multiple antibodies, and dendrimers were miniaturized on the micropatterned surface. The results on the multifunctional surfaces are summarized as follows:

- Cell-type dependent responses of several different types of cancer cells (MDA-PCa-2b, MDA-MB-361, and MCF-7) were screened on the antibody-functionalized surfaces at a shear stress of 0.08 dyn/cm^2: All cell lines showed interactions with anti-EpCAM; On anti-HER2-immobilized surface, two cell lines except MCF-7 were stationary binding; Only MDA-PCa-2b cells interacted with anti-PSA-coated surfaces, forming stationary binding.
- The micropatterned surfaces for multiple antibodies were defined as 500 μm antibody-immobilized patterns with 2 mm distance between patterns to maximize the capture efficiency under flow and miniaturize the surface size.
- The biomimetic combination on the micropatterned surfaces with multiple antibodies showed the enhancement in terms of capture efficiency: multiple antibodies (μA) < μA in addition of dendrimer (μAG_7) < μA in addition of dendrimer (μAE) < μAG_7 in addition of E-selectin (μAG_7E).
- The unique combination of the two physiological processes (μAG_7E) leads to a significantly improved surface detection of CTC model cells spiked into human blood, up to 82% capture efficiency and 90% capture specificity (purity).

In addition, CD24 overexpressed CD24 overexpressed on MCF-7 cells, in chapter 3, is identified as one of E-selectin ligands by the following investigations:

- The binding kinetics between CD24 and E-selectin was directly measured using SPR, which revealed that CD24 has a binding affinity against E-selectin ($K_D = 3.4 \pm 0.7$ nM).
- The involvement of CD24 in MCF-7 cell rolling was confirmed by the rolling behavior that was completely blocked when cells were treated with anti-CD24.
- A simulated study by flowing microspheres coated with CD24 onto E-selectin-immobilized surfaces further revealed that the binding is Ca^{2+} dependent.

- Additionally, actin filaments are involved in the CD24-mediated cell rolling, as observed by the decreased rolling velocities of the MCF-7 cells upon treatment with cytochalasin D (an inhibitor of actin-filament dynamics) and the stationary binding of CD24-coated microspheres (the lack of actins) on the E-selectin-immobilized slides.

This dissertation demonstrates that cell-specific detection and separation is achieved through mimicking the biological processes of cell rolling and stationary binding, which leads to a CTC detection device with significantly enhanced specificity and sensitivity without any complex fabrication process. Eventually, the developed diagnostic device via mimicking these natural phenomena could measure the number of CTCs from the peripheral blood samples of cancer patients and predict the cancer metastasis. In addition to the potential use of this device as a metastatic cancer treatment tool by filtering CTCs from the bloodstream, the advantages of this device include the ability to collect CTCs from whole blood under continuous flow without labeling or damaging the CTCs. Therefore, the collected CTCs can be extracted and potentially be subject of further analysis such as genetic understanding and responses for currently available therapeutic drugs by culture expansion.

The versatile surface platform with biomimetic approaches that is developed in this dissertation for CTC detection can be applied for other diagnostic purposes. A large class of hematological cells, including leukocytes, platelets, neutrophils, mesenchymal and hematopoietic stem cells, exhibits rolling on E-selectin. If the cell recruitments of E-selectin from flow are combined with the targeting moieties with selective binding affinity to target cells, this biomimetic surfaces will provide the technology to a clinically significant device to capture any disease-related hematological cells in blood with high sensitivity and specificity. On the other hand, dendrimer-mediated multivalent binding has not only been utilized to enhance targeting efficacy of tumor cells as demonstrated in this dissertation, rather it has also been leveraged to

develop highly sensitive devices for the detection of DNA [1], toxins [2], and antigens [3]. For instance, the dendrimer functionalization on substrates was able to enhance the capture of oligomers by 2-fold in nucleic acid hybridization experiments using fluorophore-labeled complementary oligonucleotide targets, compared to the untreated intact substrate [4, 5]. Disease-related molecules such as circulating DNA released by necrosis, apoptosis, and active release from tumor [6], human immunodeficiency virus (HIV)-p24 antigen [7], and choleragen (cholera toxin) [8] can be targeted. However, these detection methods under the static condition have a limitation to analyze the clinical samples with large quantity. The continuous analysis system under flow developed in this dissertation using dendrimers also can be used for detection of the disease-related DNA, toxins, and antigens in clinical samples.

Although the biomimetic surfaces developed in this dissertation showed the enhanced detection sensitivity, we need further investigations to improve the surface properties for clinical samples. This dissertation presents quantitative analysis on the multifunctional surfaces with biomimetic techniques using *in vitro* cancer cell lines. Since the properties of *in vitro* cancer cells could be different from real CTCs, we cannot exclude the possibility of the CTCs in blood specimens withdrawn from patients to be captured differently. On the other hand, because our technique for surface functionalization is based on simple covalent bindings of random amine groups of the antibodies or E-selectin, the three-dimensional structure, binding site orientation, and surface distribution of the proteins may be varied from batch to batch. To control the orientation of antibodies, one method would be to modify the protein reactive groups. For example, the carboxylate groups in antibody Fc regions may be altered to thiol group that will bind with the thiol-terminated dendrimers. The disulfide bond between antibodies and the dendrimer-immobilized surface can dissociate using free thiol chemicals to release the captured cells such as tumor cells from the surface. The captured cells could be transferred to post-analysis without releasing damage using enzyme, and the dendrimer-immobilized surface can be

reused. The surface functionalized with protein combinations also need to be further characterized. Although the quantitative analysis between EpCAM and anti-EpCAM-immobilized dendrimer conjugates using SPR, the anti-EpCAM immobilized conditions such as the density and orientation on the dendrimer-immobilized surfaces may be different from the free anti-EpCAM-dendrimer conjugates. The direct measurement of EpCAM affinity to the anti-EpCAM-dendrimer-immobilized surface using AFM may give important clues to characterize the surfaces. These future efforts combined with work presented in this dissertation will play a critical role to advance surface engineering for early diagnosis of cancer metastasis.

6.1. REFERENCES

1. Stears, R.L., R.C. Getts, and S.R. Gullans, *A novel, sensitive detection system for high-density microarrays using dendrimer technology.* Physiological genomics, 2000. **3**(2): p. 93-9.

2. Song, X.D. and B.I. Swanson, *Direct, ultrasensitive, and selective optical detection of protein toxins using multivalent interactions.* Analytical Chemistry, 1999. **71**(11): p. 2097-2107.

3. Angenendt, P., et al., *Next generation of protein microarray support materials: evaluation for protein and antibody microarray applications.* Journal of chromatography. A, 2003. **1009**(1-2): p. 97-104.

4. Benters, R., et al., *DNA microarrays with PAMAM dendritic linker systems.* Nucleic Acids Res, 2002. **30**(2): p. E10.

5. Benters, R., C.M. Niemeyer, and D. Wohrle, *Dendrimer-activated solid supports for nucleic acid and protein microarrays.* Chembiochem, 2001. **2**(9): p. 686-94.

6. Mouliere, F. and A.R. Thierry, *The importance of examining the proportion of circulating DNA originating from tumor, microenvironment and normal cells in colorectal cancer patients.* Expert Opin Biol Ther, 2012. **12 Suppl 1**: p. S209-15.

7. Lee, K.B., et al., *The use of nanoarrays for highly sensitive and selective detection of human immunodeficiency virus type 1 in plasma.* Nano Lett, 2004. **4**(10): p. 1869-1872.

8. Richards, R.L., et al., *Choleragen (Cholera Toxin) - Bacterial Lectin.* Proc Natl Acad Sci USA, 1979. **76**(4): p. 1673-1676.

BIBLIOGRAPHY

Aeed, P.A., et al., *Partial characterization of the N-linked oligosaccharide structures on P-selectin glycoprotein ligand-1 (PSGL-1).* Cell Res, 2001. **11**(1): p. 28-36.

Aigner, S., et al., *CD24 mediates rolling of breast carcinoma cells on P-selectin.* Faseb J, 1998. **12**(12): p. 1241-51.

Aigner, S., et al., *CD24, a mucin-type glycoprotein, is a ligand for P-selectin on human tumor cells.* Blood, 1997. **89**(9): p. 3385-95.

Ajikumar, P.K., et al., *Carboxyl-terminated dendrimer-coated bioactive interface for protein microarray: high-sensitivity detection of antigen in complex biological samples.* Langmuir, 2007. **23**(10): p. 5670-7.

al Baba, M.A., et al., *Experience of Jeddah Kidney Center in Pediatric Renal Transplantation.* Transplant Proc, 1998. **30**(7): p. 3679-80.

Al-Bassam, A., et al., *Congenital H-type anourethral fistula with severe urethral hypoplasia: case report and review of the literature.* J Pediatr Surg, 1998. **33**(10): p. 1550-3.

al-Faleh, F.Z., et al., *Treatment of chronic hepatitis C genotype 4 with alpha-interferon in Saudi Arabia: a multicenter study.* Hepatogastroenterology, 1998. **45**(20): p. 488-91.

Al-Hajj, M., et al., *Prospective identification of tumorigenic breast cancer cells.* Proc Natl Acad Sci U S A, 2003. **100**(7): p. 3983-8.

Albrecht, H., *Trastuzumab (Herceptin(R)): overcoming resistance in HER2-overexpressing breast cancer models.* Immunotherapy, 2010. **2**(6): p. 795-8.

Ali, A., S.B. Naqvi, and D. Sheikh, *Resistance pattern of clinical isolates from cases of chronic ear infection II.* Pak J Pharm Sci, 1998. **11**(2): p. 31-7.

Alix-Panabieres, C., V. Muller, and K. Pantel, *Current status in human breast cancer micrometastasis.* Curr Opin Oncol, 2007. **19**(6): p. 558-63.

Allard, W.J., et al., *Tumor cells circulate in the peripheral blood of all major carcinomas but not in healthy subjects or patients with nonmalignant diseases.* Clin Cancer Res, 2004. **10**(20): p. 6897-904.

Almutairi, A., et al., *Biodegradable dendritic positron-emitting nanoprobes for the noninvasive imaging of angiogenesis.* Proc Natl Acad Sci U S A, 2009. **106**(3): p. 685-90.

Ambrosini, P.J. and R.M. Sheikh, *Increased plasma valproate concentrations when coadministered with guanfacine.* J Child Adolesc Psychopharmacol, 1998. **8**(2): p. 143-7.

Ammons, W.S., et al., *In vitro and in vivo pharmacology and pharmacokinetics of a human engineered monoclonal antibody to epithelial cell adhesion molecule.* Neoplasia, 2003. **5**(2): p. 146-54.

Andre, S., et al., *Lactose-containing starburst dendrimers: influence of dendrimer generation and binding-site orientation of receptors (plant/animal lectins and immunoglobulins) on binding properties.* Glycobiology, 1999. **9**(11): p. 1253-61.

Angenendt, P., et al., *Next generation of protein microarray support materials: evaluation for protein and antibody microarray applications.* Journal of chromatography. A, 2003. **1009**(1-2): p. 97-104.

Arifov, S.S., et al., *[Removal of the stapes from the tympanic cavity while cleaning the ear with cotton wool].* Vestn Otorinolaringol, 1998(6): p. 53.

Ashworth, T.R., *A case of cancer in which cells similar to those in the tumors were seen in the blood after death.* Aus Med J, 1869. **15**: p. 146-149.

Atherton, A. and G.V. Born, *Relationship between the velocity of rolling granulocytes and that of the blood flow in venules.* J Physiol, 1973. **233**(1): p. 157-65.

Attard, G., et al., *Reporting the capture efficiency of a filter-based microdevice: a CTC is not a CTC unless it is CD45 negative--letter.* Clin Cancer Res, 2011. **17**(9): p. 3048-9; author reply 3050.

Bae, J.W., et al., *Dendron-mediated self-assembly of highly PEGylated block copolymers: a modular nanocarrier platform.* Chem Commun (Camb), 2011. **47**(37): p. 10302-4.

Balasubramanian, S., et al., *Micromachine-enabled capture and isolation of cancer cells in complex media.* Angew Chem Int Ed Engl, 2011. **50**(18): p. 4161-4.

Balzar, M., et al., *The biology of the 17-1A antigen (Ep-CAM).* J Mol Med, 1999. **77**(10): p. 699-712.

Barthel, S.R., et al., *Targeting selectins and selectin ligands in inflammation and cancer.* Expert Opin Ther Targets, 2007. **11**(11): p. 1473-91.

Baumann, P., et al., *CD24 expression causes the acquisition of multiple cellular properties associated with tumor growth and metastasis.* Cancer Res, 2005. **65**(23): p. 10783-93.

Baumhoer, D., et al., *Expression of CD24, P-cadherin and S100A4 in tumors of the ampulla of Vater.* Mod Pathol, 2009. **22**(2): p. 306-13.

Benters, R., et al., *DNA microarrays with PAMAM dendritic linker systems.* Nucleic Acids Res, 2002. **30**(2): p. E10.

Benters, R., C.M. Niemeyer, and D. Wohrle, *Dendrimer-activated solid supports for nucleic acid and protein microarrays.* Chembiochem, 2001. **2**(9): p. 686-94.

Bevilacqua, M.P., et al., *Endothelial Leukocyte Adhesion Molecule-1 - an Inducible Receptor for Neutrophils Related to Complement Regulatory Proteins and Lectins.* Science, 1989. **243**(4895): p. 1160-1165.

Brodt, P., et al., *Liver endothelial E-selectin mediates carcinoma cell adhesion and promotes liver metastasis.* Int J Cancer, 1997. **71**(4): p. 612-9.

Brorson, S.H., *Bovine serum albumin (BSA) as a reagent against non-specific immunogold labeling on LR-White and epoxy resin.* Micron, 1997. **28**(3): p. 189-95.

Brunk, D.K., D.J. Goetz, and D.A. Hammer, *Sialyl Lewis(x)/E-selectin-mediated rolling in a cell-free system.* Biophys J, 1996. **71**(5): p. 2902-7.

Budd, G.T., et al., *Circulating tumor cells versus imaging--predicting overall survival in metastatic breast cancer.* Clin Cancer Res, 2006. **12**(21): p. 6403-9.

Carlsson, R., et al., *Gastro-oesophageal reflux disease in primary care: an international study of different treatment strategies with omeprazole. International GORD Study Group.* Eur J Gastroenterol Hepatol, 1998. **10**(2): p. 119-24.

Cattini, P.A., Y. Jin, and F. Sheikh, *Detection of 28S RNA with the FGF-2 cDNA at high stringency through related G/C-rich sequences.* Mol Cell Biochem, 1998. **189**(1-2): p. 33-9.

Chang, S.F., et al., *Tumor cell cycle arrest induced by shear stress: Roles of integrins and Smad.* Proc Natl Acad Sci U S A, 2008. **105**(10): p. 3927-32.

Chen, S. and T.A. Springer, *An automatic braking system that stabilizes leukocyte rolling by an increase in selectin bond number with shear.* J Cell Biol, 1999. **144**(1): p. 185-200.

Cheng, G.Z., et al., *Twist transcriptionally up-regulates AKT2 in breast cancer cells leading to increased migration, invasion, and resistance to paclitaxel.* Cancer Res, 2007. **67**(5): p. 1979-1987.

Chiang, A.C. and J. Massague, *Molecular basis of metastasis.* N Engl J Med, 2008. **359**(26): p. 2814-23.

Chiu, S.J., N.T. Ueno, and R.J. Lee, *Tumor-targeted gene delivery via anti-HER2 antibody (trastuzumab, Herceptin) conjugated polyethylenimine.* J Control Release, 2004. **97**(2): p. 357-69.

Christensen, T., et al., *Additivity and the physical basis of multivalency effects: a thermodynamic investigation of the calcium EDTA interaction.* J Am Chem Soc, 2003. **125**(24): p. 7357-66.

Chung, K.N., et al., *Stable transfectants of human MCF-7 breast cancer cells with increased levels of the human folate receptor exhibit an increased sensitivity to antifolates.* J Clin Invest, 1993. **91**(4): p. 1289-94.

Citro, G., et al., *Inhibition of leukaemia cell proliferation by folic acid-polylysine-mediated introduction of c-myb antisense oligodeoxynucleotides into HL-60 cells.* Br J Cancer, 1994. **69**(3): p. 463-7.

Cooke, R.M., et al., *The conformation of the sialyl Lewis X ligand changes upon binding to E-selectin.* Biochemistry, 1994. **33**(35): p. 10591-6.

Cristofanilli, M., et al., *Circulating tumor cells, disease progression, and survival in metastatic breast cancer.* N Engl J Med, 2004. **351**(8): p. 781-91.

Danila, D.C., et al., *Circulating tumor cell number and prognosis in progressive castration-resistant prostate cancer.* Clin Cancer Res, 2007. **13**(23): p. 7053-8.

Danila, D.C., et al., *Circulating tumors cells as biomarkers: progress toward biomarker qualification.* Cancer J, 2011. **17**(6): p. 438-50.

De Giorgi, U., et al., *Circulating tumor cells and [18F]fluorodeoxyglucose positron emission tomography/computed tomography for outcome prediction in metastatic breast cancer.* J Clin Oncol, 2009. **27**(20): p. 3303-11.

Deng, G., et al., *Enrichment with anti-cytokeratin alone or combined with anti-EpCAM antibodies significantly increases the sensitivity for circulating tumor cell detection in metastatic breast cancer patients.* Breast Cancer Res, 2008. **10**(4): p. R69.

Dijkgraaf, I., et al., *Synthesis of DOTA-conjugated multivalent cyclic-RGD peptide dendrimers via 1,3-dipolar cycloaddition and their biological evaluation: implications for tumor targeting and tumor imaging purposes.* Org Biomol Chem, 2007. **5**(6): p. 935-44.

Dimitroff, C.J., et al., *Rolling of human bone-metastatic prostate tumor cells on human bone marrow endothelium under shear flow is mediated by E-selectin.* Cancer Res, 2004. **64**(15): p. 5261-9.

Disibio, G. and S.W. French, *Metastatic patterns of cancers - Results from a large autopsy study.* Arch Pathol Lab Med, 2008. **132**(6): p. 931-939.

Dong, F., A.S. Budhu, and X.W. Wang, *Translating the metastasis paradigm from scientific theory to clinical oncology.* Clin Cancer Res, 2009. **15**(8): p. 2588-93.

Dustin, M.L. and A.C. Chan, *Signaling takes shape in the immune system.* Cell, 2000. **103**(2): p. 283-94.

el Hassan, A.M., et al., *Post kala-azar ocular leishmaniasis.* Trans R Soc Trop Med Hyg, 1998. **92**(2): p. 177-9.

El-Sayed, I.H., M. Lotfy, and M. Moawad, *Immunodiagnostic potential of mucin (MUC2) and Thomsen-Friedenreich (TF) antigens in Egyptian patients with colorectal cancer.* Eur Rev Med Pharmacol Sci, 2011. **15**(1): p. 91-7.

el-Sheikh, H.A. and A.M. Abdel-Hakim, *Sectional impressions for mandibular distal extension removable partial dentures.* J Prosthet Dent, 1998. **80**(2): p. 216-9.

el-Sheikh, M.M. and J.M. Powers, *Tensile bond strength of porcelain teeth to denture resin before and after aging.* Int J Prosthodont, 1998. **11**(1): p. 16-20.

El-Sheikh, S.M., et al., *Bacteria and viruses that cause respiratory tract infections during the pilgrimage (Haj) season in Makkah, Saudi Arabia.* Trop Med Int Health, 1998. **3**(3): p. 205-9.

Elkin, E.B., et al., *HER-2 testing and trastuzumab therapy for metastatic breast cancer: a cost-effectiveness analysis.* J Clin Oncol, 2004. **22**(5): p. 854-63.

Falsey, J.R., et al., *Peptide and small molecule microarray for high throughput cell adhesion and functional assays.* Bioconjug Chem, 2001. **12**(3): p. 346-53.

Fang, X., et al., *CD24: from A to Z.* Cell Mol Immunol, 2010. **7**(2): p. 100-3.

Fehm, T., et al., *HER2 status of circulating tumor cells in patients with metastatic breast cancer: a prospective, multicenter trial.* Breast Cancer Res Treat, 2010. **124**(2): p. 403-12.

Fogel, M., et al., *CD24 is a marker for human breast carcinoma.* Cancer Lett, 1999. **143**(1): p. 87-94.

Fontana, J.A., et al., *Overexpression of bcl-2 or bcl-XL fails to inhibit apoptosis mediated by a novel retinoid.* Oncol Res, 1998. **10**(6): p. 313-24.

Foxall, C., et al., *The three members of the selectin receptor family recognize a common carbohydrate epitope, the sialyl Lewis(x) oligosaccharide.* J Cell Biol, 1992. **117**(4): p. 895-902.

Franchetti, P., et al., *Potent and selective inhibitors of human immunodeficiency virus protease structurally related to L-694,746.* Antivir Chem Chemother, 1998. **9**(4): p. 303-9.

Frey, K., et al., *The recovery profile of hyperbaric spinal anesthesia with lidocaine, tetracaine, and bupivacaine.* Reg Anesth Pain Med, 1998. **23**(2): p. 159-63.

Furner, I.J., M.A. Sheikh, and C.E. Collett, *Gene silencing and homology-dependent gene silencing in Arabidopsis: genetic modifiers and DNA methylation.* Genetics, 1998. **149**(2): p. 651-62.

Fuster, M.M. and J.D. Esko, *The sweet and sour of cancer: glycans as novel therapeutic targets.* Nat Rev Cancer, 2005. **5**(7): p. 526-42.

Galanzha, E.I., J.W. Kim, and V.P. Zharov, *Nanotechnology-based molecular photoacoustic and photothermal flow cytometry platform for in-vivo detection and killing of circulating cancer stem cells.* J Biophotonics, 2009. **2**(12): p. 725-35.

Galanzha, E.I., et al., *In vivo magnetic enrichment and multiplex photoacoustic detection of circulating tumour cells.* Nat Nanotechnol, 2009. **4**(12): p. 855-60.

Gestwicki, J.E., et al., *Selective immobilization of multivalent ligands for surface plasmon resonance and fluorescence microscopy.* Anal Biochem, 2002. **305**(2): p. 149-55.

Gestwicki, J.E., et al., *Influencing receptor-ligand binding mechanisms with multivalent ligand architecture.* J Am Chem Soc, 2002. **124**(50): p. 14922-33.

Giannitsis, E., et al., *Neutrophil-derived oxidative stress after myocardial ischemia induced by incremental atrial pacing.* Pacing Clin Electrophysiol, 1998. **21**(1 Pt 2): p. 157-62.

Giavazzi, R., et al., *Rolling and adhesion of human tumor cells on vascular endothelium under physiological flow conditions.* J Clin Invest, 1993. **92**(6): p. 3038-44.

Goldman, A.J., R.G. Cox, and H. Brenner, *Slow viscous motion of a sphere parallel to a plane wall--II Couette flow.* Chemical Engineering Science, 1967. **22**(4): p. 653-660.

Gout, S., P.L. Tremblay, and J. Huot, *Selectins and selectin ligands in extravasation of cancer cells and organ selectivity of metastasis.* Clin Exp Metastasis, 2008. **25**(4): p. 335-44.

Grandoch, M., et al., *Epac inhibits apoptosis of human leukocytes.* J Leukoc Biol, 2009.

Greenberg, A.W. and D.A. Hammer, *Cell separation mediated by differential rolling adhesion.* Biotechnol Bioeng, 2001. **73**(2): p. 111-24.

Haes, A.J. and R.P. Van Duyne, *A nanoscale optical blosensor: Sensitivity and selectivity of an approach based on the localized surface plasmon resonance spectroscopy of triangular silver nanoparticles.* Journal of the American Chemical Society, 2002. **124**(35): p. 10596-10604.

Haier, J. and G.L. Nicolson, *Role of the cytoskeleton in adhesion stabilization of human colorectal carcinoma cells to extracellular matrix components under dynamic conditions of laminar flow.* Clin Exp Metastasis, 1999. **17**(8): p. 713-21.

Hammer, D.A., *Simulation of cell rolling and adhesion on surfaces in shear flow. Microvilli-coated hard spheres with adhesive springs.* Cell Biophys, 1991. **18**(2): p. 145-82.

Hammer, D.A. and D.A. Lauffenburger, *A dynamical model for receptor-mediated cell adhesion to surfaces.* Biophys J, 1987. **52**(3): p. 475-87.

Han, J.S. and P.P. Nair, *Flow cytometric identification of cell surface markers on cultured human colonic cell lines using monoclonal antibodies.* Cancer, 1995. **76**(2): p. 195-200.

Han, W., et al., *Nanoparticle Coatings for Enhanced Capture of Flowing Cells in Microtubes.* ACS Nano, 2009. **4**(1): p. 174-180.

Haynes, B.F., et al., *CD44--a molecule involved in leukocyte adherence and T-cell activation.* Immunol Today, 1989. **10**(12): p. 423-8.

Hayot, C., et al., *Characterization of the activities of actin-affecting drugs on tumor cell migration.* Toxicol Appl Pharmacol, 2006. **211**(1): p. 30-40.

He, W., et al., *Quantitation of circulating tumor cells in blood samples from ovarian and prostate cancer patients using tumor-specific fluorescent ligands.* Int J Cancer, 2008. **123**(8): p. 1968-73.

He, W., et al., *In vivo quantitation of rare circulating tumor cells by multiphoton intravital flow cytometry.* Proc Natl Acad Sci U S A, 2007. **104**(28): p. 11760-5.

Heimburg, J., et al., *Inhibition of spontaneous breast cancer metastasis by anti-Thomsen-Friedenreich antigen monoclonal antibody JAA-F11.* Neoplasia, 2006. **8**(11): p. 939-48.

Henne, W.A., et al., *Detection of folate binding protein with enhanced sensitivity using a functionalized quartz crystal microbalance sensor.* Anal Chem, 2006. **78**(14): p. 4880-4.

Hong, S., et al., *Interaction of poly(amidoamine) dendrimers with supported lipid bilayers and cells: hole formation and the relation to transport.* Bioconjug Chem, 2004. **15**(4): p. 774-82.

Hong, S., et al., *Covalent immobilization of p-selectin enhances cell rolling.* Langmuir, 2007. **23**(24): p. 12261-8.

Hong, S., et al., *The binding avidity of a nanoparticle-based multivalent targeted drug delivery platform.* Chem Biol, 2007. **14**(1): p. 107-15.

Hong, S., et al., *The Role of Ganglioside GM(1) in Cellular Internalization Mechanisms of Poly(amidoamine) Dendrimers.* Bioconjug Chem, 2009.

Hoshino, K., et al., *Microchip-based immunomagnetic detection of circulating tumor cells.* Lab Chip, 2011. **11**(20): p. 3449-57.

Hughes, A.D. and M.R. King, *Use of naturally occurring halloysite nanotubes for enhanced capture of flowing cells.* Langmuir, 2010. **26**(14): p. 12155-64.

Hughes, A.D., et al., *Microtube device for selectin-mediated capture of viable circulating tumor cells from blood.* Clin Chem, 2012. **58**(5): p. 846-53.

Hunt, B.J., et al., *Activation of coagulation and fibrinolysis during cardiothoracic operations.* Ann Thorac Surg, 1998. **65**(3): p. 712-8.

Hüsemann, Y., et al., *Systemic Spread Is an Early Step in Breast Cancer.* Cancer Cell, 2008. **13**(1): p. 58-68.

Hussain, S., et al., *Antitumor activity of an epithelial cell adhesion molecule targeted nanovesicular drug delivery system.* Mol Cancer Ther, 2007. **6**(11): p. 3019-27.

Hwang, S.Y., et al., *Adhesion assays of endothelial cells on nanopatterned surfaces within a microfluidic channel.* Anal Chem, 2010. **82**(7): p. 3016-22.

Jacobs, T.W., et al., *Specificity of HercepTest in determining HER-2/neu status of breast cancers using the united states food and drug administration-approved scoring system.* J Clin Oncol, 1999. **17**(7): p. 1983-1987.

Jawad, F., et al., *Problems of donor selection in a living related renal transplant program.* Transplant Proc, 1998. **30**(7): p. 3643.

Juranic, Z.D., et al., *The antitumor immune response in HER-2 positive, metastatic breast cancer patients.* J Transl Med, 2005. **3**(1): p. 13.

Kansas, G.S., *Selectins and their ligands: current concepts and controversies.* Blood, 1996. **88**(9): p. 3259-87.

Karnon, J., et al., *Health care costs for the treatment of breast cancer recurrent events: estimates from a UK-based patient-level analysis.* Br J Cancer, 2007. **97**(4): p. 479-485.

Kawase, M., et al., *Immobilization of ligand-modified polyamidoamine dendrimer for cultivation of hepatoma cells.* Artif Organs, 2000. **24**(1): p. 18-22.

Keller, P.J., et al., *Mapping the cellular and molecular heterogeneity of normal and malignant breast tissues and cultured cell lines.* Breast Cancer Res, 2010. **12**(5): p. R87.

Kharchenko, V.P., et al., *[Single-photon emission-computed tomography in evaluation of cerebral microcirculation of patients with epileptiform syndrome]*. Vestn Rentgenol Radiol, 1998(1): p. 4-6.

Khatibzadeh, M., et al., *Topographic pattern of advanced atherosclerotic lesions in carotid arteries.* Cardiology, 1998. **89**(3): p. 235-40.

Kiani, M.F., et al., *Effects of ionizing radiation on the adhesive interaction of human tumor and endothelial cells in vitro.* Clin Exp Metastasis, 1997. **15**(1): p. 12-8.

Kiessling, L.L. and N.L. Pohl, *Strength in numbers: non-natural polyvalent carbohydrate derivatives.* Chem Biol, 1996. **3**(2): p. 71-7.

Kim, H.J., et al., *Isolation of CD24(high) and CD24(low/-) cells from MCF-7: CD24 expression is positively related with proliferation, adhesion and invasion in MCF-7.* Cancer Lett, 2007. **258**(1): p. 98-108.

Kim, J.B., et al., *CD24 cross-linking induces apoptosis in, and inhibits migration of, MCF-7 breast cancer cells.* BMC Cancer, 2008. **8**: p. 118.

Kim, K.T., G.S. Safadi, and K.M. Sheikh, *Diagnostic evaluation of type I latex allergy.* Ann Allergy Asthma Immunol, 1998. **80**(1): p. 66-70.

Kim, M.H., et al., *Response of human epithelial cells to culture surfaces with varied roughnesses prepared by immobilizing dendrimers with/without D-glucose display.* J Biosci Bioeng, 2007. **103**(2): p. 192-9.

King, M.R., et al., *Biomolecular surfaces for the capture and reprogramming of circulating tumor cells.* J Bionic Eng, 2009. **6**(4): p. 311-317.

Kitov, P.I. and D.R. Bundle, *On the nature of the multivalency effect: a thermodynamic model.* J Am Chem Soc, 2003. **125**(52): p. 16271-84.

Kobzdej, M.M., et al., *Discordant expression of selectin ligands and sialyl Lewis x-related epitopes on murine myeloid cells.* Blood, 2002. **100**(13): p. 4485-94.

Kohler, S., et al., *E-/P-selectins and colon carcinoma metastasis: first in vivo evidence for their crucial role in a clinically relevant model of spontaneous metastasis formation in the lung.* Br J Cancer, 2009.

Koyfman, A.Y., G.B. Braun, and N.O. Reich, *Cell-targeted self-assembled DNA nanostructures.* J Am Chem Soc, 2009. **131**(40): p. 14237-9.

Kristiansen, G., M. Sammar, and P. Altevogt, *Tumour biological aspects of CD24, a mucin-like adhesion molecule.* J Mol Histol, 2004. **35**(3): p. 255-62.

Kristiansen, G., et al., *CD24 expression is a new prognostic marker in breast cancer.* Clin Cancer Res, 2003. **9**(13): p. 4906-13.

Krivacic, R.T., et al., *A rare-cell detector for cancer.* Proc Natl Acad Sci U S A, 2004. **101**(29): p. 10501-4.

Kruger, D., et al., *Cardiac release and kinetics of endothelin after uncomplicated percutaneous transluminal coronary angioplasty.* Am J Cardiol, 1998. **81**(12): p. 1421-6.

Kukowska-Latallo, J.F., et al., *Nanoparticle targeting of anticancer drug improves therapeutic response in animal model of human epithelial cancer.* Cancer Res, 2005. **65**(12): p. 5317-24.

Kuo, J.S., et al., *Deformability considerations in filtration of biological cells.* Lab Chip, 2010. **10**(7): p. 837-42.

Kuroda, K., et al., *Docetaxel down-regulates the expression of androgen receptor and prostate-specific antigen but not prostate-specific membrane antigen in prostate cancer cell lines: implications for PSA surrogacy.* Prostate, 2009. **69**(14): p. 1579-85.

Kuwada, S.K., J. Kuang, and X. Li, *Integrin alpha5/beta1 expression mediates HER-2 down-regulation in colon cancer cells.* J Biol Chem, 2005. **280**(19): p. 19027-35.

Lacroix, M., *Significance, detection and markers of disseminated breast cancer cells.* Endocr Relat Cancer, 2006. **13**(4): p. 1033-67.

Launiere, C., et al., *Channel Surface Patterning of Alternating Biomimetic Protein Combinations for Enhanced Microfluidic Tumor Cell Isolation.* Anal Chem, 2012. **84**(9): p. 4022-8.

Lawrence, M.B., *Selectin-carbohydrate interactions in shear flow.* Curr Opin Chem Biol, 1999. **3**(6): p. 659-64.

Lawrence, M.B. and T.A. Springer, *Leukocytes roll on a selectin at physiologic flow rates: distinction from and prerequisite for adhesion through integrins.* Cell, 1991. **65**(5): p. 859-73.

Lazarus, P., et al., *p53, but not p16 mutations in oral squamous cell carcinomas are associated with specific CYP1A1 and GSTM1 polymorphic genotypes and patient tobacco use.* Carcinogenesis, 1998. **19**(3): p. 509-14.

Le Berre, V., et al., *Dendrimeric coating of glass slides for sensitive DNA microarrays analysis.* Nucleic Acids Res, 2003. **31**(16): p. e88.

Lee, K.B., et al., *The use of nanoarrays for highly sensitive and selective detection of human immunodeficiency virus type 1 in plasma.* Nano Lett, 2004. **4**(10): p. 1869-1872.

Lee, R.T. and Y.C. Lee, *Affinity enhancement by multivalent lectin-carbohydrate interaction.* Glycoconj J, 2000. **17**(7-9): p. 543-51.

Ley, K., et al., *Getting to the site of inflammation: the leukocyte adhesion cascade updated.* Nat Rev Immunol, 2007. **7**(9): p. 678-689.

Lim, S.C., *CD24 and human carcinoma: tumor biological aspects.* Biomed Pharmacother, 2005. **59 Suppl 2**: p. S351-4.

Lin, C.C., et al., *Fetal congenital malformations. Biophysical profile evaluation.* J Reprod Med, 1998. **43**(6): p. 521-7.

Lin, H.K., et al., *Portable filter-based microdevice for detection and characterization of circulating tumor cells.* Clin Cancer Res, 2010. **16**(20): p. 5011-8.

Lindhorst, T., *Artificial Multivalent Sugar Ligands to Understand and Manipulate Carbohydrate-Protein Interactions*, in *Host-Guest Chemistry*, S. Penadés, Editor 2002, Springer Berlin / Heidelberg. p. 201-235.

Litvinov, S.V., et al., *Evidence for a role of the epithelial glycoprotein 40 (Ep-CAM) in epithelial cell-cell adhesion.* Cell Adhes Commun, 1994. **2**(5): p. 417-28.

Liu, Y., et al., *MCF-7 breast cancer cells overexpressing transfected c-erbB-2 have an in vitro growth advantage in estrogen-depleted conditions and reduced estrogen-dependence and tamoxifen-sensitivity in vivo.* Breast Cancer Res Treat, 1995. **34**(2): p. 97-117.

Lu, Z.M., et al., *Downregulation of caveolin-1 function by EGF leads to the loss of E-cadherin, increased transcriptional activity of beta-catenin, and enhanced tumor cell invasion.* Cancer Cell, 2003. **4**(6): p. 499-515.

Luo, H., et al., *An (125)I-labeled octavalent peptide fluorescent nanoprobe for tumor-homing imaging in vivo.* Biomaterials, 2012. **33**(19): p. 4843-50.

MacColl, R., et al., *Phycoerythrin 545: monomers, energy migration, bilin topography, and monomer/dimer equilibrium.* Biochemistry, 1998. **37**(1): p. 417-23.

Mackay, C.R., *Moving targets: cell migration inhibitors as new anti-inflammatory therapies.* Nat Immunol, 2008. **9**(9): p. 988-98.

Magro, C.M. and M.E. Dyrsen, *Cutaneous lymphocyte antigen expression in benign and neoplastic cutaneous B- and T-cell lymphoid infiltrates.* J Cutan Pathol, 2008. **35**(11): p. 1040-9.

Mahadeva, H., et al., *A simple and efficient method for the isolation of differentially expressed genes.* J Mol Biol, 1998. **284**(5): p. 1391-8.

Maheswaran, S., et al., *Detection of mutations in EGFR in circulating lung-cancer cells.* N Engl J Med, 2008. **359**(4): p. 366-77.

Makrilia, N., et al., *Cell adhesion molecules: role and clinical significance in cancer.* Cancer Invest, 2009. **27**(10): p. 1023-37.

Mammen, M., S.K. Choi, and G.M. Whitesides, *Polyvalent interactions in biological systems: Implications for design and use of multivalent ligands and inhibitors.* Angew Chem Int Ed Engl, 1998. **37**(20): p. 2755-2794.

Mani, S.A., et al., *The epithelial-mesenchymal transition generates cells with properties of stem cells.* Cell, 2008. **133**(4): p. 704-715.

Mantovani, A., et al., *Cancer-related inflammation.* Nature, 2008. **454**(7203): p. 436-44.

Marth, C., et al., *Epidermal growth factor reduces HER-2 protein level in human ovarian carcinoma cells.* Int J Cancer, 1992. **52**(2): p. 311-6.

Martin, A.L., B. Li, and E.R. Gillies, *Surface functionalization of nanomaterials with dendritic groups: toward enhanced binding to biological targets.* J Am Chem Soc, 2009. **131**(2): p. 734-41.

Martinez-Veracoechea, F.J. and D. Frenkel, *Designing super selectivity in multivalent nano-particle binding.* Proc Natl Acad Sci U S A, 2011. **108**(27): p. 10963-8.

Mason, I., et al., *The management of acid-related dyspepsia in general practice: a comparison of an omeprazole versus an antacid-alginate/ranitidine management strategy. Compete Research Group [corrected].* Aliment Pharmacol Ther, 1998. **12**(3): p. 263-71.

Matsumoto, M., et al., *CD43 collaborates with P-selectin glycoprotein ligand-1 to mediate E-selectin-dependent T cell migration into inflamed skin.* J Immunol, 2007. **178**(4): p. 2499-506.

McEver, R.P., *Selectins: novel receptors that mediate leukocyte adhesion during inflammation.* Thromb Haemost, 1991. **65**(3): p. 223-8.

Meghji, S., et al., *Surface-associated protein from Staphylococcus aureus stimulates osteoclastogenesis: possible role in S. aureus-induced bone pathology.* Br J Rheumatol, 1998. **37**(10): p. 1095-101.

Meier, R., et al., *Breast cancers: MR imaging of folate-receptor expression with the folate-specific nanoparticle P1133.* Radiology, 2010. **255**(2): p. 527-35.

Mi, Y., et al., *Herceptin functionalized polyhedral oligomeric silsesquioxane - conjugated oligomers - silica/iron oxide nanoparticles for tumor cell sorting and detection.* Biomaterials, 2011. **32**(32): p. 8226-33.

Miles, F.L., et al., *Stepping out of the flow: capillary extravasation in cancer metastasis.* Clin Exp Metastasis, 2008. **25**(4): p. 305-24.

Mittal, S., et al., *Antibody-functionalized fluid-permeable surfaces for rolling cell capture at high flow rates.* Biophys J, 2012. **102**(4): p. 721-30.

Mitusch, R., U. Stierle, and A. Sheikhzadeh, *[Atherosclerosis of the aorta as a source of arterial embolisms].* Z Kardiol, 1998. **87**(10): p. 789-96.

Momburg, F., et al., *Immunohistochemical study of the expression of a Mr 34,000 human epithelium-specific surface glycoprotein in normal and malignant tissues.* Cancer Res, 1987. **47**(11): p. 2883-91.

Moser, M., et al., *Kindlin-3 is required for beta2 integrin-mediated leukocyte adhesion to endothelial cells.* Nat Med, 2009. **15**(3): p. 300-5.

Mostert, B., et al., *Circulating tumor cells (CTCs): detection methods and their clinical relevance in breast cancer.* Cancer Treat Rev, 2009. **35**(5): p. 463-74.

Motulsky, H.J. and R.E. Brown, *Detecting outliers when fitting data with nonlinear regression - a new method based on robust nonlinear regression and the false discovery rate.* BMC Bioinformatics, 2006. **7**: p. 123.

Motulsky, H.J. and R.R. Neubig, *Analyzing binding data.* Curr Protoc Neurosci, 2010. **Chapter 7**: p. Unit 7 5.

Mouliere, F. and A.R. Thierry, *The importance of examining the proportion of circulating DNA originating from tumor, microenvironment and normal cells in colorectal cancer patients.* Expert Opin Biol Ther, 2012. **12 Suppl 1**: p. S209-15.

Mourez, M., et al., *Designing a polyvalent inhibitor of anthrax toxin.* Nat Biotechnol, 2001. **19**(10): p. 958-61.

Muraoka, R.S., et al., *Blockade of TGF-beta inhibits mammary tumor cell viability, migration, and metastases.* J Clin Invest, 2002. **109**(12): p. 1551-1559.

Murthy, S.K., et al., *Effect of flow and surface conditions on human lymphocyte isolation using microfluidic chambers.* Langmuir, 2004. **20**(26): p. 11649-55.

Myung, J.H., et al., *Direct measurements on CD24-mediated rolling of human breast cancer MCF-7 cells on E-selectin.* Anal Chem, 2011. **83**(3): p. 1078-83.

Myung, J.H., et al., *Dendrimer-mediated multivalent binding for the enhanced capture of tumor cells.* Angew Chem Int Ed Engl, 2011. **50**(49): p. 11769-72.

Myung, J.H., et al., *Enhanced tumor cell isolation by a biomimetic combination of E-selectin and anti-EpCAM: implications for the effective separation of circulating tumor cells (CTCs).* Langmuir, 2010. **26**(11): p. 8589-96.

Nagrath, S., et al., *Isolation of rare circulating tumour cells in cancer patients by microchip technology.* Nature, 2007. **450**(7173): p. 1235-9.

Navone, N.M., et al., *Establishment of two human prostate cancer cell lines derived from a single bone metastasis.* Clin Cancer Res, 1997. **3**(12 Pt 1): p. 2493-500.

Nguyen, D.X., P.D. Bos, and J. Massague, *Metastasis: from dissemination to organ-specific colonization.* Nat Rev Cancer, 2009. **9**(4): p. 274-84.

Nilsson, R. and H.O. Sjogren, *Antigen-independent binding of rat immunoglobulins in a radioimmunoassay. Solutions to an unusual background problem.* J Immunol Methods, 1984. **66**(1): p. 17-25.

Nishimura, N. and T. Sasaki, *Regulation of epithelial cell adhesion and repulsion: role of endocytic recycling.* J Med Invest, 2008. **55**(1-2): p. 9-16.

Osta, W.A., et al., *EpCAM is overexpressed in breast cancer and is a potential target for breast cancer gene therapy.* Cancer Res, 2004. **64**(16): p. 5818-24.

Owens, D.E., 3rd and N.A. Peppas, *Opsonization, biodistribution, and pharmacokinetics of polymeric nanoparticles.* Int J Pharm, 2006. **307**(1): p. 93-102.

Paget, S., *The distribution of secondary growths in cancer of the breast. 1889.* Cancer Metastasis Rev, 1989. **8**(2): p. 98-101.

Pahan, K., et al., *Sphingomyelinase and ceramide stimulate the expression of inducible nitric-oxide synthase in rat primary astrocytes.* J Biol Chem, 1998. **273**(5): p. 2591-600.

Pahan, K., et al., *N-acetyl cysteine inhibits induction of no production by endotoxin or cytokine stimulated rat peritoneal macrophages, C6 glial cells and astrocytes.* Free Radic Biol Med, 1998. **24**(1): p. 39-48.

Pantel, K., R.H. Brakenhoff, and B. Brandt, *Detection, clinical relevance and specific biological properties of disseminating tumour cells.* Nat Rev Cancer, 2008. **8**(5): p. 329-40.

Pantel, K. and M. Otte, *Occult micrometastasis: enrichment, identification and characterization of single disseminated tumour cells.* Semin Cancer Biol, 2001. **11**(5): p. 327-37.

Park, G.S., et al., *Full surface embedding of gold clusters on silicon nanowires for efficient capture and photothermal therapy of circulating tumor cells.* Nano Lett, 2012. **12**(3): p. 1638-42.

Paterlini-Brechot, P. and N.L. Benali, *Circulating tumor cells (CTC) detection: clinical impact and future directions.* Cancer Lett, 2007. **253**(2): p. 180-204.

Pauletti, G., et al., *Assessment of methods for tissue-based detection of the HER-2/neu alteration in human breast cancer: A direct comparison of fluorescence in situ hybridization and immunohistochemistry.* J Clin Oncol, 2000. **18**(21): p. 3651-3664.

Peer, D., et al., *Nanocarriers as an emerging platform for cancer therapy.* Nat Nanotechnol, 2007. **2**(12): p. 751-60.

Pepper, M.S., *Lymphangiogenesis and tumor metastasis: myth or reality?* Clin Cancer Res, 2001. **7**(3): p. 462-8.

Perl, A., et al., *Gradient-driven motion of multivalent ligand molecules along a surface functionalized with multiple receptors.* Nat Chem, 2011. **3**(4): p. 317-22.

Pinzani, P., et al., *Isolation by size of epithelial tumor cells in peripheral blood of patients with breast cancer: correlation with real-time reverse transcriptase-polymerase chain reaction results and feasibility of molecular analysis by laser microdissection.* Hum Pathol, 2006. **37**(6): p. 711-8.

Pirruccello, S.J. and T.W. LeBien, *The human B cell-associated antigen CD24 is a single chain sialoglycoprotein.* J Immunol, 1986. **136**(10): p. 3779-84.

Poon, Z., et al., *Ligand-clustered "patchy" nanoparticles for modulated cellular uptake and in vivo tumor targeting.* Angew Chem Int Ed Engl, 2010. **49**(40): p. 7266-70.

Psaila, B. and D. Lyden, *The metastatic niche: adapting the foreign soil.* Nat Rev Cancer, 2009. **9**(4): p. 285-93.

Quintana, A., et al., *Design and function of a dendrimer-based therapeutic nanodevice targeted to tumor cells through the folate receptor.* Pharm Res, 2002. **19**(9): p. 1310-6.

Ramezani, A. and R.G. Hawley, *Generation of HIV-1-based lentiviral vector particles.* Curr Protoc Mol Biol, 2002. **Chapter 16**: p. Unit 16 22.

Rana, K., J.L. Liesveld, and M.R. King, *Delivery of apoptotic signal to rolling cancer cells: a novel biomimetic technique using immobilized TRAIL and E-selectin.* Biotechnol Bioeng, 2009. **102**(6): p. 1692-702.

Raziuddin, S., et al., *Regulation of interleukin-4 production and cytokine-induced growth potential in peripheral T-cell non-Hodgkin's lymphomas.* Br J Haematol, 1998. **100**(2): p. 310-6.

Reuter, J.D., et al., *Inhibition of viral adhesion and infection by sialic-acid-conjugated dendritic polymers.* Bioconjug Chem, 1999. **10**(2): p. 271-8.

Richards, R.L., et al., *Choleragen (Cholera Toxin) - Bacterial Lectin.* Proc Natl Acad Sci USA, 1979. **76**(4): p. 1673-1676.

Riethdorf, S., et al., *Detection of circulating tumor cells in peripheral blood of patients with metastatic breast cancer: a validation study of the CellSearch system.* Clin Cancer Res, 2007. **13**(3): p. 920-8.

Riethdorf, S., et al., *Detection and HER2 expression of circulating tumor cells: prospective monitoring in breast cancer patients treated in the neoadjuvant GeparQuattro trial.* Clin Cancer Res, 2010. **16**(9): p. 2634-45.

Riethdorf, S. and K. Pantel, *Disseminated tumor cells in bone marrow and circulating tumor cells in blood of breast cancer patients: current state of detection and characterization.* Pathobiology, 2008. **75**(2): p. 140-8.

Rossi, B. and G. Constantin, *Anti-selectin therapy for the treatment of inflammatory diseases.* Inflamm Allergy Drug Targets, 2008. **7**(2): p. 85-93.

Rusnak, D.W., et al., *The effects of the novel, reversible epidermal growth factor Receptor/ErbB-2 tyrosine kinase inhibitor, GW2016, on the growth of human normal and tumor-derived cell lines in vitro and in vivo.* Molecular Cancer Therapeutics, 2001. **1**(2): p. 85-94.

Sacchettini, J.C., L.G. Baum, and C.F. Brewer, *Multivalent protein-carbohydrate interactions. A new paradigm for supermolecular assembly and signal transduction.* Biochemistry, 2001. **40**(10): p. 3009-15.

Sachs, L., *Control of growth and normal differentiation in leukemic cells: regulation of the developmental program and restoration of the normal phenotype in myeloid leukemia.* J Cell Physiol Suppl, 1982. **1**: p. 151-64.

Sadr-Ameli, M.A., et al., *Late results of balloon pulmonary valvuloplasty in adults.* Am J Cardiol, 1998. **82**(3): p. 398-400.

Sammar, M., et al., *Heat-stable antigen (CD24) as ligand for mouse P-selectin.* Int Immunol, 1994. **6**(7): p. 1027-36.

Schliwa, M., *Action of cytochalasin D on cytoskeletal networks.* J Cell Biol, 1982. **92**(1): p. 79-91.

Schott, M.E., et al., *Preparation, characterization, and in vivo biodistribution properties of synthetically cross-linked multivalent antitumor antibody fragments.* Bioconjug Chem, 1993. **4**(2): p. 153-65.

Segal, H., et al., *Complement activation during major surgery: the effect of extracorporeal circuits and high-dose aprotinin.* J Cardiothorac Vasc Anesth, 1998. **12**(5): p. 542-7.

Sekine, J., et al., *Functionalized conducting polymer nanodots for enhanced cell capturing: the synergistic effect of capture agents and nanostructures.* Adv Mater, 2011. **23**(41): p. 4788-92.

Shah, A.M., et al., *Biopolymer System for Cell Recovery from Microfluidic Cell Capture Devices.* Anal Chem, 2012.

Shaheen, F.A., et al., *Impact of donor/recipient gender, age, HLA matching, and weight on short-term graft survival following living related renal transplantation.* Transplant Proc, 1998. **30**(7): p. 3655-8.

Shaheen, F.A. and I.A. Sheikh, *Slow continuous ultrafiltration with dialysis in patients with acute renal failure in the intensive care unit.* Saudi J Kidney Dis Transpl, 1998. **9**(3): p. 294-7.

Shaheen, F.A., I.A. Sheikh, and A. al-Khader, *Cyclosporin Neoral and long-term survival of renal grafts.* Transplant Proc, 1998. **30**(7): p. 3549.

Shaheen, F.A., et al., *Renal transplantation in anti-HCV-positive patients with end-stage renal disease.* Transplant Proc, 1998. **30**(7): p. 3142-3.

Shaker, O.G., et al., *Gene expression of E-selectin in tissue and its protein level in serum of breast cancer patients.* Tumori, 2006. **92**(6): p. 524-30.

Sheikh, S. and G.B. Nash, *Treatment of neutrophils with cytochalasins converts rolling to stationary adhesion on P-selectin.* J Cell Physiol, 1998. **174**(2): p. 206-16.

Sheridan, C., et al., *CD44+/CD24- breast cancer cells exhibit enhanced invasive properties: an early step necessary for metastasis.* Breast Cancer Res, 2006. **8**(5): p. R59.

Shi, X., et al., *Synthesis, characterization, and intracellular uptake of carboxyl-terminated poly(amidoamine) dendrimer-stabilized iron oxide nanoparticles.* Phys Chem Chem Phys, 2007. **9**(42): p. 5712-20.

Shiwach, R.S. and S. Sheikha, *Delusional disorder in a boy with phenylketonuria and amine metabolites in the cerebrospinal fluid after treatment with neuroleptics.* J Adolesc Health, 1998. **22**(3): p. 244-6.

Shukla, R., et al., *Tumor angiogenic vasculature targeting with PAMAM dendrimer-RGD conjugates.* Chem Commun (Camb), 2005(46): p. 5739-41.

Shukla, R., et al., *HER2 specific tumor targeting with dendrimer conjugated anti-HER2 mAb.* Bioconjug Chem, 2006. **17**(5): p. 1109-15.

Shweiki, D., et al., *Vascular endothelial growth-factor induced by hypoxia may mediate hypoxia-initiated angiogenesis.* Nature, 1992. **359**(6398): p. 843-845.

Sieuwerts, A.M., et al., *Anti-epithelial cell adhesion molecule antibodies and the detection of circulating normal-like breast tumor cells.* J Natl Cancer Inst, 2009. **101**(1): p. 61-6.

Sieuwerts, A.M., et al., *Molecular characterization of circulating tumor cells in large quantities of contaminating leukocytes by a multiplex real-time PCR.* Breast Cancer Res Treat, 2009. **118**(3): p. 455-68.

Signoretti, S., et al., *Her-2-neu expression and progression toward androgen independence in human prostate cancer.* J Natl Cancer Inst, 2000. **92**(23): p. 1918-25.

Simon, B., et al., *Epithelial glycoprotein is a member of a family of epithelial cell surface antigens homologous to nidogen, a matrix adhesion protein.* Proc Natl Acad Sci U S A, 1990. **87**(7): p. 2755-9.

Slade, M.J., et al., *Comparison of bone marrow, disseminated tumour cells and blood-circulating tumour cells in breast cancer patients after primary treatment.* Brit J Cancer, 2009. **100**(1): p. 160-166.

Smith, D.K. and F. Diederich, *Supramolecular dendrimer chemistry: A journey through the branched architecture*, in *Dendrimers Ii*2000, Springer-Verlag Berlin: Berlin. p. 183-227.

Smith, M.L., et al., *Chromatin relaxation by overexpression of mutant p53, HPV16-E6, or cyclin G transgenes.* Exp Cell Res, 1998. **242**(1): p. 235-43.

Smith, M.R., S. Biggar, and M. Hussain, *Prostate-specific antigen messenger RNA is expressed in non-prostate cells: implications for detection of micrometastases.* Cancer Res, 1995. **55**(12): p. 2640-4.

Song, X.D. and B.I. Swanson, *Direct, ultrasensitive, and selective optical detection of protein toxins using multivalent interactions.* Analytical Chemistry, 1999. **71**(11): p. 2097-2107.

Sriram, S.M., et al., *Multivalency-assisted control of intracellular signaling pathways: application for ubiquitin- dependent N-end rule pathway.* Chem Biol, 2009. **16**(2): p. 121-31.

Stahn, R., et al., *Multivalent sialyl Lewis x ligands of definite structures as inhibitors of E-selectin mediated cell adhesion.* Glycobiology, 1998. **8**(4): p. 311-19.

Stathopoulou, A., et al., *Molecular detection of cancer cells in the peripheral blood of patients with breast cancer: comparison of CK-19, CEA and maspin as detection markers.* Anticancer Res, 2003. **23**(2C): p. 1883-90.

Stears, R.L., R.C. Getts, and S.R. Gullans, *A novel, sensitive detection system for high-density microarrays using dendrimer technology.* Physiological genomics, 2000. **3**(2): p. 93-9.

Steeg, P.S., *Tumor metastasis: mechanistic insights and clinical challenges.* Nat Med, 2006. **12**(8): p. 895-904.

Steegmaier, M., et al., *The E-selectin-ligand ESL-1 is a variant of a receptor for fibroblast growth factor.* Nature, 1995. **373**(6515): p. 615-20.

Stevens, R.A., et al., *Time course of the effects of cervical epidural anesthesia on pulmonary function.* Reg Anesth Pain Med, 1998. **23**(1): p. 20-4.

Stevens, R.A., et al., *Does the choice of anesthetic technique affect the recovery of bowel function after radical prostatectomy?* Urology, 1998. **52**(2): p. 213-8.

Stevenson, B.R. and D.A. Begg, *Concentration-dependent effects of cytochalasin D on tight junctions and actin filaments in MDCK epithelial cells.* J Cell Sci, 1994. **107 (Pt 3)**: p. 367-75.

Stierle, U., et al., *Relation between QT dispersion and the extent of myocardial ischemia in patients with three-vessel coronary artery disease.* Am J Cardiol, 1998. **81**(5): p. 564-8.

Stierle, U., et al., *Myocardial ischemia in generalized coronary artery-left ventricular microfistulae.* Int J Cardiol, 1998. **63**(1): p. 47-52.

Stott, S.L., et al., *Isolation of circulating tumor cells using a microvortex-generating herringbone-chip.* Proc Natl Acad Sci U S A, 2010. **107**(43): p. 18392-7.

Stott, S.L., et al., *Isolation and characterization of circulating tumor cells from patients with localized and metastatic prostate cancer.* Sci Transl Med, 2010. **2**(25): p. 25ra23.

Stroock, A.D., et al., *Chaotic mixer for microchannels.* Science, 2002. **295**(5555): p. 647-51.

Sulchek, T.A., et al., *Dynamic force spectroscopy of parallel individual Mucin1-antibody bonds.* Proc Natl Acad Sci U S A, 2005. **102**(46): p. 16638-43.

Sun, C., R. Sze, and M. Zhang, *Folic acid-PEG conjugated superparamagnetic nanoparticles for targeted cellular uptake and detection by MRI.* J Biomed Mater Res A, 2006. **78**(3): p. 550-7.

Sunoqrot, S., et al., *Kinetically controlled cellular interactions of polymer-polymer and polymer-liposome nanohybrid systems.* Bioconjug Chem, 2011. **22**(3): p. 466-74.

Swales, P.J. and J.I. Sheikh, *Shared symptoms of panic disorder in an elderly couple.* Am J Geriatr Psychiatry, 1998. **6**(4): p. 340-4.

Tan, S.J., et al., *Microdevice for the isolation and enumeration of cancer cells from blood.* Biomed Microdevices, 2009. **11**(4): p. 883-92.

Tedder, T.F., et al., *The selectins: vascular adhesion molecules.* Faseb J, 1995. **9**(10): p. 866-73.

Telatar, M., et al., *A model for ATM heterozygote identification in a large population: four founder-effect ATM mutations identify most of Costa Rican patients with ataxia telangiectasia.* Mol Genet Metab, 1998. **64**(1): p. 36-43.

Thalmann, G.N., et al., *LNCaP progression model of human prostate cancer: androgen-independence and osseous metastasis.* Prostate, 2000. **44**(2): p. 91-103 Jul 1;44(2).

Thierry, B., et al., *Herceptin functionalized microfluidic polydimethylsiloxane devices for the capture of human epidermal growth factor receptor 2 positive circulating breast cancer cells.* Biomicrofluidics, 2010. **4**(3): p. 32205.

Thiery, J.P., *Epithelial-mesenchymal transitions in development and pathologies.* Curr Opin Cell Biol, 2003. **15**(6): p. 740-746.

Thurin, M. and T. Kieber-Emmons, *SA-Lea and tumor metastasis: the old prediction and recent findings.* Hybrid Hybridomics, 2002. **21**(2): p. 111-6.

Tomalia, D.A., A.M. Naylor, and W.A. Goddard, *STARBURST DENDRIMERS - MOLECULAR-LEVEL CONTROL OF SIZE, SHAPE, SURFACE-CHEMISTRY, TOPOLOGY, AND FLEXIBILITY FROM ATOMS TO MACROSCOPIC MATTER.* Angew Chem Int Ed Engl, 1990. **29**(2): p. 138-175.

Tozeren, A., et al., *E-selectin-mediated dynamic interactions of breast- and colon-cancer cells with endothelial-cell monolayers.* Int J Cancer, 1995. **60**(3): p. 426-31.

Tremblay, P.L., J. Huot, and F.A. Auger, *Mechanisms by which E-selectin regulates diapedesis of colon cancer cells under flow conditions.* Cancer Res, 2008. **68**(13): p. 5167-76.

Udabage, L., et al., *The over-expression of HAS2, Hyal-2 and CD44 is implicated in the invasiveness of breast cancer.* Exp Cell Res, 2005. **310**(1): p. 205-17.

van de Stolpe, A., et al., *Circulating tumor cell isolation and diagnostics: toward routine clinical use.* Cancer Res, 2011. **71**(18): p. 5955-60.

Varki, A., *Glycan-based interactions involving vertebrate sialic-acid-recognizing proteins.* Nature, 2007. **446**(7139): p. 1023-9.

Varki, N.M. and A. Varki, *Diversity in cell surface sialic acid presentations: implications for biology and disease.* Lab Invest, 2007. **87**(9): p. 851-7.

Verbaan, F.J., et al., *Application of poly(2-(dimethylamino)ethyl methacrylate)-based polyplexes for gene transfer into human ovarian carcinoma cells.* Int J Pharm, 2005. **304**(1-2): p. 185-92.

Verdier, C., et al., *Modeling cell interactions under flow.* J Math Biol, 2009. **58**(1-2): p. 235-259.

Vincent, J.C. and A. Sheikh, *Phosphate poisoning by ingestion of clothes washing liquid and fabric conditioner.* Anaesthesia, 1998. **53**(10): p. 1004-6.

Wagers, A.J., et al., *An sLex-deficient variant of HL60 cells exhibits high levels of adhesion to vascular selectins: further evidence that HECA-452 and CSLEX1 monoclonal antibody epitopes are not essential for high avidity binding to vascular selectins.* J Immunol, 1998. **160**(10): p. 5122-9.

Wang, L., et al., *Antitumor effect of an HER2-specific antibody-toxin fusion protein on human prostate cancer cells.* Prostate, 2001. **47**(1): p. 21-8.

Wang, S., et al., *Highly efficient capture of circulating tumor cells by using nanostructured silicon substrates with integrated chaotic micromixers.* Angew Chem Int Ed Engl, 2011. **50**(13): p. 3084-8.

Wang, S., et al., *Three-dimensional nanostructured substrates toward efficient capture of circulating tumor cells.* Angew Chem Int Ed Engl, 2009. **48**(47): p. 8970-3.

Weiss, L. and D.S. Dimitrov, *A fluid mechanical analysis of the velocity, adhesion, and destruction of cancer cells in capillaries during metastasis.* Cell Biophys, 1984. **6**(1): p. 9-22.

Weissleder, R., et al., *Cell-specific targeting of nanoparticles by multivalent attachment of small molecules.* Nat Biotechnol, 2005. **23**(11): p. 1418-23.

Weitman, S.D., et al., *Distribution of the folate receptor GP38 in normal and malignant cell lines and tissues.* Cancer Res, 1992. **52**(12): p. 3396-401.

Weitz-Schmidt, G., et al., *An E-selectin binding assay based on a polyacrylamide-type glycoconjugate.* Anal Biochem, 1996. **238**(2): p. 184-90.

Welply, J.K., et al., *Multivalent sialyl-LeX: potent inhibitors of E-selectin-mediated cell adhesion; reagent for staining activated endothelial cells.* Glycobiology, 1994. **4**(3): p. 259-65.

Wendt, M.K. and W.P. Schiemann, *Therapeutic targeting of the focal adhesion complex prevents oncogenic TGF-beta signaling and metastasis.* Breast Cancer Res, 2009. **11**(5).

Went, P., et al., *Frequent high-level expression of the immunotherapeutic target Ep-CAM in colon, stomach, prostate and lung cancers.* Br J Cancer, 2006. **94**(1): p. 128-35.

Woller, E.K., et al., *Altering the strength of lectin binding interactions and controlling the amount of lectin clustering using mannose/hydroxyl-functionalized dendrimers.* Journal of the American Chemical Society, 2003. **125**(29): p. 8820-6.

Woywodt, A., et al., *Cardiomyopathic lentiginosis/LEOPARD syndrome presenting as sudden cardiac arrest.* Chest, 1998. **113**(5): p. 1415-7.

Xiao, Y., et al., *Anti-HER2 IgY antibody-functionalized single-walled carbon nanotubes for detection and selective destruction of breast cancer cells.* BMC Cancer, 2009. **9**: p. 351.

Xu, H., et al., *Antibody conjugated magnetic iron oxide nanoparticles for cancer cell separation in fresh whole blood.* Biomaterials, 2011. **32**(36): p. 9758-65.

Xu, W., et al., *Isolation of circulating tumor cells in patients with hepatocellular carcinoma using a novel cell separation strategy.* Clin Cancer Res, 2011. **17**(11): p. 3783-93.

Yang, M., et al., *Bioreactive surfaces prepared via the self-assembly of dendron thiols and subsequent dendrimer bridging reactions.* Langmuir, 2005. **21**(5): p. 1858-65.

Yesavage, J.A., et al., *A follow-up study of actigraphic measures in home-residing Alzheimer's disease patients.* J Geriatr Psychiatry Neurol, 1998. **11**(1): p. 7-10.

Yoshizawa, T., et al., *Folate-linked lipid-based nanoparticles for synthetic siRNA delivery in KB tumor xenografts.* Eur J Pharm Biopharm, 2008. **70**(3): p. 718-25.

Yu, M., et al., *Circulating tumor cells: approaches to isolation and characterization.* J Cell Biol, 2011. **192**(3): p. 373-82.

Yuan, K., et al., *Alterations in human breast cancer adhesion-motility in response to changes in cell surface glycoproteins displaying alpha-L-fucose moieties.* Int J Oncol, 2008. **32**(4): p. 797-807.

Zaher, H., et al., *The involvement of aryl hydrocarbon receptor in the activation of transforming growth factor-beta and apoptosis.* Mol Pharmacol, 1998. **54**(2): p. 313-21.

Zen, K., et al., *CD44v4 is a major E-selectin ligand that mediates breast cancer cell transendothelial migration.* PLoS ONE, 2008. **3**(3): p. e1826.

Zhang, Y., N. Kohler, and M. Zhang, *Surface modification of superparamagnetic magnetite nanoparticles and their intracellular uptake.* Biomaterials, 2002. **23**(7): p. 1553-61.

Zhao, J., et al., *Highly sensitive identification of cancer cells by combining the new tetrathiafulvalene derivative with a beta-cyclodextrin/multi-walled carbon nanotubes modified GCE.* Analyst, 2010. **135**(11): p. 2965-9.

Zheng, S., et al., *Membrane microfilter device for selective capture, electrolysis and genomic analysis of human circulating tumor cells.* J Chromatogr A, 2007. **1162**(2): p. 154-61.

Zheng, S., et al., *3D microfilter device for viable circulating tumor cell (CTC) enrichment from blood.* Biomed Microdevices, 2011. **13**(1): p. 203-13.

Zhong, H., et al., *Overexpression of hypoxia-inducible factor 1 alpha in common human cancers and their metastases.* Cancer Res, 1999. **59**(22): p. 5830-5835.

Zieglschmid, V., C. Hollmann, and O. Bocher, *Detection of disseminated tumor cells in peripheral blood.* Crit Rev Clin Lab Sci, 2005. **42**(2): p. 155-96.

Zou, X., et al., *PSGL-1 derived from human neutrophils is a high-efficiency ligand for endothelium-expressed E-selectin under flow.* Am J Physiol Cell Physiol, 2005. **289**(2): p. C415-24.

APPENDIX A. IRB Approval Letter

UNIVERSITY OF ILLINOIS
AT CHICAGO

Office for the Protection of Research Subjects (OPRS)
Office of the Vice Chancellor for Research (MC 672)
203 Administrative Office Building
1737 West Polk Street
Chicago, Illinois 60612-7227

Approval Notice
Initial Review (Response to Modifications)

March 8, 2012

Seungpyo Hong, PhD
Biopharmaceutical Sciences
833 S. Wood Street
M/C 865
Chicago, IL 60612
Phone: (312) 413-8294 / Fax: (312) 996-0098

RE: Protocol # 2012-0139
"Validation of Novel Biomimetic Circulating Tumor Cell Devices Using Clinical Blood Samples"

Dear Dr. Hong:

Your Initial Review (Response to Modifications) was reviewed and approved by the Expedited review process on March 2, 2012. You may now begin your research

Please note the following information about your approved research protocol:

Protocol Approval Period: March 2, 2012 - March 1, 2013
Approved Subject Enrollment #: 100 Total
Additional Determinations for Research Involving Minors: These determinations have not been made for this study since it has not been approved for enrollment of minors.
Performance Sites: UIC
Sponsor: None
Research Protocol(s):

a) Validation of Novel Biomimetic CTC Devices using Clinical Blood Samples, Version 2.0, 02.27.2012

Recruitment Material(s):

a) Flyer "Be part of a research study!" Version 2.0 as submitted on 2/28/12

Informed Consent/ HIPAA Authorization(s):

a) Combined Consent/Authorization: Version 2.0/02.27.2012/Validation of novel biomimetic device

APPENDIX B. Permission to Reprint Copyrighted Material

JOHN WILEY AND SONS LICENSE TERMS AND CONDITIONS

Oct 25, 2012

This is a License Agreement between Ja Hye Myung ("You") and John Wiley and Sons ("John Wiley and Sons") provided by Copyright Clearance Center ("CCC"). The license consists of your order details, the terms and conditions provided by John Wiley and Sons, and the payment terms and conditions.

All payments must be made in full to CCC. For payment instructions, please see information listed at the bottom of this form.

License Number	3016031011576
License date	Oct 25, 2012
Licensed content publisher	John Wiley and Sons
Licensed content publication	Angewandte Chemie International Edition
Book title	None
Licensed content author	Ja Hye Myung,Khyati A. Gajjar,Jelena Saric,David T. Eddington,Seungpyo Hong
Licensed content date	Oct 19, 2011
Start page	11769
End page	11772
Type of use	Dissertation/Thesis
Requestor type	Author of this Wiley article
Format	Print and electronic
Portion	Full article
Will you be translating?	No
Order reference number	None

Myung, Ja Hye

E-mail: jmyung4@uic.edu

EDUCATION

08/07-09/12	**Ph.D.**, Biopharmaceutical Sciences (Advisor: Prof. Seungpyo Hong) Department of Biopharmaceutical Sciences University of Illinois at Chicago, Chicago, IL Dissertation Title: Multivalent binding, cell rolling, and micropatterning for enhanced detection of circulating tumor cells.
03/04-02/06	**M.S.**, Pharmaceutics (Advisor: Prof. Sung-Joo Hwang) Department of Pharmaceutics Chungnam National University, Daejeon, Korea (ROK) Thesis Title: Sirolimus solid dispersions with Sucroester 15 and PVP K-30 using the solution enhanced dispersion by supercritical fluids.
03/00-02/04	**B.S.**, Pharmacy (Advisor: Prof. Sung-Joo Hwang) Department of Pharmaceutics Chungnam National University, Daejeon, Korea (ROK) Thesis Title: Preparation and evaluation of sustained-released pellets of Tamsulosin Hydrochloride using ethylcellulose.

RESEARCH EXPERIENCE

08/08-current	Graduate Research Assistant Department of Biopharmaceutical Sciences College of Pharmacy, University of Illinois at Chicago, Chicago, IL
05/06-07/07	Professional researcher Institute of Drug Research and Development Chungnam National University, Daejeon, Korea (ROK)
04/04-08/05	Graduate Research Assistant for High Performance Liquid Chromatography (HPLC) Center for Research Facilities Chungnam National University, Daejeon, Korea (ROK)

TEACH EXPERIENCE

09/10-04/11	Participation in the student inquiry and research program The Illinois Mathematics and Science Academy, Aurora, IL

08/08-05/11	Graduate Teaching Assistant Department of Biopharmaceutical Sciences College of Pharmacy at University of Illinois at Chicago, Chicago, IL

NON-ACADEMIC EXPERIENCE

2009-2011	Volunteer in Alzheimer's disease association Volunteer to organize the Chicago Memory Walk Alzheimer's Association-Great Illinois Chapter (8430 W. Bryn Mawr, Suite 800, Chicago, IL, 60631)
09/04-12/05	Graduate student council of College of Pharmacy Graduate Association at Chungnam National University, Daejeon, Korea (ROK)
09/03-10/03	International Internship GlaxoSmithKline Korea, Seoul, Korea (ROK)
09/02-08/03	President of the organization Herbal Medicine Study Club at Chungnam National University, Daejeon, Korea (ROK)

ACADEMIC AWARDS/HONORS

06/2012	Third place in 2012 COP images of research competition College of Pharmacy at UIC, USA
2011/2012	W.E. van Doren Scholar Award College of Pharmacy at UIC, USA
08/2011	Dean's Scholar Award Graduate college at UIC, USA
2010/2011	Chancellor's graduate research fellowship Graduate college at UIC, USA
03/2008	Phi Kappa Phi The honor society of Phi Kappa Phi, USA
08/2007	Global Alumni Scholarship Alumni of Chungnam National University, Daejeon, Korea (ROK)
02/2006	Best Research award of Beckma Symposium Graduate College at Chungnam National University, Daejeon, Korea (ROK)
02/2004	Excellence award in Academic Performance Chungnam National University, Daejeon, Korea (ROK)
2001-2003	Jeongsimhwa Scholarship Jeongsimhwa Scholarship Foundation, Daejeon, Korea (ROK)
08/2000	Dean's Scholarship

PUBLICATIONS

A) SUBMITTED or IN PREPARATION

1. **J.H. Myung**, K.A. Gajjar, J. Saric, D. T. Eddington, and S. Hong, Modular CTC device using a combinational approaches of dendrimer-mediated multivalent binding and E-selectin-mediated cell rolling. *in preparation*.
2. P.M. Ryan, **J.H. Myung**, and S. Hong, Engineering multifunctional devices through implementation of bio-inspired design strategies (Book Chapter). *Submitted*.

B) PEER-REVIEWED PUBLICATIONS, IN PRESS or PUBLISHED

1. **J.H. Myung**, K.A. Gajjar, Ye Eon Han, and S. Hong, The Role of Polymers in Detection and Isolation of Circulating Tumor Cells. *Polymer Chemistry,* Vol. 3, pp. 2336-2341 (2012).
2. C. Launiere, M. Gaskill, G. Czaplewski, **J.H. Myung**, S. Hong, and D.T. Eddington, Channel surface patterning of alternating biomimetic protein combinations for enhanced microfluidic tumor cell isolation. *Analytical Chemistry,*Vol. 84, No. 9, pp.4022-8 (2012).
3. **J.H. Myung**, K.A. Gajjar, J. Saric, D.T. Eddington, and S. Hong, Dendrimer-mediated Multivalent Binding for Enhanced Capture of Tumor Cells. *Angewandte Chemie-International Edition,*Vol. 50, No. 49, pp.11769-72 (2011).

   ***** This article is highlighted in UIC NEWS RELEASE as well as Faculty of 1000 by Dr. Don Tomalia who is the inventor of dendrimers. Also this article is selected as a HOT PAPER by Angewandte Chemie.
4. C.A. Launiere, G.J. Czaplewski, **J.H. Myung**, S. Hong, and D.T. Eddington, Rheologically Biomimetic Cell Suspensions for Decreased Cell Settling in Microfluidic Devices. *Biomedical Microdevices*, Vol. 13, No. 3, pp. 549-57 (2011).
5. **J.H. Myung**, K.A. Gajjar, R.M. Pearson, C.A. Launiere, D.T. Eddington, and S. Hong, Direct Measurements on CD24-Mediated Rolling of Human Breast Cancer MCF-7 Cells on E-selectin. *Ananlytical Chemistry*, Vol. 83, No. 3, pp. 1078-83 (2011).[*]

   ***** This article is highlighted by C&E News.
6. **J.H. Myung**, C.A. Launiere, D.T. Eddington, and S. Hong, Enhanced Tumor Cell Isolation by a Biomimetic Combination of E-selectin and anti-EpCAM: Implication for Effective Separation of Circulating Tumor Cells (CTCs). *Langmuir*, Vol. 26, No. 11, pp. 8589-96 (2010).
7. C.M. Kang, T.Q. Trung, K.H. Kim, **J.H. Myung**, S.J. Hwang, M.Y. Kim, and H.J. Kuh, Validation of an HPLC Method for Nadolol in Human Plasma and Evaluation of Its Pharmacokinetics after a Single-dose in Korean Volunteers. *Journal of Korean Pharmaceutical Science*, Vol.35, No.6, pp.431-436 (2005).
8. J.H. Yun, **J.H. Myung**, H.J. Kim, S. Lee, J.S. Park, W. Kim, E.H. Lee, C.J. Moon, and S.J. Hwang,

LC-MS Determination and Bioavailability Study of Imidapril Hydrochloride after the Oral Administration of Imidapril Tablets in Human Volunteers. *Archives of Pharmacal Research*, Vol.28, No.4, pp.463-468 (2005).

PATENT

1. **United State Patent Application**. PCT/US10/32266, Methods and Devices for Capturing Circulating Tumor Cells. Inventors: Seungpyo Hong, David T. Eddington, **Ja Hye Myung**, and Cari A. Launiere (2010).

CONFERENCE PRESENTATIONS

A) Oral presentation

1. **J.H. Myung**, K.A. Gajjar, J. Saric, R.M. Pearson, C.A. Launiere, D.T. Eddington, and S. Hong, Direct measurements on CD24-mediated rolling of human breast cancer MCF-7 cells on E-selectin (PD 16). The 43rd annual pharmaceutics graduate student research meeting, Jun 23-25th 2011, Madison, WI.

B) Poster presentation

1. **J.H. Myung**, K.A. Gajjar, and S. Hong, Enhanced tumor cell detection through the multivalent binding of dendrimer-integrated surfaces (#1909). Biotechnology session in 2012 AAPS Annual Meeting and Exposition, Oct 14th – 18th 2012, Chicago, IL.
2. **J.H. Myung**, K.A. Gajjar, J. Saric, D.T. Eddington, and S. Hong, Dendrimer-mediated multivalent binding for enhanced capture of tumor cells (#2388). Tumor Biology 21 session in AACR Annual Meeting, Apr 2nd 2012, Chicago, IL.
3. **J.H. Myung**, K.A. Gajjar, J. Saric, D.T. Eddington, and S. Hong, Dendrimer-mediated multivalent binding for enhanced capture of tumor cells (#74). UIC College of Pharmacy Research day, March 9th 2012, Chicago, IL.
4. **J.H. Myung**, K.A. Gajjar, J. Saric, D.T. Eddington, and S. Hong, Dendrimer-mediated multivalent binding for enhanced capture of tumor cells (#CTTI-26). Cancer Center Research Forum 2012, March 6th 2012, Chicago, IL.
5. **J.H. Myung**, K.A. Gajjar, J. Saric, D.T. Eddington, and S. Hong, Dendrimer-mediated multivalent binding for enhanced capture of tumor cells (#31). The 9th Annual Chicago Biomedical Consortium (CBC) Symposium, Oct 21st 2011, Chicago, IL.
6. **J.H. Myung**, K.A. Gajjar, J. Saric, R.M. Pearson, C.A. Launiere, D.T. Eddington, and S. Hong, Direct measurements on CD24-mediated rolling of human breast cancer MCF-7 cells on E-selectin (#7). The 3rd Controlled Release Society (CRS)-Illinois Student Chapter Symposium, Aug 12th 2011, Chicago, IL.
7. **J.H. Myung**, K.A. Gajjar, J. Saric, R.M. Pearson, C.A. Launiere, D.T. Eddington, and S. Hong,

Direct measurements on CD24-mediated rolling of human breast cancer MCF-7 cells on E-selectin (#135). UIC Student Research Forum, April 19th 2011, Chicago, IL.

8. **J.H. Myung**, K.A. Gajjar, J. Saric, R.M. Pearson, C.A. Launiere, D.T. Eddington, and S. Hong, Direct measurements on CD24-mediated rolling of human breast cancer MCF-7 cells on E-selectin (#29). UIC College of Pharmacy Research day, February 25th 2011, Chicago, IL.
9. **J.H. Myung**, K.A. Gajjar, C.A. Launiere, D.T. Eddington, and S. Hong, Effective separation of tumor cells using surfaces functionalized with a biomimetic combination of adhesive proteins (PP3.54). Materials Research Society annual meeting, November 29th 2010, Boston, MA.
10. **J.H. Myung**, C.A. Launiere, K.A. Gajjar, D.T. Eddington, and S. Hong, Effective cancer cell separation using a biomimetic combination of adhesive proteins. The 42nd Pharmaceutics Gradutate Students Research Meeting, June 17-19th 2010, Ohio, The Ohio State University.
11. **J.H. Myung**, K.A. Gajjar, C.A. Launiere, D.T. Eddington, and S. Hong, Cancer cell isolation using anti-EpCAM-dependentinteraction. The 2nd Controlled Release Society (CRS)-Illinois Student Chapter Symposium, May 17th 2010, Chicago, IL.
12. **J.H. Myung**, C.A. Launiere, K.A. Gajjar, D.T. Eddington, and S. Hong, Biomimetic combinations of adhesive protein for enhanced cancer cell separation. UIC College of Pharmacy Research day, February 26th 2010, Chicago, IL.
13. **J.H. Myung**, C.A. Launiere, K.A. Gajjar, D.T. Eddington, and S. Hong, Enhanced tumor cell separation by surfaces functionalized with combinations of bioadhesive proteins (NEMB2010-13210). Proceedings of ASME 2010 first global congress on nanoengineering for medicine and biology, February 7-10th 2010, Houston, TX.
14. **J.H. Myung** and S. Hong, Cell-type dependent responses to functionalized surfaces with adhesive proteins (PS-54). The 41st annual pharmaceutics graduate student research meeting, Jun 25-27th 2009, Lafayette, IN.
15. **J.H. Myung**, D.T. Eddington, and S. Hong, Cellular responses to biofunctionalized substrates immobilized with selectins and anti-EpCAM. The 1st controlled release society (CRS)-Illinois student chapter symposium, Jun 6th 2009, Chicago, IL.
16. **J.H. Myung**, H.Y. Lee, S.H. Ryu, and S.J. Hwang, Developed HPLC Method for Determination of Zolpidem Tartrate in Human Plasma with Fluorescence Detection and its Use in Pharmacokinetic Studies (M1268). 19th Anniversary of American Association of Pharmaceutical Scientists, November 2005, Nashville, TN.
17. M.S. Kim, H.Y. Lee, **J.H. Myung**, S.W. Jun, J.S. Kim, S.B. Lee, and S.J. Hwang, Development and Evaluation of Controlled-Release Pellets with Sodium Alginate and Surelease using Extrusion/Spheronization (W5081). 19th Anniversary of American Association of Pharmaceutical Scientists, November 2005, Nashville, TN.
18. H.J. Kim, **J.H. Myung**, S.H. Ryu, S.B. Lee, and S.J. Hwang, Studies on Drug Release Kinetics form 4-Aminopyridine-Carbomer Hydrophilic Matrix Tablets. 34th Meeting of the Korean Society of

Pharmaceutical Sciences and Technology, November 2004, Seoul, Korea.

19. H.J. Kim, **J.H. Myung**, S.H. Ryu, S.B. Lee, and S.J. Hwang, Bioequivalence of Vidcef capsule to Duricef capsule (Cefadroxil 500mg). 53rd Proceedings of the Convention of the Pharmaceutical Society of Korea, April 2004, Seoul, Korea.